Control strategy of grid connected power converter based on virtual flux approach

Nurul Fazlin Roslan

PhD Thesis

Control Strategy of Grid Connected Power Converter based on Virtual Flux Approach

Nurul Fazlin Roslan

Barcelona, September 2021

Control Strategy of Grid Connected Power Converter based on Virtual Flux Approach

Nurul Fazlin Roslan

Dissertation submitted to the Doctorate Office of the Universitat Politècnica de Catalunya in partial fulfillment of the requirements for the degree of Doctor of Philosophy by the

UNIVERSIDAD DE MÁLAGA

UNIVERSIDAD DE SEVILLA

UNIVERSIDAD DEL PAÍS VASCO/EUSKAL ERRIKO UNIBERTSITATEA

UNIVERSITAT POLITÈCNICA DE CATALUNYA

Joint Doctoral Programme in Electric Energy Systems

Barcelona, September 2021

Control Strategy of Grid Connected Power Converter based on Virtual
Flux Approach

UNIVERSITAT POLITÈCNICA DE CATALUNYA
Escola de Doctorat
Edifici Vèrtex. Pl. Eusebi Güell, 6 08034 Barcelona
Web: http://www.upc.edu

UNIVERSIDAD DE MÁLAGA
Escuela de Doctorado
Pabellón de Gobierno - Plaza el Ejido, s/n 29013 Málaga
Web: http://www.uma.es

UNIVERSIDAD DE SEVILLA
Escuela Internacional de Doctorado
Pabellón de México - Paseo de las Delicias, s/n 41013 Sevilla
Web: http://www.us.es

UNIVERSIDAD DEL PAÍS VASCO/EUSKAL ERRIKO UNIBERTSITATEA
Escuela de Máster y Doctorado Edificio Aulario II - Barrio Sarriena, s/n 48940 Leioa (Bizkaia)
Web: http://www.ehu.eus/es

Acknowledgements

Abstract

Distributed Generation (DG) provides an alternative to the Centralized Generation (CG) by means of generating electricity near to the end user of power with the employment of small-scale technologies to produce electricity, mainly using Renewable Energy Sources (RES). The prospects of renewable energy integration during the next years are still very optimistic. In fact, RES has become one of the most cost-competitive options for energy generation. Power electronic converter technology enables flexible interconnection between renewable energy generation systems and the electrical network. Therefore, power converters and their control systems play an important role in the grid integration of renewable energy systems like wind turbines and photovoltaic installations. With a stochastic behavior and inconsistency of the RES, it is difficult to guarantee power balancing in the system, hence the power electronics-based converters should have a specific functionality to make them compatible with the synchronous power systems dominated in most traditional power systems. Extensive research has been done and different control algorithms have been introduced with the purpose to improve the power quality in the distributed generation system.

This PhD dissertation is made to provide an alternative control framework for the grid connected power converter by adopting the virtual flux concept in the control layer. This dissertation can be divided into three main topics. The 1st topic presents the voltage sensorless control system for the grid-connected power converter. The control system presented is done without depending on AC-voltage measurement where the grid synchronization is based on the Virtual Flux (VF) estimation. In this regard, the Frequency Locked Loop (FLL) is used in conjunction with the estimation scheme to make the system fully adaptive to the frequency changes. This voltage sensorless application is useful for reducing cost and complexity of the control hardware. It is also can be utilized in case of limited reliability or availability of voltage measurements at the intended point of synchronization to the grid. Considering that most previous studies are based on the VF estimation for the case of power converter connected to the grid through the L-filter or LC-filter, this dissertation is focused on the power converter connected to the grid through the

LCL filter. The Proportional Resonant (PR) current controller is adopted in the inner loop control of the power electronics-based converter to test the performance of such system.

Another control method based on VF synchronization that permits to control the active and reactive power delivery in a remote point of the grid is also presented in this dissertation. This is due to the fact that the VF is implemented that the voltage in a remote point of the line can be estimated. As it will be shown in simulations and experiments, the proposed control scheme provides a good tracking and dynamic performance under step changes in the reference power. The fast synchronization and the smooth reference tracking achieved in transient conditions have demonstrated the effectiveness of the Dual Second Order Generalized Integrator controlled as Quadrature Signal Generator (DSOGI-QSG) and also the current controller used in the proposed system. In addition to the power control itself, this study could also benefit the frequency and the voltage regulation methods in distributed generation applications as for instance in microgrid.

Considering the fact that the grid connected power converter can be controlled as a virtual synchronous generator where the flux is a variable to be used for controlling its operation, this dissertation also presents a Virtual Synchronous Flux Controller (VSFC) as a new control framework of the grid connected power converter. In this regard, a new control strategy in the inner loop control of the power converter will be proposed. The main components of the outer loop control of VSFC are based on the active and reactive power control. The results presented show that the VSFC works well to control the active and reactive power without considering any synchronization system. The inner loop control is able to work as it is required, and the measurement flux is able to track the reference flux without any significant delays.

All the work presented in this dissertation are supported by mathematical and simulation analysis. In order to endorse the conclusions achieved, a complete experimental validations have been conducted before wrapping this dissertation with a conclusion and recommendation for future enhancement of the control strategies that have been presented.

.

Contents

List of Tables

Nomenclature

DG	Distributed Generation
CG	Centralized Generation
RES	Renewable Energy Sources
VF	Virtual Flux
FLL	Frequency Locked Loop
PR	Proportional Resonant
DSOGI-QSG	Dual Second Order Generalized Integrator configured as Quadrature Signal Generator
VSFC	Virtual Synchronous Flux Controller
IEA	International Energy Agency
TSO	Transmission System Operator
PLL	Phase Locked Loop
DPC	Direct Power Control
VOC	Voltage Oriented Control
PWM	Pulse Width Modulation
PI	Proportional Integral
VSC	Voltage Source Converter

HV	High Voltage
MV	Medium Voltage
LV	Low Voltage
RE	Renewable Energy
PCC	Point of Common Coupling
ESS	Energy Storage System
EMS	Energy Management System
VSG	Virtual Synchronous Generator
VISMA	Virtual Synchronous Machine
SSG	Static Synchronous Generator
PSC	Power Synchronization Control
SPC	Synchronous Power Controller
MC	Magnetic Controller
PNS	Positive Negative Sequence
IEC	International Electrotechnical Commission
THD	Total Harmonics Distortion
MPPT	Maximum Power Point Tracking
DFIG	Doubly Fed Induction Generator
SG	Synchronous Generator
SCIG	Squirrel Cage Induction Generator
SRF-PLL	Synchronous Reference Frame Phase Locked Loop
DDSRF-PLL	Decoupled Double Synchronous Reference Frame-Phase Locked Loop
DSOGI-PLL	Dual Second Order Generalized Integrator based on Phase Locked Loop
3phEPLL	Three Phase Enhanced PLL

ISC	Instantaneous Symmetrical Component
EPLL	Enhanced PLL
DSOGI-FLL	Dual Second Order Generalized Integrator based on Frequency Locked Loop
MSOGI-FLL	Multiple Second Order Generalized Integrator based on Frequency Locked Loop
SOGI-QSG	Second Order Generalized Integrator configured as a Quadrature Signal Generator
DDSRF	Decoupling network in the Double Synchronous Reference Frame
NPC	Neutral Point Clamp
HERIC	Highly Efficient and Reliable Inverter Concept
DSC	Delayed Signal Cancellation
PS-SRF	Positive Sequence Synchronous Reference Frame
PV	Solar Photovoltaic
PNS-VF	Positive and Negative Sequence Virtual Flux
DSOGI-VF	Dual SOGI-based VF estimation
P	Active Power
Q	Reactive Power
PNSC	Positive and Negative Sequence Component
VCO	Voltage Controlled Oscillator
PLC	Power Loop Controller
ZOH	Zero Order Hold

Introduction

*T*his chapter provides a depth understanding of the research topic area. The chapter starts with an explanation of the research background that also emphasized the transition of global power generation from the conventional resources to the renewable energy resources that includes the forecast of renewable energy penetration. The chapter continues with the research motivation and highlights the issues and problems in the research area. The dissertation is not complete without the research objectives indicating the solution and method that aims to solve the problems that has been highlighted. Chapter 1 will be continued with the scope of work, research question, research contributions and outlined of the dissertation before concluding the chapter with a list of publications.

1.1. Background

Synchronous generations have been used for a very long time to produce electricity by means of utilizing the synchronous generators. The electricity generated by these plants is radially transmitted long distances. Due to the long transmission distances, the current generation faced a low efficiency as the generation of electrical power is dependent on limited resources, hence highly contributed to the negative impact of emissions on the environment.

The progression of renewable energy in the early 2000s has change the energy scenario. In the last ten years, the global perceptions on renewable energy have shifted considerably from the conventional to the rapid deployment of many renewable energy technologies [1]. The recent attentiveness on the renewable distributed energy generation has been motivated by the necessity to reduce the high environmental impact of fossil fuel-based energy system.

Based on the figure shown in Fig. 1.1, the renewable energy increase steadily in global energy demand with the capacity data begin in the year of 2004 until 2013. It is clearly seen that the hydropower leads the total installed capacity followed by the wind energy systems and solar photovoltaic.

Total Installed Capacity		2004	2005	2006	2007	2008	2009	2010	2011	2012	2013
Solar Photovoltaic	GW	2.6	3.1	4.6	7.6	13.5	21	40	71	100	139
Concentrating Solar Power	GW	0.4	0.4	0.4	0.4	0.5	0.7	1.1	1.6	2.5	3.4
Wind Power	GW	48	59	74	94	121	159	198	238	283	318
Bio Power	GW	39	41	43	45	46	51	70	74	78	88
Geothermal Power	GW	8.9	9.8	10	10.4	10.7	11	11.2	11.4	11.7	12
Hydro Power	GW	715	–	–	920	950	980	935	960	990	1,000

Fig. 1.1. Total installed capacity of renewable energy technologies from 2004 until 2013 [1] .

The updated info provided in [2] shows the renewable energy transition from 2012 to 2018. Based on the graph shown in Fig. 1.2, solar PV, wind power and hydropower are the leading technologies in the renewable energy platform with a higher total additions since 2012. The graph also shown that the renewable energy still shows a good progression in 2018 with a total addition of 181GW.
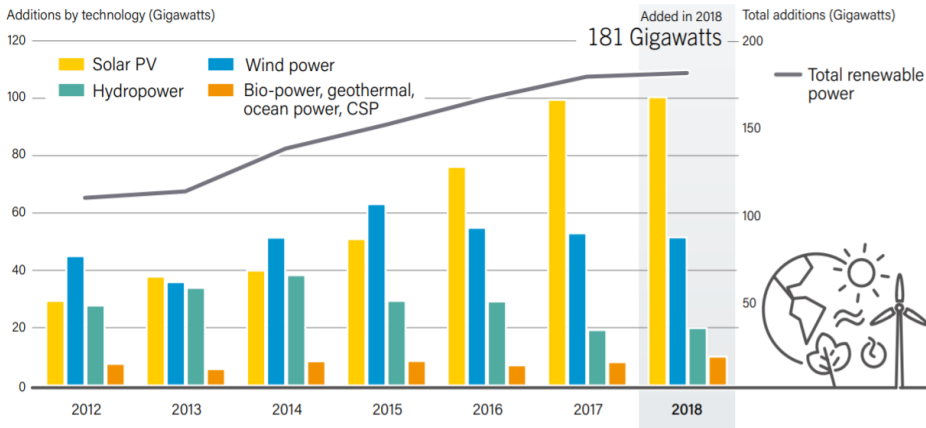
Fig. 1.2. Total additions of renewable energy by technology from 2012 until 2018 [2].

In line with an abrupt cost reduction and supported by the policy as well as the advancement in digital technologies, the renewables energy sector is expected to rapidly developed [3]. Fig. 1.3 shows the cost in solar and wind power systems are expected to drop until 2030.
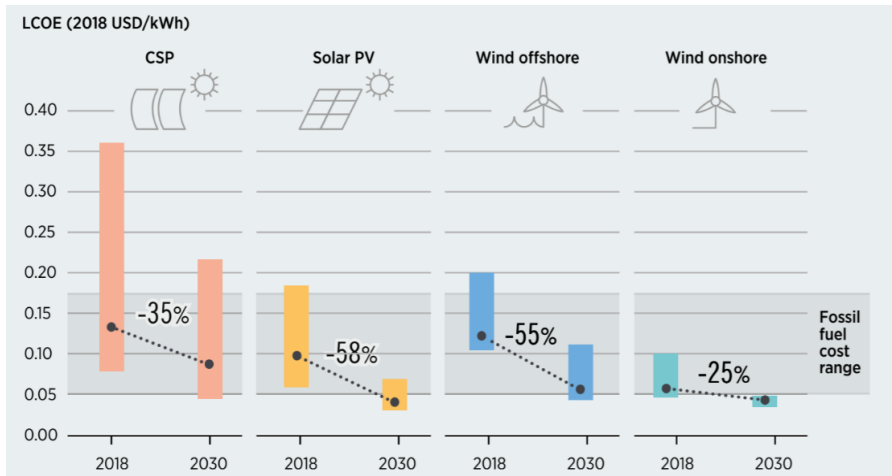
Fig. 1.3. Cost reduction in renewable energy from 2018 to 2030 [3].

However, in the year of 2020, the world has been shocked with the Covid-19 pandemic that has significantly affected all aspect of life. In this regards, this pandemic caused an extraordinary global economic impact that includes the negative impact on renewables energy sector and social predicament. As most countries faced lockdown situation, the construction of energy facilities and infrastructure have been delayed or stopped [4]. Fig. 1.4 shows the net capacity addition and forecast to 2025 [5], according to the International Energy Agency (IEA). The total capacity net addition shown from 2020 to 2025 include the accelerated cases while considering the impact of Covid-19 pandemic. Therefore, the renewable energy industry globally should bounce back quickly and steadily from the challenges of the Covid-19 crisis. In this regard, the recovery plan must be aligned with the long term national and global objectives on energy resilient and sustainable development [6].

As the renewable energy sector is still growing, the main issue is not only producing electricity but to maintain the stability in the AC network and offering a more reliable performance of the control system which suits with the specific requirements set by the national Transmission System Operator (TSO) in each country. In AC system, the frequency is the most important global magnitude and it should be ideally maintained by all interconnected elements. Even though the grid voltage is not a global magnitude, but it should have remained stable within certain limits over the electrical network. In order to maintain the voltage stability, a precise control of active and reactive power is essential. In renewable energy generation systems, the used of power converters and its controllability are the key elements for achieving an effective control of grid integration especially in solar PV and wind power plants [7, 8].
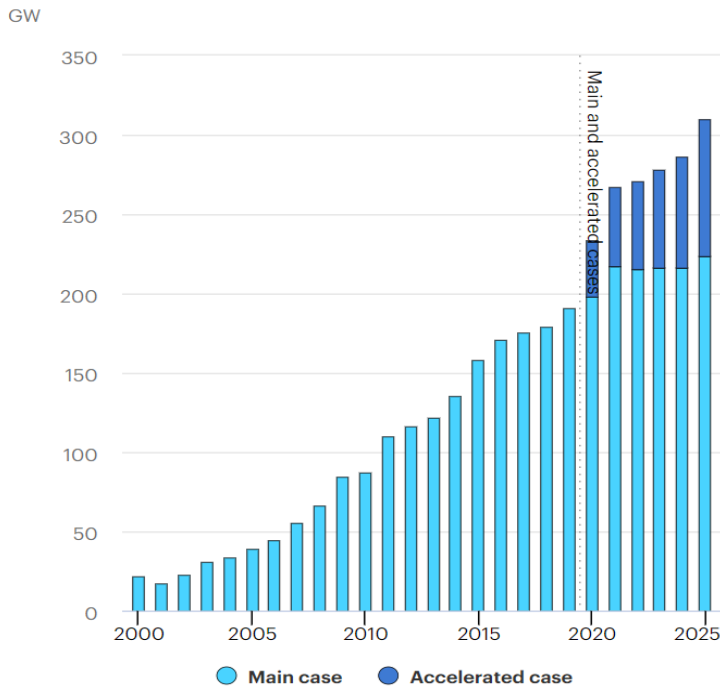
Fig. 1.4. World total capacity net additions and forecast of renewable energy to 2025 [6].

Utilization of power electronics-based generation with an appropriate control has tremendously increased with the determination to maximize the power output from the renewable resources while ensuring the reliability and controllability at minimum cost. Power electronic converter technology enables flexible interconnection between renewable energy generation systems and the electrical network. The performance of power electronics based converter has become very important to perform advanced function such as dynamic response control of the active and reactive power, reactive current injection during faults and also operation on the wide range of voltage and frequency in order to comply with the grid code requirement [9].

1.1.1   Classical Control of Grid Connected Power Converters

The power electronics based converters are capable to convert the electrical energy from AC to DC and vice versa where voltage source and current source are the two possible types that can be considered for the conversion process [10, 11]. For the conventional control scheme of a grid connected power converter, grid synchronization methods become highly important to ensure the safe running of the grid connected of three phase converters especially when the grid voltage disturbances occurred in the system.

The synchronization method should consider the accuracy, frequency and phase angle adaptivity, distortion rejection capability, dynamics response and its structural simplicity. A perfect synchronization method is able to correctly filter a grid side harmonic in order to track the fundamental cleanly when harmonics pollution exists. During the weak grid condition, the system frequency may deviate from its nominal value and the synchronization method selected must be able to withstand with the changes without losing its synchronism. In order to synchronize the power converter with the grid, the Phase Locked Loop (PLL) is commonly used to obtain the phase angle, θ and the angular speed, ω of the grid voltage. In this regard, the grid connected power converter response and its interaction with the grid is strongly influenced by the PLL dynamics.

The synchronization of power converters with the grid can be performed either by direct measurement of the grid voltage [12-14] or by adopting a voltage sensorless [15-17] control solution. Voltage sensorless control has become an attractive solution because it can reduce costs by means of reducing the number of sensors needed. The voltage sensorless control could lead to the increasing of system reliability where in this case, the possibilities of interruption due to the component failure can be reduced. Other advantages of implementing the voltage sensorless operation is that, the voltage measurement can be utilized in normal condition while the voltage sensorless will allow the converter to remain operated in case of voltage sensor fails to function. In the implementation of voltage sensorless control, the Direct Power Control (DPC) and the Voltage Oriented Control (VOC) strategies are commonly used [18-20]. Virtual Flux estimation is one of the simplest ways to achieve voltage sensorless control by means of estimating the grid voltage condition. By utilizing the virtual flux estimation, it is also possible to increase the performance and flexibility of the converter control system. This feature makes it possible to estimate the grid voltage condition that are not easily available for measurement [21, 22]. If the parameters needed are available, the estimation can be done at any point of the grid.

Considering the power converter is controlled as a voltage source, the lowest control hierarchy is the Pulse Width Modulation (PWM) control. The PWM control will generate the pulses needed for the IGBTs in the converter. The pulses are very important to ensure the converter is switched at appropriate instance. The reference needed by the PWM is normally from the output of the inner loop control. The inner loop control is a current controller that controls the grid injection current. In conventional control of grid connected power converter, the Proportional Integral (PI) and Proportional Resonant (PR) current controller have been considered in most publications.

The outer loop control [23] will influence the dynamics of AC system because the active and reactive power as well as the DC and AC voltage control is performed in this control loop [24-28]. The objectives of having the outer loop control is to provide the current reference signals needed by the inner loop and control the active and reactive power injected to the grid. The current reference generated can be either in synchronous reference frame ($i_d{}^*$ & $i_q{}^*$) or stationary reference frame ($i_\alpha{}^*$ & $i_\beta{}^*$) depending on the implementation of the control strategies. In this regard, the current reference signals generated will influence both active and

reactive power flow. The active and reactive power control can be achieved by using the PI controller in the closed loop and instantaneous power calculation in the open loop system. The highest control hierarchy of the Voltage Source Converter (VSC) is known as ancillary control. This control loop is not mandatory to be added in the control layer of the VSC but by having this control, it will greatly enhance the VSC performances. Normally the frequency control, damping control as well as the AC voltage control will be performed at this stage.

Considering the control system is implemented in stationary reference frame, $\alpha\beta$, Fig. 1.5 shows the general schematic of the main components in VSC control systems. The converter current $I_{c,\,abc}$ as well as the measured voltage, V_{abc} is converted in $\alpha\beta$ sequence, denoted as $I_{c,\,ab}$ and V_{ab}.
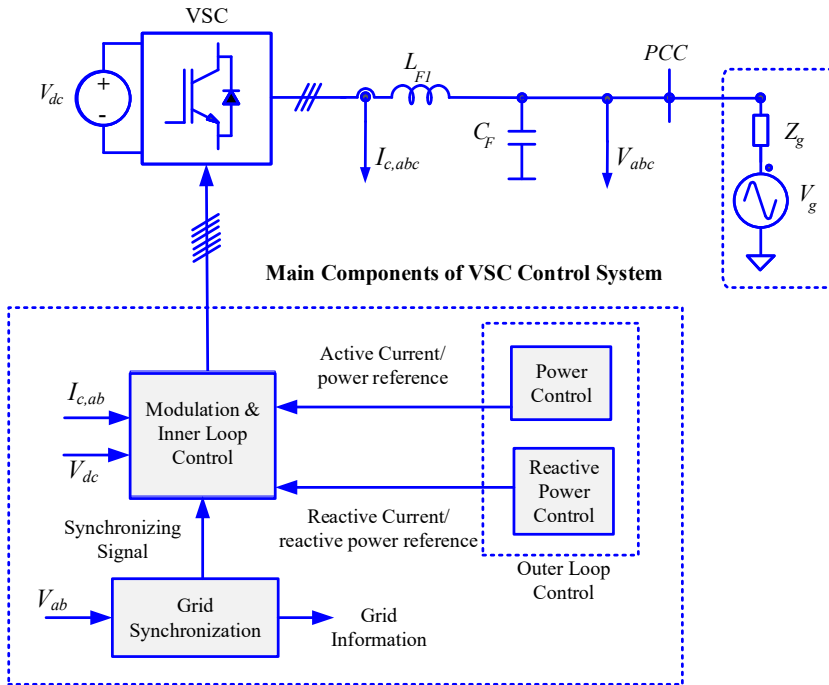
Fig. 1.5. Overview of the main components of VSC control systems.

1.1.2   Frequency and Voltage Droop Control

In renewable distributed generation, the grid connected power converters should interact with the grid, and automatically react to the frequency and voltage variations by providing the frequency and voltage support. The frequency and voltage support can be achieved by implementing the droop controller [29, 30]. It should be noted that the characteristics of the droop control are provided by the national grid codes, therefore, it might be different in each

country. The droop controller provides frequency and voltage control by adjusting the active and reactive power set point proportional to the deviation of frequency and AC voltage magnitude. The principle of a droop control can be described by analyzing the power transfer between point A and point B as shown in Fig. 1.6 [31]. Referring to Fig. 1.6 (a), the active and reactive power flowing into line A is given by (1.1) and (1.2).

$$P_A = \frac{V_A^2}{Z}\cos\theta - \frac{V_A V_B}{Z}\cos(\theta + \delta) \tag{1.1}$$

$$Q_A = \frac{V_A^2}{Z}\sin\theta - \frac{V_A V_B}{Z}\sin(\theta + \delta) \tag{1.2}$$

where the δ is the power angle and θ is the power factor angle at section A. As stated in [31] and [9], this analysis is valid for both single and three phase system. Assume the power converter is an ideal controllable voltage source and $Z\cos\theta = R$, $Z\sin\theta = X$, the active and reactive power can be obtained by (1.3) and (1.4) respectively.
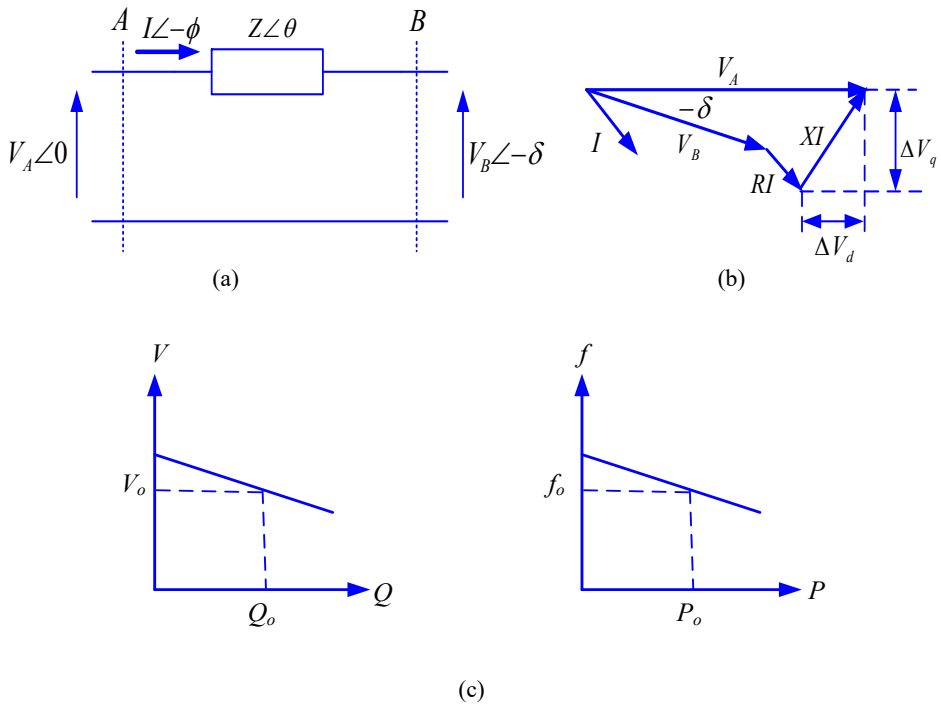
Fig. 1.6. (a) Power flow through a line, (b) Phasor diagram, (c) Q/V and P/f droop control.

$$P_A = \frac{V_A}{R^2 + X^2}[R(V_A - V_B \cos \delta) + XV_B \sin \delta] \tag{1.3}$$

$$Q_A = \frac{V_A}{R^2 + X^2}[-R(V_B \sin \delta + X(V_A - V_B \cos \delta)] \tag{1.4}$$

Therefore,

$$\Delta V_d = V_A - V_B \cos \delta = \frac{RP_A + XQ_A}{V_A} \tag{1.5}$$

$$\Delta V_q = V_B \sin \delta = \frac{XP_A - RQ_A}{V_A} \tag{1.6}$$

The resistive part can be neglected in the case of DG inverter connected to the grid through a purely inductive line impedance because the inductive component in the line impedance in High Voltage (HV) and Medium Voltage (MV) network are typically higher than resistive. Additionally, the power angle δ is relatively small, it can be assumed that $\sin \delta \approx \delta$ and $\cos \delta \approx 1$ that is possible to simplify (1.3) and (1.4) to (1.5) and (1.6) respectively. The direct relationship between power angle and active power as well as the relationship between the voltage difference and the reactive power can be directly seen from (1.7) and (1.8) as stated in [31]. The grid frequency and voltage at the point of connection of the converter is regulated by means of controlling the value of active and reactive power delivered to the grid.

$$P_A = \frac{V_A}{X}(V_B \sin \delta) \Rightarrow \delta \approx \frac{XP_A}{V_A V_B} \tag{1.7}$$

$$Q_A = \frac{V_A}{X}(V_A - V_B \cos \delta) \Rightarrow V_A - V_B \approx \frac{XQ_A}{V_A} \tag{1.8}$$

Therefore, the droop expression for the inductive lines can be derived as (1.9) and (1.10).

$$f - f_0 = -k_P(P - P_0) \tag{1.9}$$

$$V - V_0 = -k_Q(Q - Q_0) \tag{1.10}$$

where f_0 and V_0 are the rated frequency and voltage while P_0 and Q_0 are the set points for the active and reactive power. The *P/f* and *Q/V* droop characteristics based on (1.9) and (1.10) can be illustrated in Fig. 1.6 (c) where the slope of the voltage and frequency droop is

depending on the coefficients k_P and k_Q. Based on this theoretical, it is easy to understand that the frequency and voltage can be regulated by controlling its active and reactive power according to its droop characteristics. For the case of Low Voltage (LV) network that mainly based on the resistive, the inductive part can be ignored which contrary to the case in both high and medium voltage. In the low voltage network, the droop regulation in (1.7) and (1.8) is no longer valid. The effect on the voltage amplitude can be seen when the active power, P has been adjusted and the effect on the frequency can be observed while adjusting the reactive power, Q. Equation (1.7) to (1.10) can be modified to (1.11) to (1.14) in order to suit with the resistive line case.

$$P_A \approx \frac{V_A}{R}(V_A - V_B \cos\delta) \Rightarrow V_A - V_B \approx \frac{RP_A}{V_A} \tag{1.11}$$

$$Q_A = -\frac{V_A.V_B}{R}\sin\delta \Rightarrow \delta \approx -\frac{RQ_A}{V_A V_B} \tag{1.12}$$

$$V - V_0 = -k_P(P - P_0) \tag{1.13}$$

$$f - f_0 = k_Q(Q - Q_0) \tag{1.14}$$

In general, both resistive and inductive effect must be taken into account in order to regulate the frequency and voltage droop.

1.1.3 Emulation of Synchronous Generator

In conventional power system, synchronous generator has a robust connection to a weak grid, capable to naturally perform a load sharing and also work well during the unbalanced voltage conditions. Therefore, the idea of emulating the synchronous generator behavior (that includes its electrical and mechanical characteristics) on grid connected power converter control layer are most welcomed by the grid operators. In synchronous generator operation, a good control of the output impedance will influence the electrical characteristics. On the other hand, the rotor inertia will react on the mechanical response by guaranteeing a good dynamic response of the power systems.

The dynamic response of the power electronics-based converter is totally different from the synchronous generator because it depends on the PLL dynamics. The distributed generator resulting from the power electronics-based converter does not naturally implement either any inertia or inductive output impedance. Therefore, the performance of grid connected power converters differ from the synchronous generator. The odd transient dynamics as well as lack

of inertia gives rise to the negative impact on power system operation especially under weak grid or islanded grid condition. Emulating the effect of inertia and impedance somehow is very important in order to respond to any disturbances that may appear in the power systems. In order to ensure the effectiveness of the distributed generators and to make them compatible with the operational principles of synchronous generators, specific functionalities should be considered in the control systems thus motivates the research topic for this dissertation.

Extensive research has been carried out in the control of grid connected power electronics-based converter with the aim to improve the interaction between the power converter and the electrical grid. Many works presented were also aim to provide the inertial characteristics to the grid connected power converters. The method for inertia emulation can be achieved by implementing an extra loop [32-35] or by modifying the PLL [36]. In this implementation, the inertia emulation is dependent on an external voltage source. In this regard, extra control scheme is needed in order to form a grid, in case of islanded operation condition. However, the active power transfer dynamics are still different with synchronous machine even though the dynamic interaction of the converter with the grid has been modified. Considering this drawback, power loop controller has been presented as another option to emulate the virtual inertia. There are three different methods that can be implemented in the power loop controller as for instance, cascaded voltage-current control [37, 38], open loop modulation [39-45] or virtual impedance/virtual admittance configuration [46-56].

1.2. Summary of the Remarkable Works

With a high variability of renewable energy sources, it is so difficult to maintain the stability of the AC network. There were many control algorithm being presented by the research community to enhance the performance of grid connected power converters. However, it is possible to classify the past contributions into two main groups even though there are slight differences. The first group gathers the contributions achieved in the control strategies of the grid connected power converters for the microgrid application. The second group oriented to reproduce the same dynamical behavior of synchronous generator in the control layer of grid connected power converters.

Microgrids are proposed into electric power systems in order to manage the extensive penetration of Renewable Energy (RE) and DG in power distribution networks [57, 58]. A microgrid systems consisting of generation units, loads and storage units [59-61]. Microgrid system has attained a significant consideration due to its desired characteristics such as improved reliability [62-64], efficiency [65, 66], stability and expandability [67, 68]. Application of microgrid can be divided into two clusters which are AC Microgrid and DC Microgrid. AC microgrid is connected to the utility grid at the Point of Common Coupling (PCC) is the most studies microgrid structure [69], [30]. However, in recent years, DC microgrids have attracted additional attentions because majority of the emerging RES, storage components and loads are inherently DC [70, 71], [58], [61], [66].

The hierarchical control structure of microgrids can be divided into three control levels which are primary control level, secondary control level and tertiary control level [58], [72, 73]. The primary control level focuses on the stability of the frequency and voltage. Normally the droop control is applied in this level in order to achieve the active and reactive power sharing without using the communication channels. In the secondary control level, the elimination of the frequency and voltage deviations that caused by the droop control will be performed. The tertiary control on the other hands deals with economic dispatch, operating schedule and power flow between the microgrid and the utility grid. The Energy Storage Systems (ESS) as well as the Energy Management Systems (EMS) are also required in order to ensure a smooth transition between islanded and grid connected modes [73-75]. Since the accuracy and the dynamic stability of active power sharing is very important, therefore, an early study of static droop compensator has been presented in [76] in order to perform an active power sharing. In [77], enhanced droop control with a transient droop performance has been proposed. An optimized droop control has been presented in [78] in order to improve the dynamic stability of the active power sharing. Earlier study by the same author has been carried out in [79] with the objective to adjust the dynamic performance of the power sharing without affecting the static droop gain. In order to achieve the objective, an adaptive decentralized droop-based power sharing control has been implemented.

According to [73], the active power can be regulated well by using the improved droop control schemes when the DG units operate at the same frequency in the steady state conditions. However, the reactive power sharing is still poor. A various control strategies have been proposed with the objective to share the reactive power. The strategies include the improved primary droop control methods [80-84], the improved virtual impedance methods [85-90] and the improved hierarchical control strategies [91-94].

The new grid codes demanded that the distributed generation should perform as similar performance as a conventional generation which particularly based on synchronous generator in term of transient response, grid regulation and efficiency of the system. To deal with such condition, a Virtual Synchronous Generator (VSG) has been introduced as a new control strategy that signifies the VSC operated in a similar way to synchronous generator [95-98]. In this regard, the swing equation of synchronous generator has been modelled in the control layer of VSC. In the case of VSG, the regulation of frequency and voltage of the network still count on the external droop controller. However the added value in this control system is the introduction of the virtual inertia concept [44], [99, 100].

The VSYNC project is one of the examples of initial works related to VSG concept [101, 102]. This project runs under 6th European Research Framework Program. The power converters controlled as VSGs present a similar frequency dynamic response as synchronous generator hence the system is not capable to store the energy. As a result, it also requires a supplementary energy storage unit. The work done in [50] and [55] introduces a Virtual Synchronous Machine (VISMA). As similar to the VSG, the idea of VISMA is to reproduce the static and dynamic properties of synchronous machine into the grid connected power converter. However, the tuning accuracy may deviate due to the high number of controller

parameters and potential interaction between the loops. The cascaded structure may contribute in a slow dynamic response thus simplification of the control structure is reasonable. A Static Synchronous Generator (SSG) has been presented in [39] and [103]. In this work, the power regulation is also based on the classical method of frequency and voltage drooping mechanism. The SSG performs as a voltage control that may contributes to the derivative term problems and also has a low damping that makes it necessary to use filters.

Mimicking the dynamic behavior of the synchronous generator into the control layer of the grid connected power converter in general will not solve any problems on the one that conventional generator has. Direct emulation of the synchronous machine does not improve the electrical side of the grid connected power converter since the generator equations are still literally used in some works thus issues on the low damping still arise. The problem of a low damping of electrical transients and resonance will contribute to a very slow dynamic when there are changes in the electromotive force or in the distribution network, hence it is necessary to improve this situation.

In [104-106], the Power Synchronization Control (PSC) for the VSC or more specifically for the HVDC application are presented. By using the PSC, the VSC avoids the instability caused by the PLL in a weak AC system connection. The author adopts power synchronization to directly control the active and reactive power by means of controlling the phase angle and voltage magnitude. In order to ensure a safe stability margin during the weak grid, the VSC shall run with a control system with a low bandwidth and the needs of protection and filters against perturbations are highly recommended.

The control strategies based on Synchronous Power Controller (SPC) has been presented in [52]. The SPC based power converter controls the power converter as improved synchronous generator. The implementation of SPC is based on controlling the current at the output of power converter that emulated the generator. The electrical controller is based on the virtual admittance concept as presented in [53] and it plays an important role in load sharing and presents a natural voltage magnitude droop feature for grid voltage support [107]. The electromechanical damping and inertia can be controlled, as a result it can attenuate the power oscillation, hence counteract the drawbacks of conventional generators. Contrary to the conventional synchronous generator, the SPC does not need any software protection against perturbation and short circuit as it works inherently to reduce them. The electromechanical damping and inertia can be controlled as a result it can attenuate the power oscillation hence counteract the drawbacks of conventional generators.

It should be noted that all the previous contributions have been focusing on the classic current control for inner regulations of the grid connected power converter. However, to the best of author knowledge, there is no research to date considering to deliberate the theoretical of flux into the inner regulation. Thus, the research in this particular area should be committed since it is already long overdue. The goal of this thesis is to investigate various kinds of control strategies and propose a new control strategy for the grid connected power converter based on virtual flux approach that could provide an advanced synchronous performance to make them comply with the grid code requirements further performs an inherent synchronous connection

with the grid. Other than that, this dissertation will also present the control strategy based on VF estimation for power converter connected to the grid through the LCL filter.

1.3. Objectives of This PhD Dissertation

The research work in this PhD dissertation is directed towards the general goal of proposing control strategies for the grid connected power converter based on virtual flux approach. Several objectives were specified to guide the PhD project, which are summarized in the following:

- To attain a detailed design, analysis and experimental validation of the VF estimation for the grid connected voltage source converter with LCL filter.

- To attain a detailed design, analysis and experimental validation of the control strategy to control the active and reactive power in remote point.

- To attain a detailed design, analysis and validation of the Virtual Synchronous Flux Controller with the Magnetic Controller (MC) used in the inner loop control and power loop controller used in the outer loop control.

These objectives contribute to develop the particular details of the control strategies based on VF approach in terms of implementation with a consideration of specific needs in different scenarios.

1.4. Scope of Work

The focus of this dissertation can be limited to two main parts. Firstly, this dissertation will focus on the area of virtual flux-based synchronization as illustrated in Fig. 1.7.
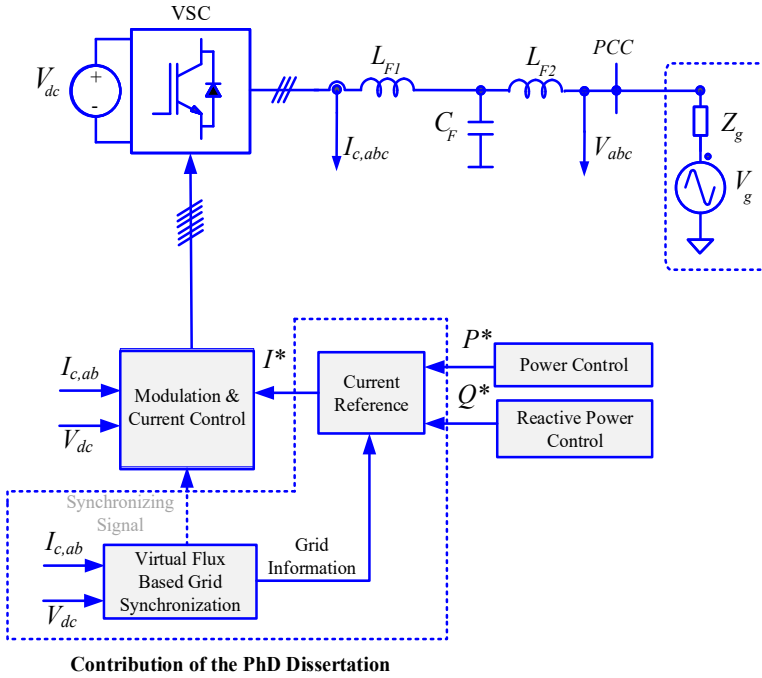
Fig. 1.7. Overview of VSC control system with the implementation of virtual flux-based grid synchronization.

In this regard, the virtual flux based synchronization for the case of LCL filter will be investigated. As the capacitor current cannot be ignored, the estimation of the grid voltage condition will be presented in three different methods. The design features of the control system can be summarized by the following:

- The precision and dynamic response of the grid synchronization method should not be swayed by discrepancies in the grid frequency.

- The control system should be able to provide a very fast synchronization with the generation of reliable output of virtual flux estimation at the grid side. A good estimation is essential to generate the perfect sinusoidal of current reference that is needed by the current controller.

- The control system is worked in stationary reference frame and the current controller used in this work can be based on the conventional linear current controller.

- The applied method is suitable for both balanced and unbalanced condition and the system should be able to control both active and reactive power in specific conditions.

- The virtual flux estimation in the case of the power converter connected to the grid through the LCL Filter can be done in three different methods.

- The proposed method should be able to control the active and reactive power remotely.

Secondly, a new concept for controlling the VSC will be investigated. This concept is known as Virtual Synchronous Flux Controller (VSFC) where it is capable to control the flux at the output of power converter. The VSFC does not require any specific hardware or power converter topology as it can be applied in any commercial power converter just by changing its control layer. The VSFC combines the MC in the inner loop control and the power loop control in the electromechanical part of the systems as shown in Fig. 1.8. The outer loop control is used to generate the flux reference needed by the MC. Considering the VSC is connected to the grid through the LCL Filter, the desired features of this concept can be summarized in the following:

- The applied method of VSFC should be designed suitable for both balanced and unbalanced grid voltage conditions as well as capable in controlling the active and reactive power in a flexible manner.

- The VSFC should be able to naturally synchronize with the electrical grid without external grid synchronization.

- The magnetic controller should be able to emulate the electrical behavior and responding well in case of any perturbations occurred such as transient grid voltage sags.

- The VSFC based power converter should be able to control the active and reactive power effectively.

- The proposed method is tested under normal operating condition considering the power converter is connected to a strong grid.

- The control strategy will be based on stationary reference frame where the current and voltage measurement should be transformed from *abc* sequence to *αβ* sequence.

Due to the time constraint, only the validation of the proposed system on balanced conditions were completed. The test work for under unbalanced condition was not achieved. Thus, it is the limitations for this dissertation topic.
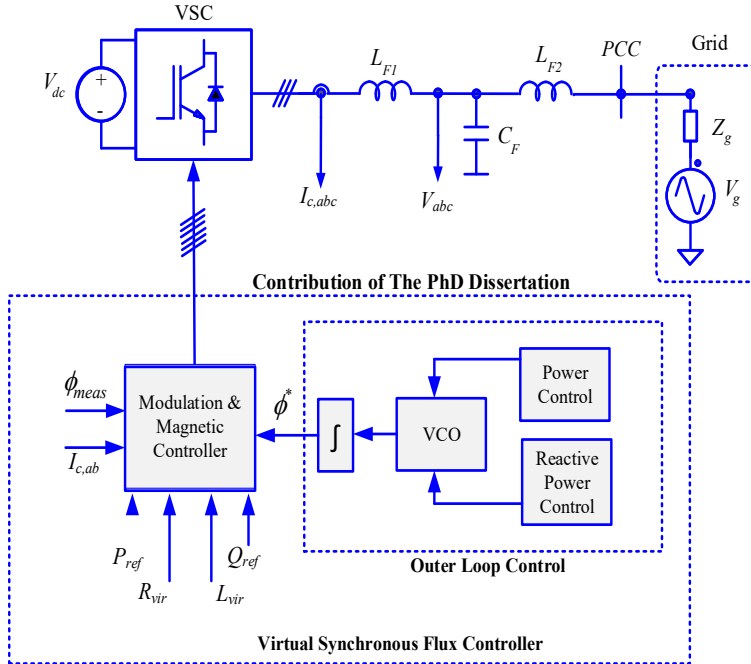
Fig. 1.8. Overview of the control system of Virtual Synchronous Flux Controller.

1.5. Identification of Research Question

From the previous sections, it can be seen that conventional current controllers are used to accommodate the inner loop control of VSC, and it has been comprehensively studied in the literature. The design, operation and performance of inner loop control for some extent can be reviewed and further investigated hence provide an alternative control to the conventional ones. The main research question constitutes behind the results and analysis that will be presented in this dissertation can be described as:

How to develop and analyze a control system of a grid connected power converter that utilized a virtual flux approach that should be able to fulfill the grid code requirements?

1.6. Research Contributions

Previous contributions that have been used as an important reference as well as the important background of this research studies constitutes the research gap in Table 1.1. The theoretical, development and the analysis from both simulation and experimental work of the proposed control strategies that will be discussed in the following chapters will benefit the researcher in education industry as well as in the renewable energy application industry. In education industry, the findings of this study will provide a reference to the researchers particularly in the area of virtual flux control. As for the distributed generation industries, the virtual flux approaches presented in this dissertation is significant and will definitely provide an alternative solution to the conventional control strategies.

Table 1.1. Research Gap and Contributions

Research Gap	Research Contribution
A. Previous research on virtual flux approach considering the power converter is connected to the grid through the LCL Filter is very limited.	Proposed new control strategies that embraced the concept of virtual flux-based synchronization with the LCL Filter that utilized the Second Order Generalized Integrator configured as Quadrature Signal Generator with a sequence separation.
B. There are no detail studies on controlling the active and reactive power remotely by using the virtual flux estimation approach.	The proposed control strategy permits to control the power injection not at the local connection point of the converter, but at the connection point of the line taking an advantage of virtual flux estimation approach.
C. The existing flux oriented controller are just used for the control and regulation of machines but not for the control of grid connected converter. No attempt was done to explore the potential of using the flux controller in the inner regulation of grid connected power converters.	Proposed a new control strategy that is based on controlling the flux in the inner loop control of grid connected power converter by means of implementing the Virtual Synchronous Flux Controller.

A brief description of the research contributions listed in Table 1.1 can be summarized as follows;

A.   VF estimation with LCL Filter

The development and analysis of the simulation and experimental studies of the VF will be done in the stationary reference frame. For VF-based synchronization to the grid side of an LCL filter, it is necessary to consider the influence of the currents in the filter capacitors. Therefore, three options for VF-based synchronization to the PCC are presented for converters with LCL filters, and Positive Negative Sequence (PNS) separation is considered as part of the VF estimation. This topic will serve as the first contributions of the PhD Dissertation. Only a few studies have previously considered VF-based voltage sensorless grid synchronization with LCL filters [108-111]. The DSOGI-VF estimation described in [112] is an extended version of the work presented in [113], [16, 17]. In this work, the PR current controller is used as an inner control of the VSC. However, as discussed in [22] and [111], VF estimation can also be useful if capacitor voltage measurements are available. As a result, estimation of the grid-side current is also included in the VF-based synchronization strategy, in order to obtain an accurate voltage or flux across the grid-side inductor. This kind of estimation strategy has not been studied in detail in the existing literature. Therefore, the transient and steady state response of the system will be investigated in detail.

B.   Remote Power Control Injection based on VF

The second contribution is the development of the remote power control strategies. The analysis, simulation and experimental validation of the proposed systems extend thus the work done in [108], [110-112] and [17]. The VF estimation enables to calculate the power at any point in the network and built controllers to regulate the active and reactive power delivery. Therefore, the VF estimation can regulate the active and reactive power not only at the output of the converter, but it is also possible to regulate the active and reactive power at the connection transformer that interfaces a plant with the main grid. Normally the connection point with the electrical company is far away from the converter. In this point, it is necessary to guarantee the cos phi required by the electrical company in many cases, hence the control proposed in this dissertation permits to regulate the active and reactive power delivery in a remote point. The fact of controlling the power in a remote point is relevant as the standards are asking to regulate the power at the connection point, which is not necessarily the output of the grid-side converter. In this case, the control system will be designed in a stationary reference frame, and thus a PR current controller will be adopted in the inner control loop. This is due to the fact that the VF is implemented in such a way that the voltage in a remote point of the line can be estimated. In addition to the power control itself, this study could also benefit the frequency and the voltage regulation methods in distributed generation applications as for instance in microgrid system.

C. VSFC with a new control strategy in the inner and outer loop

The third contribution of this PhD dissertation is the development, analysis and experimental verification of VSFC. This will also include the general expression used in the magnetic controller as well as the outer loop controller. The VSFC provides control solution based on controlling the virtual output flux of the converter. Control of flux is derived from the main idea that the power converter can be controlled as a virtual synchronous generator where flux is used as a variable for controlling the operation. A power converter that equipped with the VSFC is able to conduct an inherent synchronous connection with the grid without additional synchronization system. Magnetic controller is responsible to regulate the virtual flux at the output of the power converter and the power loop controllers on the other hands generate the flux reference to be tracked. It is worth to mention that this is the first control solution that adopts such structure in the control of grid connected power converters.

1.7. Outline of the PhD Dissertation

This dissertation can be divided into six chapters. Chapter 1 is exclusively presented to introduce the basic control of power electronics-based converters. Issues and problems in the control strategies of grid connected power converters have been highlighted and served as a basis for identifying the research objectives, research question as well as the main focus of the dissertation. In this chapter, new contributions to an area of knowledge have been emphasized to demonstrate the originality of the work.

Chapter 2 focuses on the review method of the control strategies of grid connected power converters particularly involving the virtual flux approach. It also includes the review on the general structure of the control strategies in both solar photovoltaic and wind energy system as well as highlighting the research gap that could lead to the present studies. In this chapter, the grid synchronization method based on voltage measurement as well as voltage sensorless will be reviewed in detail. In this regard, a review on the implementation of virtual flux estimation will be presented as a basis for the following chapters.

In Chapter 3, three options for VF-based synchronization to the PCC is studied for power converters with LCL filters, and PNS separation is considered as part of the VF estimation. Estimation of the grid-side current is also included in the VF-based synchronization strategy, in order to obtain an accurate voltage or flux across the grid-side inductor. This chapter also present a brief introduction of the current controller used in the control strategies and also demonstrate on how the output of the virtual flux estimation is used to generate the reference current. The proposed methods are validated through simulation and experimental work and the performance of the proposed methods are discussed accordingly.

Chapter 4 goes further in the analysis of a control method based on the VF approach, which is able to control the power injection not only at the second inductor of the filter, but also in a remote point of the line where it is connected. This is because the VF is implemented in such a way that the voltage in a remote point of the line can be estimated. The simulation and experimental results will show a broad variety of testing scenarios, where the line impedance is changed and the power tracking at remote points offers a good performance.

Chapter 5 presents the control strategy of VSFC including the parameters used in the experimental validation. In this chapter, the mathematical equations as well as the overview of the proposed system including the MC in the inner loop as well as the outer loop control will be explicitly explained. The performance of proposed system is analyzed and verified based on the scope of work listed in Chapter 1.4. The concluding remarks as well as the recommendations for possible topic for further research are summarized in Chapter 6 respectively.

1.8. List of Publications

This section lists the main contributions of the PhD work, classified as journal or conference papers, and contributions on related topics that might diverge slightly from the main focus of the thesis. The publications focus on the improved control scheme in order to enhance the controllability of grid connected VSC. The selected journal papers present the main results toward completing this dissertation. The topics range from the development of the virtual flux estimation for the case of VSC connected to the grid through the LCL filters to the enhanced control strategy based on virtual flux. The theory and the results presented in these papers are discussed in detail in the following chapters.

1. **N. F. Roslan**, A. Luna, J. Rocabert, J. I. Candela, and P. Rodriguez, "Remote Power Control Injection of Grid Connected Power Converters Based on Virtual Flux," in *Energies,* vol. 11(3), pp. 488, 2018.

2. M. Shahparasti, P. Catalán, **N. F. Roslan**, J. Rocabert, R. S. Muñoz, and A. Luna, "Enhanced Control for Improving the Operation of Grid Connected Power Converters Under Faulty and Saturated Conditions," in *Energies,* vol. 11(3), pp. 525, 2018.

3. **N. F. Roslan**, J. A. Suul, J. Rocabert, and P. Rodriguez, "A Comparative Study of Methods for Estimating Virtual Flux at the Point of Common Coupling in Grid-Connected Voltage Source Converters with LCL Filter," *in IEEE Transactions on Industry Applications,* vol. 53(6), pp. 5795 - 5809, 2017.

4. **N. F. Roslan**, A. Luna, J. Rocabert, J. I. Candela, and P. Rodriguez, "Remote Power Control Strategy based on Virtual Flux Approach for the Grid Tied Power

Converters", in *Proc. 2018 IEEE Energy Conversion Congress and Exposition (ECCE 2018)*, Portland, OR, USA, 2018, pp. 7114–7120.

(This paper has been awarded as 1st Prize paper by IEEE IAS Renewable and Sustainable Energy Conversion Systems Committee)

5. **N. F. Roslan**, J. A. Suul, A. Luna, J. Rocabert, I. Candela, and P. Rodriguez, "A Comparative Study of Methods for Estimating Virtual Flux at the Point of Common Coupling in Grid Connected Voltage Source Converters with LCL Filter", in *Proc. 2016 IEEE Energy Conversion Congress and Exposition (ECCE 2016)*, Milwaukee, WI, USA, 2016, pp. 0–5.

6. **N. F. Roslan**, J. A. Suul, A. Luna, I. Candela, and P. Rodriguez, "A Simulation Study of Proportional Resonant Controller Based on the Implementation of Frequency- Adaptive Virtual Flux Estimation with the LCL Filter", in *Proc. 41st Annual Conference of IEEE Industrial Electronics Society (IECON 2015)*, Yokohama, Japan, 2015, pp 1934–1941.

State of the Art
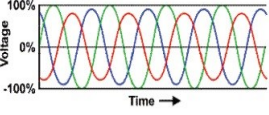
*T*his chapter introduces the most relevant topics in developing this dissertation. The state of the art starts with the explanation on the power quality issues in modern power systems. As the Renewable-based generation system progressively evolved, grid codes requirement becomes one of the most important documents in electrical power system. Therefore, a brief explanation on grid codes requirement is included in the sub-section of this chapter. The state of the art continues with a description of the control of DG system that includes the control structure of typical PV inverter and wind turbine system. In the following sections, a summary of the virtual flux control implementation is disclosed. This information is relevant for the development of the proposed control principles that will be explained in Chapter 3, 4 and 5.

2.1. Power Quality in Distribution Systems
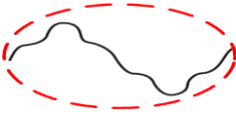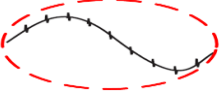
In distribution systems, the power quality is defined as a set of boundaries that allows a piece of equipment to function in its intended manner without significant loss of performance. The electrical boundaries include the voltage, current and frequency. In this regard, the power quality problems are defined as any problems manifested in deviation of these three elements that results in failure or missed operation of end user equipment or appliances. At the generation level, the power quality is assessed by the capability of the generator to generate power at the designed frequency of 50 Hz or 60 Hz depending on the country requirements. The power quality at the transmission and the distribution level is assessed by the capability of the distribution systems to provide and maintain the voltage within ± 5% of the nominal voltage. With the increasing complexity of electrical power systems and its interconnected elements, power disturbance occur in all electrical systems.

The common power quality problems including their causes and effects are described in Table 2.1 [114, 115].

Table 2.1. Common power quality problems.

Power Quality Problems	Causes	Effects
Voltage sags	➤ Faults occured in the transmission or distribution network ➤ Starting of a large motors or heavy loads	➤ Reduced energy delivered to the end user ➤ Loss of efficiency in electric rotating machine
Voltage unbalanced	➤ Incorrect distribution of loads in three phase systems ➤ Large single phase loads (traction loads, induction furnaces)	➤ Motors & transformers can be overheated thus shortened the life of the equipments
Voltage fluctuation	➤ Frequent start/stop of electrical motors ➤ Equipments that have rapid changes in load current	➤ Most of the concequences are similar to under voltages ➤ Flickering on lighting and screen
Voltage swells	➤ Transfer of loads to one power source to another ➤ Start/stop a large load ➤ Poorly regulated transformer	➤ Damage of sensitive equipments due to increases of energy in voltage swells
Interruptions	➤ Disturbances occurred in the systems (Generation, transmission, distribution or end user)	➤ Shutting down of equipments ➤ Loss of production in industrial factory,

		causing the protection devices to activate.	retail market and office
Transients		➤ Lightning strikes ➤ Power lines switching at the utility's power systems ➤ Switching of inductive or capacitive loads	➤ Damage to electronics components ➤ Total failure or misoperation of computers or micro-processor-based equipments.
Harmonics distortion		➤ Increase use of non-linear loads (adjustable speed drive, three phase rectifier, flourocent lighting)	➤ Loss of efficiency on electrical machines ➤ Problems in relay tripping ➤ Conductor overheating or overheating of transformer, power cables and motors
Noise		➤ Improper grounding ➤ Electromagnetic interferences	➤ Degrade telecommunication equipment, radio and television reception ➤ Data losses and data processing errors ➤ Disturbances on sensitive electronics equipments

Obviously, the voltage sag is the most common problems in electrical power systems. The voltage sag is a reduction in voltage magnitude that occurred for a short time. It normally happens when the rms voltage decreases in magnitude between 10% to 90% from its nominal for half cycle to one minute [116]. There are seven types of voltage sags as tabulated in Table 2.2. In three phase systems, the voltage magnitude should remain stable in term of its magnitude with a phase displacement of 120° with each phases. The voltage can be classified as unbalance if the phase voltages have an inequality values. Most equipments especially motors can only tolerate up to 2% of unbalanced voltage. The voltage fluctuations on the other hand is the rapid changes in voltage. It is also known as a flicker.

The voltage fluctuation described by the International Electrotechnical Commission (IEC) as a random voltage variation that up to ±10% of the nominal voltage.

Contrary to the voltage sags, the voltage swell is the momentary of over-voltages. In this event, the magnitude of the rms voltage increases above the nominal voltage. The duration of the event is normally less than 1 minute and the frequency of occurrence is less frequent compared to the voltage sags event. In electrical power systems, interruption is something that need to be avoided. Interruption is the complete loss of voltage and it can be categorized in three different types depending on the durations of the event. Normally, the momentary interruption occurred between half cycle or 8msecs to 3secs. However, if the voltage drops below 10% of the nominal voltage between 3 secs and 1 minute, it can be categorized as a temporary interruption or short duration interruption. If the event last longer than 1 minute, it could be categorized as a long duration interruption.

Transients on the other hand are the sudden increase or decrease of current or voltage. It is also called as surges or spikes. There are two types of transients which are impulsive and oscillatory transients. Compared to the other power quality problems, the transients normally decay quickly. The other common problems in the power system is harmonics. Harmonics are the integral multiples of fundamental frequency of the sine wave. The current harmonics will distort the voltage waveform and later will create distortion in the power systems that can cause many problems. In electrical system, noise is unwanted electrical interference signal. It can cause serious problems if the electromagnetic interference produced by wireless communication equipment that can affect medical equipments especially the one used to monitor patient's life.

Table 2.2. Voltage sag types.

Voltage Sag Types	Fault Types
Type A	Three Phase
Type B	Single-phase to ground
Type C	Phase to phase
Type D	Phase to phase fault (experienced by delta connected load) ; Single-phase to ground (zero sequence component removed)
Type E	Two-phase to phase fault (experienced by wye connected load)
Type F	Two-phase to phase fault (experienced by a delta connected load)
Type G	Two-phase to phase fault (experienced a load connected through a non-grounded transformer removing the zero sequence component)

The fact that the power quality has become an issue in the distribution generation systems, the power quality standard is very important in order to ensure safe operation at generation, transmission and distribution level. The most popular international organizations that responsible to develop the power quality standards are Institute of Electrical and Electronics Engineer (IEEE) and IEC. The example of the power quality standards developed by these two organizations are tabulated in Table 2.3 [117-119]. The utility companies conduct the power quality assessments by means of evaluating the power quality and reliability of the electrical power systems by using some indexes such as SAIFI, CAIDI and SAIDI [120].

Table 2.3. Power Quality Standards

Phenomena	Standards
Power Quality Characterizations	IEEE 1159:1995, IEC 61000-2-5: 1995, IEC 61000-2-1: 1990
Voltage sag/swell and interruption	IEEE 1159: 1995, IEC 61009-2-1: 1990
Harmonics	IEEE 519:1992, IEC 61000-2-1: 1990, IEC 61000-4-7: 1991
Transients	IEEE 1159:1995, IEEE C62.41: (1991), IEC 61000-2-1: 1990, IEC 816: 1984
Voltage flicker	IEC 61000-4-15: 1997

2.2.   Grid Codes Requirements

The rules and regulations used to organize various electricity supply activities of the electrical producer, operator, distributor and the consumer is known as grid and distribution codes. Sometimes, the grid code is also known as an interconnected guideline. The main concern of the grid code is normally associated with the variations of transmission system voltage and frequency, faults events, active and reactive power control capabilities, safety and security of the entire power systems. In each country, the transmission system operator is responsible to ensure a safe operation and stability of the transmission system by controlling and monitoring the different levels of electrical network. It is worth to mention that the rules and regulation that includes a specific requirements regarding the transient and steady state operation of the generation unit of each country is not the same. However, there are three important elements that need to be taken into account while considering to connect any kind of power generation plants to the electrical grid as stated in Section 2.2.1, 2.2.2 and 2.2.3.

In Europe, there are two regional grid codes which are the Nordic Grid Code and the ENTSO-E Network Code [121]. The Nordic Code has been used in Denmark, Norway, Finland and Sweden. However, the ENTSO-E have been signed into European Law which means all the European grid code including the Nordic Grid Code should comply with the

requirements stated in the ENTSO-E Network Code. The followings are the other examples of grid code providers or regulators [122];

- Ministerio de Industria y Energia (Spain)
- National Grid Electricity Transmission plc (Great Britain)
- VDN (Germany)
- RTE (France)
- TERNA S.p.A. (Italy)
- SwissGrid (Switzerland)
- Energie-Control Kommission (Austria)
- Belgian Ministry of Economy (Belgium)
- Autoriteit, Consument & Markt (Netherlands)

2.2.1 Operational window for a generation unit

The amplitude of the grid voltage and frequency will keep changing and do not remain constant over time but these variations should be around their rated values. The operational window is very important especially during the unbalanced situation. In this regard, the generation units that are connected to the electrical network should be able to operate within the operational margin specified by the grid codes. The operational window may vary in different countries depending on the requirement sets by the TSO. Normally the frequency window sets by the TSO is around the range of 2-3Hz and the voltage amplitude may vary in the range of 5-10% around its rated value.

Table 2.4. Frequency Variation in European Country as stated in [122].

Country	Steady State Range, Hz	Transient Range, Hz
Austria	49 – 50.5	47.5 – 51.5
Belgium	48.5 – 51	47.5 – 52.5
Bulgaria	48.75 – 51.25	Nil
Czech Republic	48.5 – 50.5	47.5 – 51.5
France	49.5 – 50.5	47 - 55
Great Britain	49 – 51	47.5 – 51.5
Germany	49 – 50.5	47.5 – 51
Greece	49.5 – 50.5	47 – 53
Italy	49 – 51	47.5 – 52
Lithuania	Nil	Nil
Netherlands	49.85 – 50.15	48 – 51
Poland	49 – 51	47.5 – 52.5
Romania	49.5 – 50.5	49 – 52
Scandinavia	49 – 50.3	47.5 – 52
Spain	48 – 51.5	47 – 51.5

2.2.2   The capacity for controlling the grid voltage and frequency

The amplitude of the grid voltage as well as the frequency are associated with the reactive power and active power controls. Therefore, any deviations in voltage amplitude and the frequency will surely affect the regulation of both reactive and active power. A good control of the grid voltage amplitude and the frequency definitely will enhance the whole performance of the grid in both steady state and transient conditions.

In the steady state conditions, the grid code stated that the reactive power should be injected to the grid by the distributed generators in case of any deviations in voltage amplitude. The injection of the reactive power should be made at the point of connection. It is also important for the generation unit to have the capability to track the reactive power set points specified by the TSO.

Likewise, the TSO also specified the amount of active power that needs to be injected by the distributed generators in order to respond to the frequency variations. In this regard, the distributed generators should automatically reduce the active power delivered to the grid when the grid frequency increases and vice versa. It is also possible to increase the active power delivered to the grid when the frequency decreases below its rated value, if the generation units are accommodated with the energy storage, power curtailment or primary source control. As similar to the regulation of the grid voltage amplitude, the TSO also demand that the generation units should have the capability to track the active power set points.

2.2.3   The setting of transient response

The grid code also sets a strict requirement to the distributed generation units during the transient conditions especially when the faults occurred in the systems. Therefore, the control of the grid connected power converters should have a good response not only during the steady state conditions, but also during the transient conditions. The grid code demands the distributed generators to stay connected to the grid in case of voltage sags occurred in the systems. As stated in Table 2.1, the voltage sags occurred when fault happens in the system. The fault ride-through capability required by different countries may differ from one to another. The grid codes asking the grid connected power converter to have the ability to instantaneously inject the reactive current in order to obtain a fast grid voltage recovery during the voltage sags event that caused by the transient faults [123]. The magnitude of the reactive current needed depends on the depth of the sag event. However, if the overvoltage occurs in the system, the control of grid connected converter should be able to withdraw the reactive current.

2.3.   Basic Control Structures of Solar PV and Wind Power Systems

The swift growth of PV cell technologies and the incessant cost reduction of PV modules as well as the advancement of power electronics have been the main motivation for the intensive employment of PV distributed power generation systems [8, 9], [124-126]. In order to certify the dependable, efficient and less harmful transfer of solar PV energy to the distributed grid, the PV distributed power generation system is essential to comply with a strict requirements than ever before [127]. Fig. 2.1 shows the general structures of the grid connected power converter for PV systems. The basic functions for all grid connected inverters are the grid current control, DC voltage control and grid synchronization. These three basic controllers should be capable to ride-through the grid disturbances.
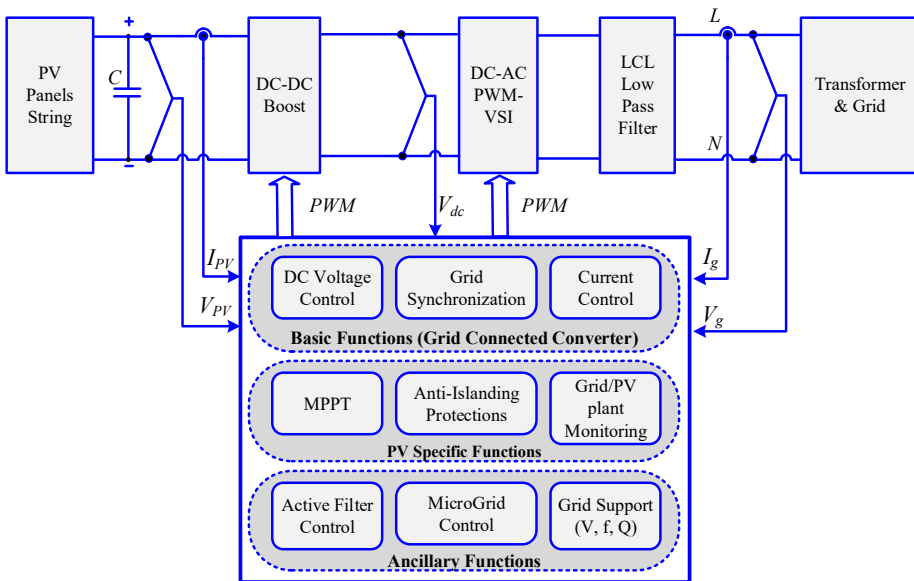
Fig. 2.1. Generic control structure for a PV inverter with boost stage [9].

A good grid current control will ensure that the system will remain stable in case of large grid impedance variations occur. It is also important to make sure that the system achieve a low Total Harmonics Distortion (THD) as required by the standards. The function of having the DC voltage control in the control layer of the inverter is to adapt with the discrepancies of grid voltage and the control is able to respond accordingly. As mentioned in Chapter 1.2, the main issue of connecting the power converter with the grid is the grid synchronization. The standards asking that the grid synchronization operates at the unity power factor. The grid synchronization is critical because the information generated by the grid

synchronization will be used at different level of control systems in the grid connected converter.

Even though there are a variability and system configurations of the inverter topologies that increase the control difficulty, but the PV system should performs the specific functions that include the Maximum Power Point Tracking (MPPT), Anti-islanding protection as required by standards (VDE 0126, IEEE 1574) and grid/PV plant monitoring [9]. The MPPT is significant in PV system because it will maximize the power output of PV array for a given set of conditions. The maximum power point is totally depends on the irradiance and the solar panels temperature [128]. The MPPT controls should have a stable operation during low irradiance levels and fast dynamic response is required when irradiance is rapidly changes. During the steady state, the MPPT algorithms is expected to have a very high efficiency.

In economic point of view, a very high efficiency of MPPT can reduced the number of PV array and batteries used thus leads to a lower implementation cost [129]. The most common MPPT techniques include perturb & observed [128], [130-132], incremental conductance [133-135], ripple correlation [136-138] and short circuit current techniques [139]. The grid monitoring on the other hands is the algorithm used to detect the grid state in a fast and accurate way in order to meet the requirements demanded by the grid codes in term of precision and time response. Monitoring the grid variables at the PCC is essential in order to trip the disconnection procedure when the variables go beyond the limit boundaries set by the grid codes, hence the grid monitoring is closely linked with the grid synchronization. Typically, the ancillary functions include an active filter control, microgrid control and the grid support. The grid support provides a local voltage control, reactive power compensation, harmonic compensation and also fault ride-through capability.

In wind power systems, the elementary of power conversion is made of two parts which are the mechanical and an electrical. The mechanical part extracts the energy from the wind and makes the kinetic energy of the wind available to a rotating shaft. The function of electrical part is to transform the energy to electrical, making it suitable to electrical grid. This two subsystems are connected through the electrical generator (which is an electromechanical system) and later converts the mechanical energy into electrical energy [9], [140, 141]. Based on the description stated above and also the figure shown in Fig. 2.2, it shows that the wind turbine control has 3 different stages which are the mechanical, electromechanical and electrical.

The first stage will control the pitch of the blades, the yaw of the turbine shaft and the speed of the motor shaft. The second stage can have a variable structure (pole pairs, rotor resistors, etc), an external excitation and/or a power converter that adapts the speed or the torque of the motor shaft and the waveforms of the generator voltages/currents. The third stage adapts the waveforms of the grid currents and the power converters may be presented in the second and/or third stage [9].
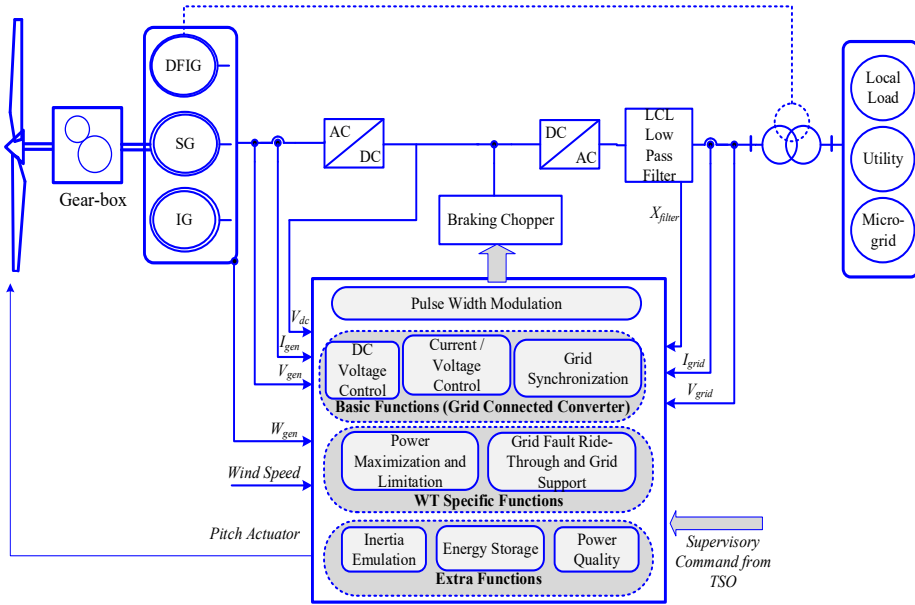
Fig. 2.2. Typical wind turbine control structure [9].

The mechanical and an electrical part are categorized by diverse control goals, but it related with the main aim which is to control the power injected into the grid. The electrical control is responsible of the interconnection with the grid, active/reactive power control and overload protection. The mechanical control on the other hands is important for the power limitation, maximum energy capture, speed limitation and reduction of the acoustical noise. These two control loops can be treated autonomously since it has a different bandwidth. The wind turbine shown in Fig. 3.2 will vary proportionally with the wind speed and keep the pitch angle fixed when the power production is maximum. When the turbine reaches the nominal power, the pitch angle controller will directly limit the power.

The function of the generator-side converter is to extract the maximum power from the wind and to limit power braking the wind turbine. The types of the generator can be based on Doubly Fed Induction Generator (DFIG) [142-146], Synchronous Generator (SG) [147-150] and Squirrel Cage Induction Generator (SCIG) [151-155]. The grid-side converter is to ensure that the DC link voltage is fixed. As it can be seen from Fig. 3.2, an internal current and voltage loops in both converters are used in the control. As for the stability purposes, the state variables of the LCL filter is also considered.

The specific function of the wind turbine is important to prepare the systems especially during the grid faults condition. Therefore, the grid fault ride-through and the support to the grid voltage restoration after the fault is essential in the wind turbine systems. The extra functions of the wind turbine system include the inertia emulation, energy storage and power quality. The main objective of the inertia emulation is to emulate the relation between active

power and frequency by providing a large inertia to the system. The aim of energy storage is to smooth the power output and it can be achieved by storing the energy in the inertia of the generator, in the dc-link or using an additional storage. The power quality refers the probability to use the grid converter of the wind turbine to provide benefits in term of grid power quality.

2.4.   Grid Synchronization Methods

The method of synchronization can be established based on the frequency domain and time domain detection method. The frequency domain is a discrete implementation while the time domain is an adaptive loop that allows an internal oscillator to track the component of interest. In closed loop system, the conventional method that is still gain its popularity up until now is PLL and FLL.

For the three-phase converter, the grid synchronization can be implemented in natural *abc* reference frame, synchronous reference frame (rotating *dq* coordinates) and stationary reference frame (*αβ* coordinates). The basic PLL structure in Synchronous Reference Frame is called SRF-PLL. The SRF-PLL has satisfactory performance during the balanced condition, but it shows inadequate response under unbalanced condition where the needs of advanced method are required [156, 157]. The extended version of SRF-PLL is the Decoupled Double Synchronous Reference Frame-Phase Locked Loop (DDSRF-PLL) has been presented in [158, 159] with the aim to overcome the drawback introduced by the SRF-PLL. The synchronization based on DDSRF-PLL exploits two synchronous reference frames rotating at fundamental utility frequency with one counterclockwise and the other one is clockwise in order to achieve an accurate detection of positive and negative sequence components of the grid voltage vector when it is affected by unbalanced grid fault.

Other improved and advanced versions of PLL in SRF are Dual Second Order Generalized Integrator based on Phase Locked Loop (DSOGI-PLL) and Three Phase Enhanced PLL (3phEPLL) as presented in [14]. The implementation of DSOGI-PLL is based on the dual second order generalized integrator together with the phase locked loop and the control strategy is done in stationary reference frame. The author used an Instantaneous Symmetrical Component (ISC) and positive sequence calculation block to detect the positive and negative sequence voltage. To make the system frequency adaptive, the SRF-PLL is applied to the positive sequence voltage vector. In order to do that, it is necessary to transform the positive sequence voltage in *αβ* to rotating *dq*. The 3phEPLL on the other hand is an adaptation of three single phase of Enhanced PLL (EPLL) where the phase voltage is independently processed by the EPLL. The positive sequence components for this structure also can be obtained based on the ISC method.

In [12, 13] and [160, 161], Dual and Multiple Second Order Generalized Integrator based FLL (DSOGI-FLL & MSOGI-FLL) structure have been presented. The FLL is responsible to make the synchronization process adaptive to the frequency changes. Nevertheless, the

frequency in the grid does not experience sudden changes therefore a feedforward is used, ω_{ff}, in order to enhance the dynamical performance of the FLL. Of course, this ω_{ff}, is not the final value, as the DSOGI-FLL is self-adaptive and it would match the final frequency whatever it will be. Since the SOGIs are working at the same frequencies, only one FLL is used. Fig. 2.3 shows the diagram of a single block of a Second Order Generalized Integrator configured as a Quadrature Signal Generator (SOGI-QSG) including the structure of the FLL with a normalized gain.

(a)

(b)
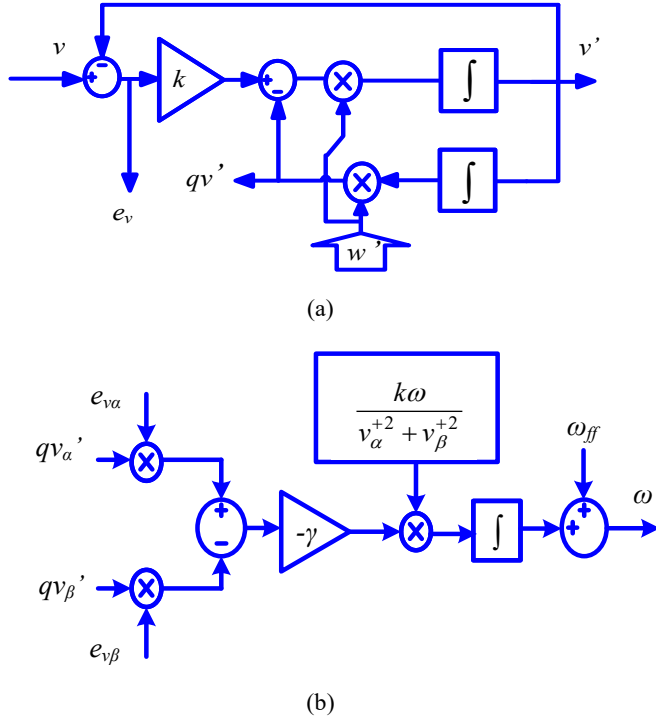
Fig. 2.3. SOGI-FLL diagram. (a) A structure of SOGI-QSG, (b) FLL with gain normalization.

The input of the SOGI is the signal to be integrated, namely v. If the input signal is sinusoidal, both the direct output voltage v' and the in-quadrature signal qv' will always be sinusoidal. The two outputs from the SOGI-QSG will always have the same amplitude if the input signal and the resonance frequency of the SOGI are equal. By referring to the structure of SOGI-QSG shown in Fig. 2.3 (a), the direct output voltage v' will be in phase with the input voltage v, while qv' will lag the direct output voltage v' by 90°. The error between the input and direct output voltage is denoted as 'e_v' and the frequency of the system is symbolized as ω'.

Considering the control implementation is done in stationary reference frame, the input of the FLL is provided by the SOGI-QSG where the error signal and the in-quadrature output

signal both in alpha beta components have been used. The integral controller with a negative gain, $-\gamma$ is used to make the dc component of the frequency error equivalent to zero by shifting the SOGI resonance frequency ω' to match with the value of the input frequency, ω. The transfer functions of the SOGI-QSG for the direct output voltage, v' and the in-quadrature output voltage, qv' with respect to the input voltage, v is given by (2.1) and (2.2) respectively.

$$D(s) = \frac{v'}{v}(s) = \frac{k\omega' s}{s^2 + k\omega' s + \omega'^2} \tag{2.1}$$

$$Q(s) = \frac{qv'}{v}(s) = \frac{k\omega'^2}{s^2 + k\omega' s + \omega'^2} \tag{2.2}$$

The frequency response of the previous transfer functions is shaped by the value of the gain constant, k. Selecting the gain constant, $k = \sqrt{2}$ a good trade-off between overshoot and stabilization time can be obtained. In order to understand how the system adapts to the frequency changes, it is worth to consider the behavior of the FLL by looking at the relationship between the error signal, ε_v and in-quadrature output signal qv'. The transfer functions of the input signal, v to the error signal ε_v is given by (2.3).

$$E(s) = \frac{\varepsilon v}{v}(s) = \frac{s^2 + \omega'^2}{s^2 + k\omega' s + \omega'^2} \tag{2.3}$$

Bode diagram shown in Fig. 2.4 is plotted by considering the both transfer functions of $E(s)$ and $Q(s)$. It can be observed that error signal and the in-quadrature output are in phase when the input frequency is lower than the SOGI resonant frequency ($\omega < \omega'$). Both signal is counter phase when ($\omega > \omega'$). Therefore, frequency error, ε_f can be defined as the product of qv' and ε_v. The average value of the frequency error will be positive when ($\omega < \omega'$), negative when ($\omega > \omega'$) and zero when ($\omega = \omega'$). The integral controller with a negative gain, $-\gamma$ can be used to make zero the dc component of the frequency error by shifting the SOGI resonance frequency ω' until the value is matching with the input frequency, ω. The input frequency in this case will be directly detected by the FLL. By referring to the transfer function stated in (2.1) and the frequency responses shown in Fig. 2.4, it can be clearly seen that the direct output voltage v' has a band pass characteristics with unitary gain and zero phase shift at the fundamental angular frequency, ω_0.
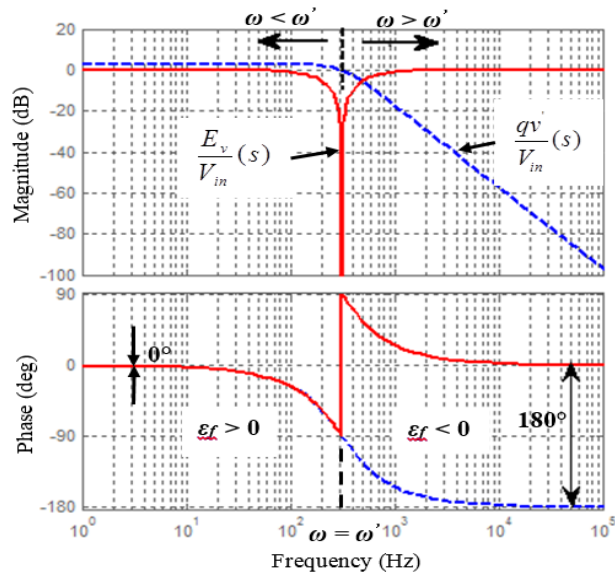
Fig. 2.4. Bode diagram of the input variables of FLL.
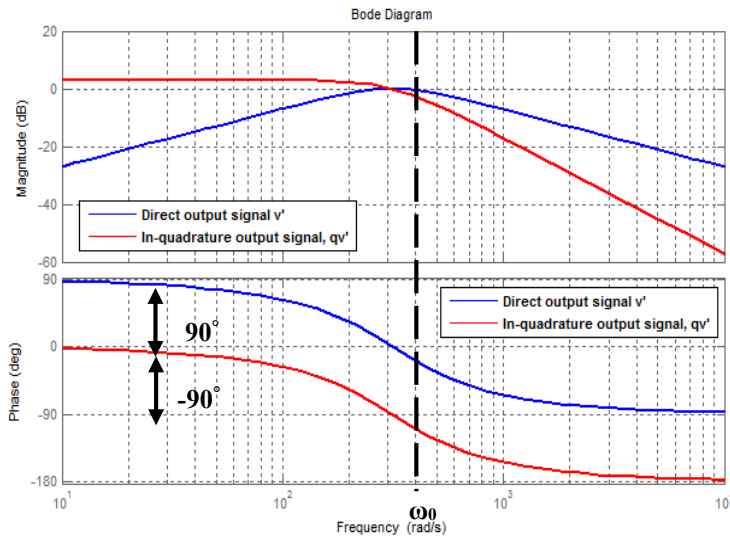
Fig. 2.5. Bode diagram of SOGI-QSG block.

On the other hand, the transfer function stated in (2.2) as well as the frequency response of the in-quadrature signal, *qv'* shown in Fig. 2.5 has a low pass characteristic with unitary gain and −90° phase shift at the fundamental frequency. As shown in [13], the SOGI-QSG settling time on the other hands can be calculated based on (2.4).

$$t_{s(SOGI-QSG)} = \frac{10}{k\omega'} \tag{2.4}$$

2.5. Current Controller

As the main perturbation of the voltage waveform is due to the system transient operation or power fluctuation thus controlling the current is necessary. The classification of the current control method shown in Fig. 2.6 is based on the PWM current control methods. This control method can be divided into two parts which are by employing the ON/OFF controller or with a pulse width modulator.
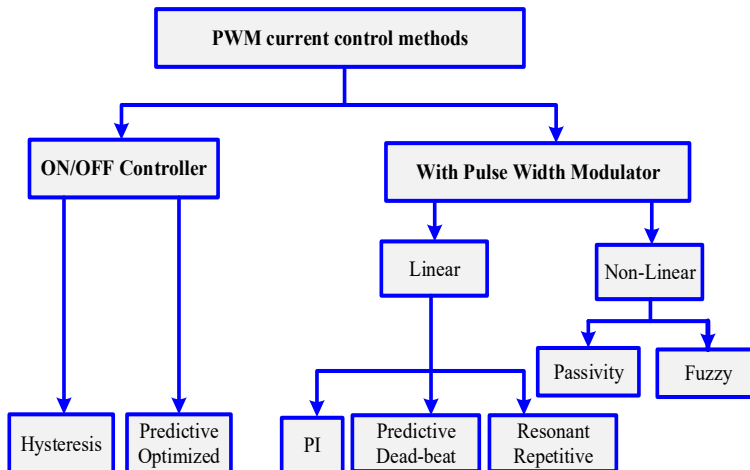
Fig. 2.6. Classification of current control methods.

If the wind power system or PV power system are using the VSC as the front-end, the grid current is usually controlled and becomes important in order to control the quality for active and reactive power exchange [9]. The current controller with a pulse width modulator can be divided into two main groups of linear and non-linear current control.

The most popular current control techniques used in the literature up until now is the linear current controller such as PI current controller, the PR [162-165] current controller and Deadbeat current Controller [166]. Conventionally, the proportional (P) controller has been considered in the part of grid connected inverter control. By using this controller, it suffers from the inherent steady state error and with the aim to reduce the error, the integral component has been added to the transfer function [167].

The transfer function of the PI current controller can be defined as (2.5) where K_p is the proportional gain and K_I is the integral term.

$$G_{PI}(s) = K_p + \frac{K_i}{s} \tag{2.5}$$

The drawbacks of classical PI controller have been highlighted in [9] and [168, 169]. Even though the used of the grid voltage feed forward is to help the controller to try to reach the steady state faster but typically poor THD of the current will be obtained due to the presence of the grid voltage background harmonics in the current waveform. Since PI in SRF can't remove the undesirable twice fundamental frequency, the implementation of decoupling network in the Double Synchronous Reference Frame (DDSRF) has been implemented in [158] to counteract the oscillations caused by the positive and negative sequence.

The PR current controller is usually employed in the inner loop control of the inverter because of its capability to provide a smooth tracking and achieve a zero error during the steady state condition [112, 170]. Normally, the PR current controller is implemented in stationary reference frame. Even though PR current controller has overcome the drawback of PI current controller but it still needs an additional harmonic compensation to compensate the harmonics in order to comply with the regulation standards [168]. It has been proven in previous works that the PR current control performs a very good performance and in term of the implementation wise, it is less complex if compared to the other linear or non-linear current control. The PR current controller can be described in ideal or non-ideal cases. The Laplace transformation of the ideal PR current controller is shown in (2.6), and it can be implemented by using a SOGI-QSG.

$$G_{PR}(s) = K_p + K_r \frac{s}{s^2 + \omega^2} \tag{2.6}$$

Where the K_p is the proportional gain, K_r is the resonant gain and ω is the resonant frequency. The proportional gain, K_p determines the dynamics of the controller while the K_r determines the amplitude gain at selected frequency. The bode diagram of ideal PR current controller characteristic is shown in Fig. 2.7.

(a)   (b)
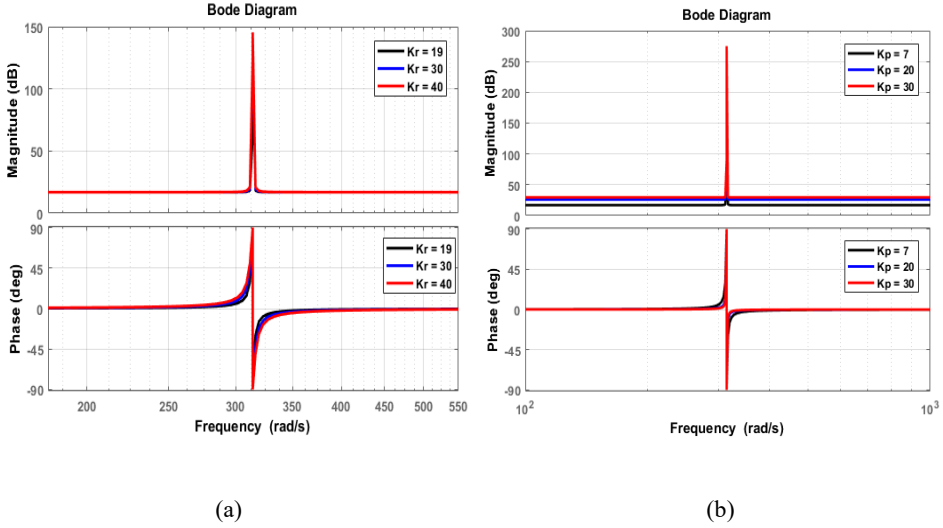
Fig. 2.7. Bode diagram of the PR controller considering ideal cases (a) Response when $K_p = 7$ with different values of K_r, (b) Response when $K_r = 19$ with different values of K_p.

However, in real implementation the non-ideal cases are more preferable due to its stability. For the case of non-ideal cases of PR current controller, the implementation will be based on the transfer function stated in (2.7).

$$G_{PR}(s) = K_p + K_r \frac{2\omega_c s}{s^2 + 2\omega_c s + \omega^2} \tag{2.7}$$

It is possible to control the bandwidth by adjusting the value of ω_c. The smaller the value of ω_c, the filter will become more sensitive to the frequency variations. In practical implementation, normally the value of ω_c used is between 5 – 15 rad/s. As compared to the PR current controller, the PI Controller is normally implemented in the synchronous reference frame [171]. However, using the classical PI Controller unveils two significant drawbacks which are inability of PI controller to track the sinusoidal reference without steady state error and somehow it has a poor disturbance rejection. The grid voltage feed forward and decoupling network is normally added to obtain a good dynamic response and improve grid disturbance rejection [31, 172, 173]. As presented in [174], selecting the proportional gain involves a trade-off between the dynamic response and the disturbance rejection capability.

Deadbeat controller is developed based on the model of a filter and a grid therefore the controller is sensitive to model and parameter mismatches. The controller is defined as dead beat because the error at the end of the following sampling period is zero. The switching state of the converter is decided from the information on the model. In order to compensate the parameter mismatch and the sample time delay, an observer is introduced in the controller structure.

The deadbeat controller has a high dynamic and prove to be superior in a situation of grid fault [166]. In [175-177], there are some examples of the work related to hysteresis current controller that belongs to a non-linear type. A current set point needed to trigger the current controller is normally known as a current reference, which is the output generated by the outer loop control. Fig. 2.8 shows the bode diagram of the non-ideal PR current controller.

(a)

(b)

(c)
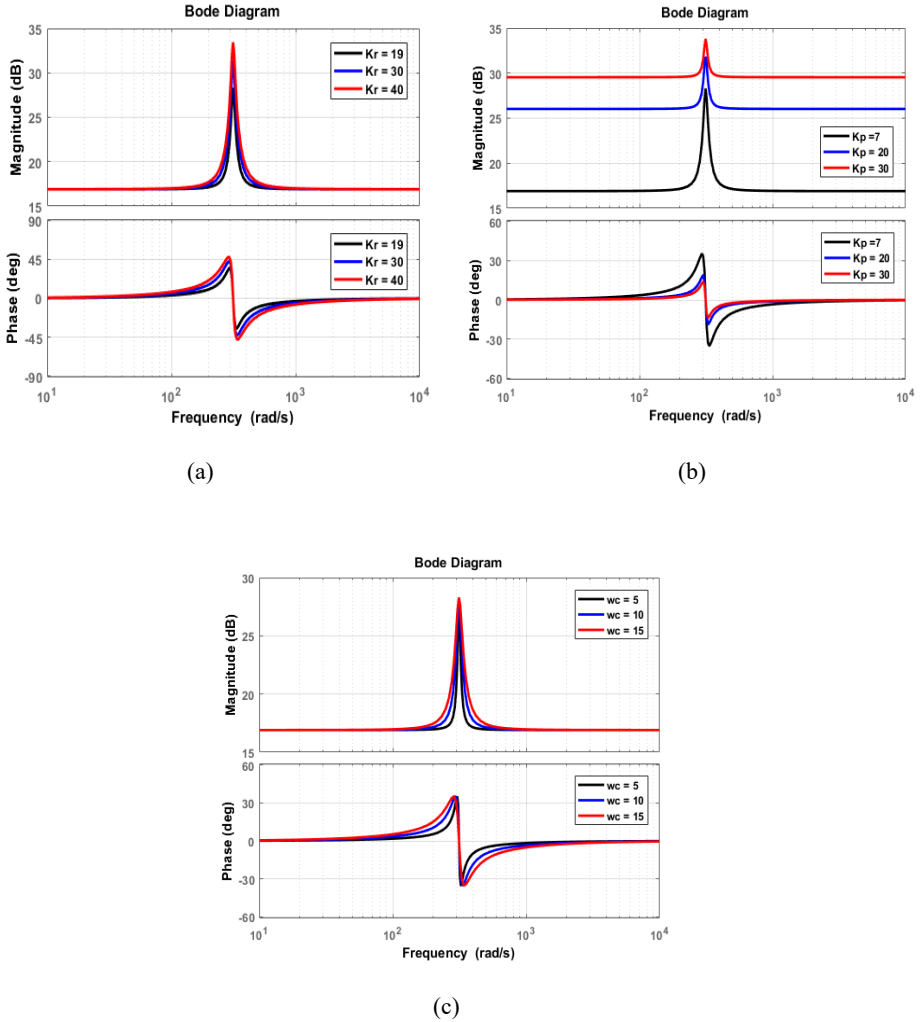
Fig. 2.8. Bode Diagram of the PR controller considering non-ideal cases (a) Response when $K_p = 7$ with different values of K_r, (b) Response when $K_r = 19$ with different values of K_p, (c) Response when $K_p = 7$, $K_r = 19$ and different values of ω_c.

2.6.   General Configurations of Power Electronics Converters in Wind Energy and Solar PV Systems

In [178], the developing trends and most commonly used power electronics converters for both wind and solar PV application has been presented. In wind energy system, the converter usually configured as back to back structure with a transformer on the grid side. However, with the increasing of power and voltage level, this structure may suffer from larger switching losses, lower efficiency and higher *dv/dt* stresses to the generator and transformer thus three level neutral point diode clamped topology has become one of the alternative as this topology achieves one more voltage level and less *dv/dt* stress compared to the two level back to back structures. The configurations of both converters are shown in Fig. 2.9.

(a)   (b)
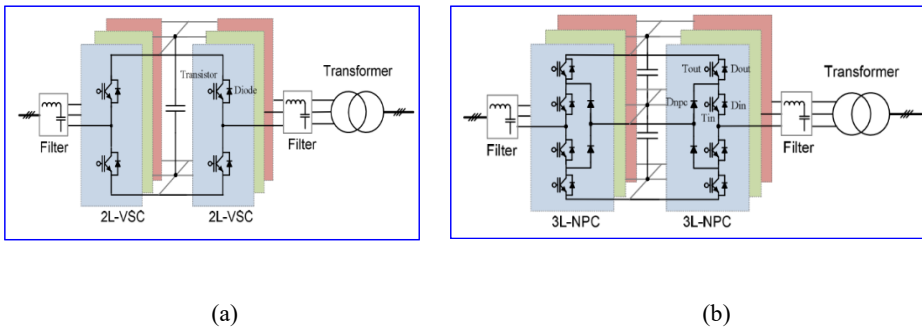
Fig. 2.9. Two level back to back converter. (b) Three level Neutral Point Clamped back to back converter.

However, the general configuration of grid connected PV inverters is shown in Fig. 2.10. The PV plants larger than 10kWp arranged in parallel string normally connected to the central converter. This configuration needs high voltage DC cables between PV and inverters. However, with that configuration, the power may loss due to common MPPT, module mismatch and losses in the string diodes because the reliability of the whole system depends solely on one inverter as shown in Fig. 2.10 (a). A string inverter is based on a modular concept where a series connected of solar panel will be connected to the separate inverters as shown in Fig. 2.10 (b). Another configuration is module-based inverter where a single PV module is connected to grid via its own inverter. The power production can be maximized because every single PV module has its own inverter and MPPT as shown in Fig. 2.10 (c). The Multi-string inverter as shown in Fig. 2.10 (d) combines the advantages of string and module inverters by having many DC-DC converters with individual MPPT which feed energy into common inverters.
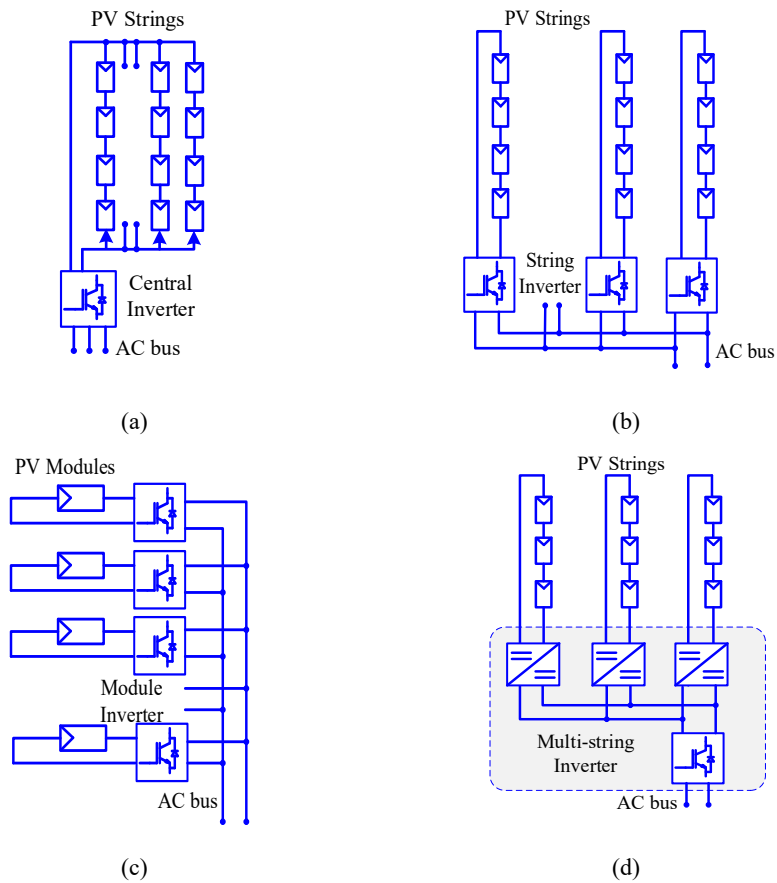
Fig. 2.10. Configuration of grid connected PV inverters. (a) Central Inverter, (b) String Inverter, (c) Module Inverter, (d) Multi-String Inverter.

In [9], the author described that inverter structures are derived from H-Bridge and neutral point clamp (NPC) topology. Three main modulation strategies are based on the bipolar, unipolar and hybrid modulation have been considered in the design. However, those three types are not suitable for transformer-less system. Manufacturers such as SMA, Sunways, Conergy, Ingeteam, Danfoss and Refu have offering transformer-less PV inverters with high European efficiency typically up to 98% on the maximum level [9]. Similar review on the suitable inverter for transformer-less system has done by [179] where H5 bridge topology, Highly Efficient and Reliable Inverter Concept (HERIC) and NPC topology have been highlighted.

2.7. Sensorless Control Strategies

In three phase three-wire voltage source converter configuration, at least five sensors have been considered in the control strategies where two sensors are used to measure the AC currents, one sensor is used to measure the DC-link voltage and two sensors are used to measure the AC voltage at the grid side of the filter inductors [180-184]. However, the AC current sensors are crucial in the over current protection of the converter. Therefore the designers of the converter are not prefer to remove the current sensors compared to the voltage sensors [185].

Over the last 20 years, voltage sensorless control has become an attractive solution for reducing cost and complexity of the control hardware. In this regard, the voltage sensorless control is possible to reduce the cost by means of ignoring at least two voltage sensors including its wiring, signal conditioning and integration to the digital control system [181, 186]. Other than that, the reliability of the converter system can be improved since the voltage sensorless control system reduces a few component thus avoiding the possibility of interruptions due to component failure [187], [17].

The work presented in [185] is the example of the early implementation of voltage sensorless grid synchronization that adopts the DPC concept in the control strategy. The grid voltage has been estimated by adding the voltage drop on the AC filter with the input voltage. However, the AC line current derivatives are still required, hence it contributes to the high noise sensitivity. Similarly, the work presented in [186] had proposed the voltage sensorless grid synchronization based on VOC concept.

The virtual flux estimation is one of the approaches that can achieve voltage sensorless operation. With a known parameter values of connection filter, duty cycle as well as the converter output current that is normally measured, the VF estimation capable to estimate the grid voltage condition. Previous research works prove that the virtual flux produce highly dependent results without the voltage measurement [15, 17], [188-190].

Other than virtual flux-based control, there are a few types of sensorless control strategies presented with the determination to avoid high noise sensitivity such as disturbance observer [191, 192], Kalman filters [193, 194], adaptive full order observers [195, 196] and neural networks [181, 197].

2.7.1 Implementation Issues Related to Virtual Flux Estimation

In the practical implementation of view, there are possibilities of drift and saturation occurred on the estimated virtual flux due to the DC-offset in the integrated signals. The DC-offsets can be caused by the converter dead time and the converter switches characteristics. Other than that, the DC-offsets also can be caused by the inaccuracy of analogue and digital signal conditioning, noise that appeared in the integrated signal and the

offsets by the current sensors. This condition should not happen and must be avoided at all times in the practical implementation. The work presented in [15] suggested a drift compensation solution in order to achieve offset free of virtual flux estimation with the determination to overcome the sensitivity of the system in case of grid frequency variation occurs.

The other control strategies that have been proposed in order to avoid the drift and saturation issues in the implementation of virtual flux estimation control include the analogue and digital filters, adaptive integration and advanced estimation techniques. The low pass filter with a crossover frequency particularly below the grid frequency is a common approach in the filter based implementation of virtual flux estimation. The crossover frequency value is normally to be one decade below the nominal angular frequency [15], [198, 199]. This implementation gives more freedom to shape the frequency response. However, a small phase error does appear in the system apart from the attenuation of the amplitude. The amplitude attenuation will imply the DC-component, therefore the band pass filters have been used to eliminate the DC-component in the estimated virtual flux signals [200]. Another filter based method is two cascaded low pass filters with a crossover frequency is equal to the nominal angular frequency [15]. The method presented in [15] achieved a fast transient response and the amplitude as well as the phase angle characteristics are correspond to a unity gain and 90° phase shift at fundamental frequency. The control strategy presented in [200] somehow is an attractive filter-based strategies compared to adaptive integration or more advanced estimation techniques.

Adaptive integration for estimating the flux has been presented by taking into account a basis of ideal integrators incorporated with different types of feedback from the estimated flux signals [17, 201-204]. In this kind of control, the main idea is to utilize the feedback signal in order to retain centricity of the trajectory of the estimated flux in the stationary reference frame [17].

The virtual flux estimation based control as presented in the previous studies [17, 112] shows that the accuracy of the estimation of the grid voltage condition will depends on the precision of the accessible filter parameters. As the filter configurations may involve the resistive and inductive elements, the virtual flux estimation only involved in arithmetic operations. Therefore, any deviations in parameters will not affect the stability of the estimation structure but it will give an impact on the accuracy of the grid synchronization. As a consequence, the accuracy of the active and reactive power at the PCC will be also affected [19].

2.7.2 Positive and Negative Sequence Separation Techniques in Virtual Flux Estimation Based Control in Stationary Reference Frame

Before going further to the analysis of the sequence separation techniques in VF estimation based control, it is imperative to understand the two phase representation of the

three phase variables. As the main results presented in this dissertation are based on the stationary reference frame, $\alpha\beta$, the three phase variables will be simplified to an equivalent set of two phase signals by using the Clarke Transformation [205]. This type of transformation is common in grid synchronization and control of grid connected power converters analysis. The transformation stated in (2.8) includes a separation of the three phase *abc* variables into the $\alpha\beta$ and *0* components.

$$\begin{bmatrix} x_\alpha \\ x_\beta \\ x_0 \end{bmatrix} = \frac{2}{3} \begin{bmatrix} 1 & -\frac{1}{2} & -\frac{1}{2} \\ 0 & \frac{\sqrt{3}}{2} & -\frac{\sqrt{3}}{2} \\ \frac{1}{2} & \frac{1}{2} & \frac{1}{2} \end{bmatrix} \begin{bmatrix} x_a \\ x_b \\ x_c \end{bmatrix} \tag{2.8}$$

The reverse transformation from $\alpha\beta 0$ to the three phase *abc* signals can be obtained in (2.9).

$$\begin{bmatrix} x_a \\ x_b \\ x_c \end{bmatrix} = \begin{bmatrix} 1 & 0 & 1 \\ -\frac{1}{2} & \frac{\sqrt{3}}{2} & 1 \\ -\frac{1}{2} & -\frac{\sqrt{3}}{2} & 1 \end{bmatrix} \begin{bmatrix} x_\alpha \\ x_\beta \\ x_0 \end{bmatrix} \tag{2.9}$$

The positive and negative sequence components are important especially in unbalanced analysis. The expression for calculating the positive and negative sequence component with a generic variable x is given in (2.10) where q is the phase shifting operator that corresponds to 90° delay from the fundamental frequency[12], [13], [160], [161].

$$\begin{bmatrix} x_\alpha^+ \\ x_\beta^+ \end{bmatrix} = \frac{1}{2} \begin{bmatrix} 1 & -q \\ q & 1 \end{bmatrix} \cdot \begin{bmatrix} x_\alpha \\ x_\beta \end{bmatrix}$$
$$\begin{bmatrix} x_\alpha^- \\ x_\beta^- \end{bmatrix} = \frac{1}{2} \begin{bmatrix} 1 & q \\ -q & 1 \end{bmatrix} \cdot \begin{bmatrix} x_\alpha \\ x_\beta \end{bmatrix} \tag{2.10}$$

However, the required phase shift has been presented in several different methods. The sequence separation based on low pass filters configuration has been presented in [160] in order to find two phase shifted signals that can be used in the sequence separation. In [206] and [207], the sequence separation presented is based on the Delayed Signal Cancellation (DSC). The other implementation of q by using the two cascaded low pass filter has been presented in [15] where in [208], the sequence separation presented is made obviously for online frequency adaptive by using the SOGI-QSG.

2.7.3 Summary of Previous Contributions in Virtual Flux Estimation Based Control that Served as the Main Reference of the Dissertation

The pioneer researcher on the VF estimation topic is Malinowski where the author starts the research on VF estimation specifically for three phase PWM rectifiers application [18], [198]. The work in [18] was improved in [20] with the used of space vector modulation and a slow PLL is applied in order to track the positive sequence of the estimated VF. A further comparative study was presented in [19] where the method in [186] was compared with the performance of [18] and [20]. In [209], the notch filters and low pass filters were applied in the Positive Sequence Synchronous Reference Frame (PS-SRF) in order to cancel out the influence of negative sequence grid voltage components on the VF estimation.

In [15], the first study of VF based voltage sensor-less controlled taking into consideration the estimation of both Positive and Negative Sequence Virtual Flux (PNS-VF) components in the stationary reference frame was presented by Kulka. The VF estimation was implemented by cascading two low pass filters with cut off frequency identical to the grid frequency, produce a 90° phase shift for the VF estimation. The development of an online frequency-adaptive VF based approach for voltage sensor-less control of the grid integrated VSC under unbalanced condition was later studied in details in [16, 17] and [113].

VF-based power control under unbalanced conditions, including strategies for operating under current limitation was also analyzed in [17]. The voltage sensorless grid synchronization was achieved by means of the frequency adaptive VF estimation, taking advantage of the Second Order Generalized Integrator Configured as a Quadrature Signal Generator (SOGI-QSG). The frequency adaptive Dual SOGI-based VF estimation (DSOGI-VF) with inherent sequence separation was first proposed in [210] with the objective to simplify the method used in [15] and to avoid cascaded flux estimation and sequence separation that could lead to relatively slow transients. However, sequence separation of current is needed in the work done in [16], [17], [21] and [113] since the current induced flux needs to be subtracted separately for each sequence component once the positive and negative sequence VF have been estimated.

The work presented in [112] is the extended version of the work done in [17] where the VF estimation has been carried out considering that the inverter is connected to the grid through the LCL filter. However, the work performed in [112] constitutes just an initial analysis and it is only validated through simulation results.

2.7.4 Virtual Flux Estimation Based Control for VSC with L-Filter

Considering the structure shown in Fig. 2.11, a VSC is connected to the grid through the *L*-filter as proposed in [16, 17] and [113]. In this configuration, VF estimation is utilized for synchronizing the converter control system to the voltage conditions at the PCC. It should

be noted that the VF estimation is based on the current measurement at the convertor side, I_{conv}. The concept of VF is based on the voltage integral as stated in (2.11).

$$\Psi = \int V_{conv} dt + \Psi_0 \tag{2.11}$$

This concept is similar to the estimation method for voltage sensorless control of VSC as proposed in [15], [18], [198], [200].
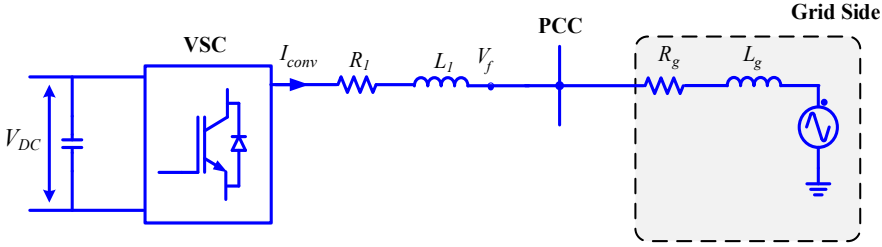
Fig. 2.11. An overview of the structure of VSC connected to the grid through L-Filter.

Based on the structure shown in Fig. 2.11, voltage at the grid side of the filter inductor, V_f in the stationary reference frame can be described according to (2.12). Before integrating the converter output voltage, the voltage drop caused by the conduction losses of the converter and the primary filter inductor, represented by the equivalent resistance R_1, should be taken into account.

$$V_{f,\alpha\beta}(t) = \left(V_{conv,\alpha\beta} - R_1 \cdot I_{conv,\alpha\beta}\right) - \left(L_1 \cdot \frac{dI_{conv,\alpha\beta}}{dt}\right) \tag{2.12}$$

The estimation of the converter output voltage is based on the multiplication of the pulse width modulation reference signal, $m_{ref,\,\alpha\beta}$ with the dc-link voltage, V_{DC}. Considering equation (2.11) and (2.12), the estimated VF at the PCC can be expressed by (2.13).

$$\Psi_{f,\alpha\beta} = \int \left(m_{ref,\alpha\beta} \cdot \frac{1}{2} V_{DC} - R_1 \cdot I_{conv,\alpha\beta} \right) dt - \left(L_1 \cdot I_{conv,\alpha\beta} \right) \tag{2.13}$$

Using the base values in (2.14), the per unit expression for VF at the grid side is given by (2.15).

$$V_b = V_{phase,} \qquad V_b = 2 \cdot V_b, \qquad \Psi_b = \frac{V_b}{\omega_b} \tag{2.14}$$

$$\psi_{f,\alpha\beta} = \omega_b \int \left(m_{ref,\alpha\beta} \cdot v_{DC} - r_1 \cdot i_{conv,\alpha\beta} \right) dt - \left(l_1 \cdot i_{conv,\alpha\beta} \right) \tag{2.15}$$

The synchronization process is based on the DSOGI-FLL as proposed in [17, 113]. The output of the FLL is the frequency, ω' needed by the SOGIs. By using the DSOGI-FLL for estimating the grid voltage, it is possible to avoid the issues related to the sensitivity of ideal integration in (2.11) to drift and offset in the real implementation. Referring to Equation stated in (2.2) and the structure of the SOGI-QSG in Fig. 2.3 (a), it can be understood that and the quadrature output signal, qv' corresponds to the VF integral of the bandpass-filter signal v' scaled by the per unit angular frequency as indicated in (2.16). According to [16], this signal can be defined as the frequency scaled VF labelled as χ.

$$qv' = \omega' \cdot \frac{1}{2} \cdot v' = \omega'_{pu} \cdot \underbrace{\omega_b \cdot \frac{1}{s} \cdot v'}_{\psi'} = \omega'_{pu} \cdot \psi' = \chi \qquad (2.16)$$

As the virtual flux is the integral of voltage, the estimation of virtual flux components will always be lagging the voltage by 90° phase shift. Considering the vector rotation, the positive sequence component can be described by a clockwise rotating vector and the negative sequence component will be in counter clockwise rotation. For sequence separation, 90° phase shift is needed. This phase shift is already available from the direct output signal v' of the SOGI-QSG where in this regard, it leads the virtual flux signal by 90°. Considering that this signal is equivalent to the derivative of the VF, changing the sign will make it correspond to a 90° phase lag [16, 17]. Thus, the per unit (p.u.) positive sequence VF components can be described in (2.17) and (2.18) respectively.

$$\chi_\alpha^+(s) = \frac{1}{2}qv'_\alpha(s) + \frac{1}{2}v'_\beta(s) \qquad (2.17)$$

$$\chi_\beta^+(s) = \frac{1}{2}qv'_\beta(s) + \frac{1}{2}v'_\alpha(s) \qquad (2.18)$$

Fig. 2.12 shows the positive and negative sequence of VF estimation for the case of VSC is connected to the L-filter where the ω_{pu} is the per unit frequency. The sequence separation of current is shown in Fig. 2.13.
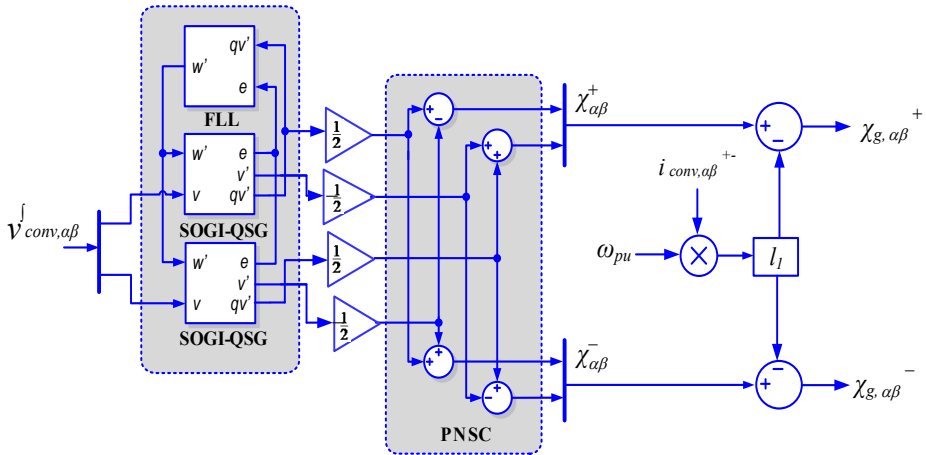
Fig. 2.12. Positive and Negative Sequence of VF estimation.
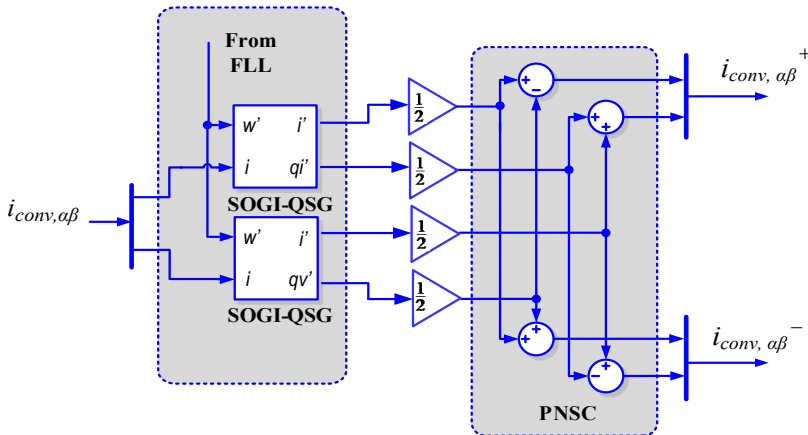
Fig. 2.13. Sequence separation of the converter current.

2.8.   Summary of the Chapter

This chapter has presented the state of the art for grid connected power converter control. The main purpose of this chapter is to provide a background studies for the following chapters. The state of the art of the Sensorless Control Strategies presented in Chapter 2.7 is really important to provide an understanding on the virtual flux based synchronization control specifically for Chapter 3 and Chapter 4. However, the explanation on Chapter 2.7 is just focussing on the estimation strategies for the case of power converter connected to the grid using the L-filter.

VF Estimation for VSC with LCL Filter

*T*his chapter introduces a grid synchronization based on VF estimation that allows a control of grid-connected power converter without depending on AC-voltage measurements. For the case of VSC with LCL filters, the influence of the capacitor currents must be taken into account to ensure an accurate VF estimation at the PCC with the grid. In this chapter, three options for VF-based synchronization to the PCC are studied and the positive as well as the negative sequence separation is taken into account as part of the VF estimation. Estimation of the grid-side current is also included in the VF-based synchronization strategy, in order to obtain an accurate voltage or flux across the grid-side inductor. Since the VF estimation is implemented in the stationary reference frame, PR current controllers will be used as the inner loop control of the VSC. A simulation and experimental work of the proposed system will be presented in this chapter. As it will be shown in both simulation and experiments, the VF estimation is reliable in estimating the conditions of the grid-side voltage, and hence it can provide the basis for controlling the active and reactive power injection without voltage sensors at the PCC and/or currents sensors in the grid-side inductance of the LCL-filter. The chapter continues with an overview of the proposed VF estimation for VSCs with LCL filter, including filter configuration and the current reference generation. Then, the three investigated methods for VF estimation with LCL filters are presented. Furthermore, the simulation cases are presented and the obtained results are compared and discussed, before experimental verification of voltage-sensorless VF-based control is presented in the last section.

3.1   Overview of Proposed System

The case study that will be considered in this chapter is shown in Fig. 3.1. Based on the structure, the capacitor current, I_{cf}, cannot be ignored and should be included in the estimation.
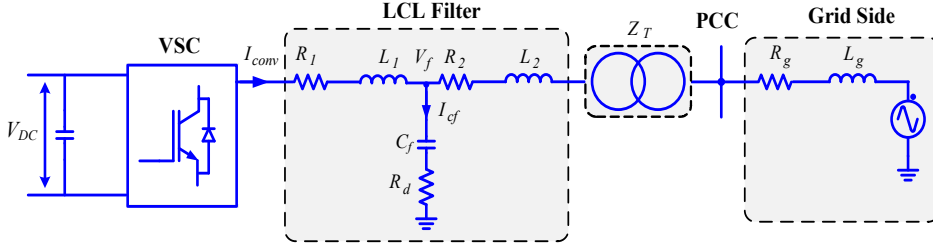
Fig. 3.1. An overview of the structure of investigated system.

In this chapter, three possible methods of estimating the VF at the PCC are investigated. The first method is based on the voltage sensorless control. In this regard, an estimation is done without an additional sensor in the LCL-filter, where the capacitor current will be estimated based on the estimated capacitor voltage, V_f. The second possible method for obtaining the capacitor current is based on using a voltage sensor to measure the capacitor voltage, V_f which later can be used for estimating the capacitor current. Finally, the third method implements the VF estimation by means of using a direct measurement of the capacitor current.

In order to synchronize the VSC with the grid, the DSOGI-QSG with FLL is used. As mentioned in Chapter 2, the VF corresponds to the integral of voltage. Therefore, an instantaneous phase angle, γ_g lags the voltage phase angle by 90° for the fundamental frequency signals. From the above statement, it can be understood that the voltage phase angle, θ_g can be obtained by; $\gamma_g + 90°$ where $\gamma_g = \arctan(\chi_{g,\beta}/\chi_{g,\alpha})$. In this regard, the $\chi_{g,\beta}$ is the positive sequence of VF estimation at the PCC in beta component and $\chi_{g,\alpha}$ is the positive sequence of virtual flux estimation at the PCC in alpha component. The main principles of the DSOGI-QSG and FLL are similar to the ones that have been presented in Chapter 2. The inner loop current control will be based on the PR current controller as presented in Chapter 2.5. Therefore, the equation stated in (2.7) will be considered in both simulation and experimental work.

3.1.1   Configurations of LCL Filter

This work contributes to the actual state of the art by means of designing an application oriented to LCL filter-based configurations, which is broadly extended in the industry. In this work, a passive damping has been considered for the LCL filter and, hence damping

resistors are placed in series with the capacitor branch [211]. Considering the per phase model of the LCL filter shown in Fig. 3.1, a passive damping has been included in the LCL filter configuration of the study case in order to smoothen the spike that might appear when considering only capacitive and inductive element of the filter. Based on the per phase model in Fig. 3.1, the transfer function of the LCL filter can be described in two scenarios which are with and without the damping resistor as given in (3.1) and (3.2) respectively.

$$G_{F,d}(s) = \frac{C_f R_d s + 1}{L_1 C_f L_2 s^3 + C_f (L_1 L_2) R_d s^2 + (L_1 L_2) s} \tag{3.1}$$

$$G_F(s) = \frac{1}{L_1 C_f L_2 s^3 + (L_1 + L_2) s} \tag{3.2}$$

These two transfer functions are used to compare the performance of the LCL filter with and without the damping element. Fig. 3.2 shows the bode diagram of the transfer function stated in (3.1) and (3.2).
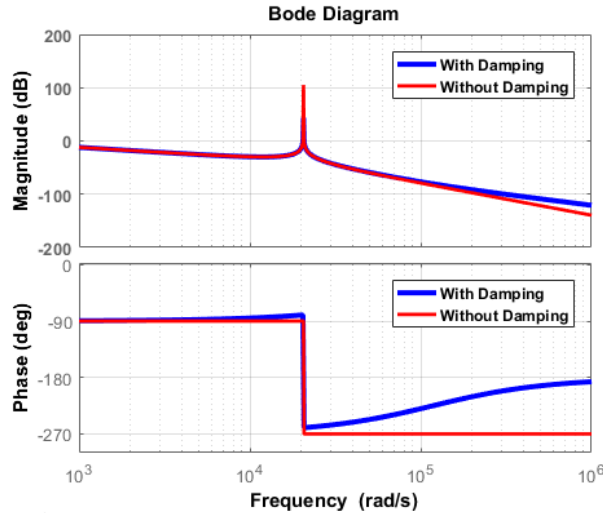
Fig. 3.2. Bode Diagram of the filter transfer function.

It can be seen clearly from the bode diagram that the magnitude of the spike is quite high when the transfer function stated in (3.2) is considered. Based on the bode diagram shown in Fig. 3.2, the overall response is smooth when considering a damping resistor. In this regard, it can be seen that the response is rolling off to -180° instead of -270° for high frequencies. This condition is more realistic to be considered in the practical implementation.

3.1.2   Current Reference Generation

In addition to the current controller and the VF estimation, it is also necessary to calculate the set point to be provided to the current controller. The current set point, which is normally known as current reference is the output generated by the outer loop controller. The current reference generation is based on the power calculation where the active and reactive power reference are also required. The positive sequence of the VF estimation at both alpha and beta components will be used to calculate the current reference. Since the current is controlled at the converter side, the capacitor current needs to be added with the current at PCC in order to match with the current at the converter side. The current references in the alpha and beta reference frame can be calculated by (3.3) and (3.4).

$$i_\alpha^* = \left[\frac{P_{ref} \cdot \chi_{g,\alpha+} + Q_{ref} \cdot \chi_{g,\beta+}}{\chi_{g,\alpha+}^2 + \chi_{g,\beta+}^2} \right] + i_{cf,\alpha} \tag{3.3}$$

$$i_\beta^* = \left[\frac{P_{ref} \cdot \chi_{g,\beta+} + Q_{ref} \cdot \chi_{g,\alpha+}}{\chi_{g,\alpha+}^2 + \chi_{g,\beta+}^2} \right] + i_{cf,\beta} \tag{3.4}$$

3.2   Implementation of VF Estimation

3.2.1   First Method; Voltage Sensorless VF Estimation

As different from the classical grid synchronization approaches (based on processing the grid voltage measurements), the concept of VF-based synchronization relies on the estimation of the grid voltage conditions without any voltage sensor at the point where the active and reactive power flow should be controlled. As similar to the implementation presented in Chapter 2.7.4, the estimation depends on the measurement of the converter-side currents, I_{conv}. The three phase quantities of the converter output current are transformed into the alpha-beta domain as shown in (3.5).

$$\begin{bmatrix} I_{conv,\alpha} \\ I_{conv,\beta} \end{bmatrix} = \sqrt{\frac{2}{3}} \cdot \begin{bmatrix} 1 & -\dfrac{1}{2} & -\dfrac{1}{2} \\ 0 & \dfrac{\sqrt{3}}{2} & -\dfrac{\sqrt{3}}{2} \end{bmatrix} \cdot \begin{bmatrix} I_{conv,a} \\ I_{conv,b} \\ I_{conv,c} \end{bmatrix} \tag{3.5}$$

Throughout this analysis, the converter current is denoted as $I_{conv}^{\alpha\beta}$. The capacitor current, $I_{cf}^{\alpha\beta}$ in this case will be estimated based on the estimated capacitor voltage. In order to avoid measuring additional currents, the grid current, $I_g^{\alpha\beta}$ is obtained by subtracting the estimated

capacitor current, I_{cf} from the converter current, I_{conv}. Considering the use of per unit frequency, ω_{pu} in the estimation, the capacitor voltage in $\alpha\beta$ components can be obtained as shown in (3.6) and (3.7) respectively.

$$v_f^\alpha(t) = \left(\left(v^\int {}_\alpha \right) dt + \left[\left(\omega_{pu} \cdot l_1 \right) \cdot \left(i_{conv}^\beta(t) \right) \right] \right) \tag{3.6}$$

$$v_f^\beta(t) = \left(\left(v^\int {}_\beta \right) dt + \left[\left(\omega_{pu} \cdot l_1 \right) \cdot \left(i_{conv}^\alpha(t) \right) \right] \right) \tag{3.7}$$

Based on the equation stated in (3.6) and (3.7), the $v_{\alpha\beta}^\int$ is the compensated converter output voltage. Fig. 3.3 shows the block diagram that permits to obtain the compensated converter output voltage and the capacitor voltage estimation in $\alpha\beta$.

(a)   (b)
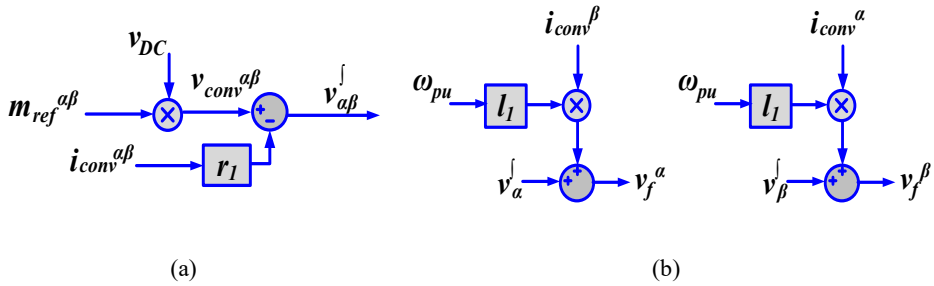
Fig. 3.3. (a) Estimation of converter output voltage and compensation of voltage drop at R_1; (b) Estimation of capacitor voltage.

The compensated converter output voltage, $v_{\alpha\beta}^\int$ in Fig. 3.3 (a) will be used later in the integration in order to obtain the VF estimation in both positive and negative sequence. The estimation of the capacitor voltage shown in Fig. 3.3 (b) is essential for obtaining the capacitor current, since the proposed system is based on fully estimation and voltage sensorless measurements. The estimation of the capacitor current based on the estimated capacitor voltage is shown in Fig. 3.4.
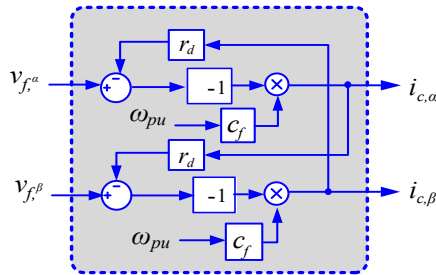
Fig. 3.4. Estimation of the capacitor current based on the estimated capacitor voltage.

In Fig. 3.5, the sequence separation of the converter and the integral of the grid current are presented. In order to obtain the positive and negative sequence of converter current and also to perform the integral of the grid current, four SOGI-QSG are used, where the frequency value comes from the FLL. The configuration of the PNSC is similar to the configuration presented in Fig. 2.12 and Fig. 2.13.
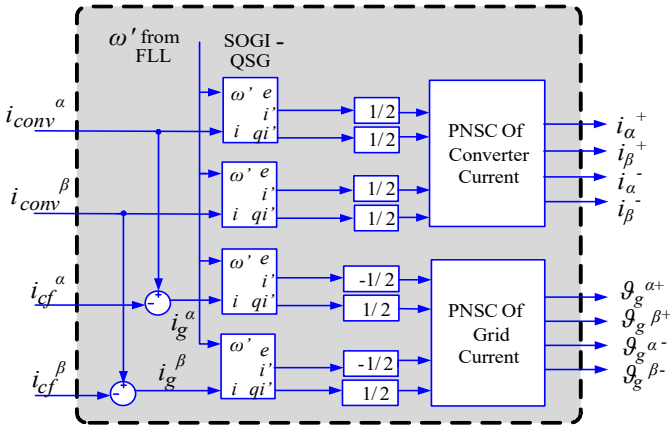
Fig. 3.5. Sequence separation of converter currents and the grid current integral.

Considering the frequency-scaled VF, the virtual flux is expressed as χ. The positive and negative sequence of the virtual flux is shown in Fig. 3.6.
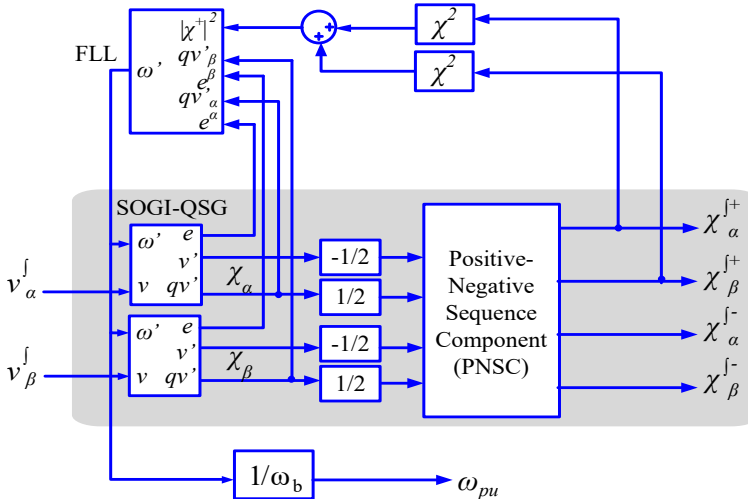
Fig. 3.6. Positive & negative sequence of virtual flux.

In balanced condition, only positive sequence of VF will be considered in the analysis, hence the equations stated in (2.17) and (2.18) are valid to be considered in this estimation. Without considering the positive and negative sequence separation, the virtual flux estimation at the filter capacitor can be found using equation (3.8). In this regard, the $\chi^{\int}_{\alpha\beta}$ is the DSOGI virtual flux estimation in alpha-beta sequence. Since the DSOGI VF estimation is the integral of compensated converter output voltage, $v^{\int}_{\alpha\beta}$, it can be calculated as in Fig. 3.3 (a).

$$\chi_c^{\alpha\beta}(t) = \chi^{\int}_{\alpha\beta}(t) - (l_1 \cdot i_{conv\alpha\beta}(t)) \tag{3.8}$$

Considering only the positive sequence component, Fig. 3.7 shows the block diagram to obtain the positive sequence of the capacitor current from the positive sequence of the VF estimation at the capacitor.
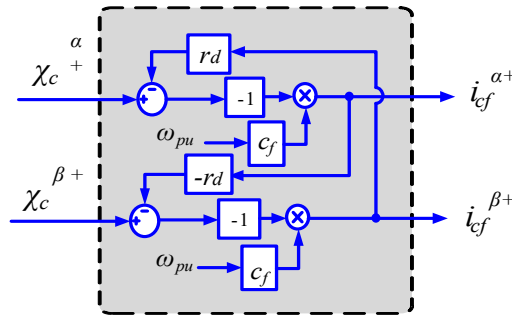
Fig. 3.7. Estimation of positive sequence of capacitor current.

The estimation is continued with the compensation for the resistive voltage drop on the virtual flux at the grid side of the LCL filter. Thus, influence from the resistive drop across the R_2 must be subtracted from the VF estimation at the filter capacitor. This is obtained by multiplying the integral of the grid current, ϑ_g with R_2. Before reaching the final estimation at the grid side, the induced flux drop at the grid side must be also subtracted. The induced flux drop can be calculated by multiplying the sum of L_2 and L_T with the PNSC of grid currents. In this work, the L_T is considered as the transformer leakage inductance and the value of L_T is based on 6% of the base impedance value. The resulting VF estimation is given by (3.9).

$$\chi_g^{\alpha\beta+} = \chi_{\alpha\beta}^{\int+} - r_2 \cdot \vartheta_g^{\alpha\beta+} - (l_2 + l_T) \cdot i_g^{\alpha\beta+} \tag{3.9}$$

where:

$$i_g^{\alpha\beta+} = i_{conv}{}^{\alpha\beta} - i_{cf}{}^{\alpha\beta+} \tag{3.10}$$

3.2.2 Second Method; VF Estimation with Voltage Sensor at Filter Capacitor.

Since one of the advantages of the utilization of VF estimation is to synchronize a control system to a different remote points in the grid, it is reasonable to have a sensor to measure the capacitor voltage, V_f. The presence of a voltage sensor permits to check the existence of voltage in the network and to simplify the connection as well as the start-up of the converter. The active and reactive power at a remote point can still be controlled on a basis of the VF estimation. This can be possible as long as the LCL parameters, duty cycle and converter output current are known. In a practical implementation, the voltage sensors normally included in the LCL filter configuration. The voltage sensors in this case is mainly used to obtain the capacitor voltage and later estimate the capacitor's current. This voltage measurement is a stable output and it will contribute positively to carry out a good estimation of the virtual flux at the PCC. However, when combined with VF estimation-based on the 1st method, the synchronization method can also maintain operation and could be more reliable in case of voltage sensor failure. The method for obtaining the capacitor current is the same as the one described previously in Fig. 3.1. As different to the method described in Chapter 3.2.1, the capacitor voltage is measured using the voltage sensor. Therefore, the expression given by (2.12, 2.13, and 3.8 - 3.10) are still valid for obtaining the resulting VF estimation in the second method.

3.2.3 Third Method; VF Estimation with Additional Current Sensor to Measure Capacitor Current

In this method, the current sensor is used to measure the capacitor current, I_{cf} directly. Following the same implementation as in the previous two methods, the estimation of the converter output voltage as well as the positive and negative sequence component of the virtual flux estimation is based on the schemes from Fig. 3.3 (a) and Fig. 3.6. The only difference in this case is that the block diagram of the capacitor current estimation in Fig. 3.4 is not necessary because the capacitor current is obtained by direct measurement using an additional current sensor. In this case, the capacitor current will be separated in positive and negative sequence component so that another two sets of SOGI-QSGs and PNSC blocks will be required. The implementation of sequence separation for the capacitor current is the same as the sequence separation of converter current shown in Fig. 2.13. The grid current integral is still necessary, since this current is also included in the VF estimation. By following the same approach used in the previous methods, the grid current is obtained by subtracting the capacitor current from the converter current before it is integrated to obtain the PNS. In this method, the expression described in (3.9) is still valid for obtaining the estimated VF at the PCC.

3.3   Simulation Results of VF Estimation

Based on the structure of the investigated system shown in Fig. 3.1, an overview of the complete configuration for the simulation studies is shown in Fig. 3.8.
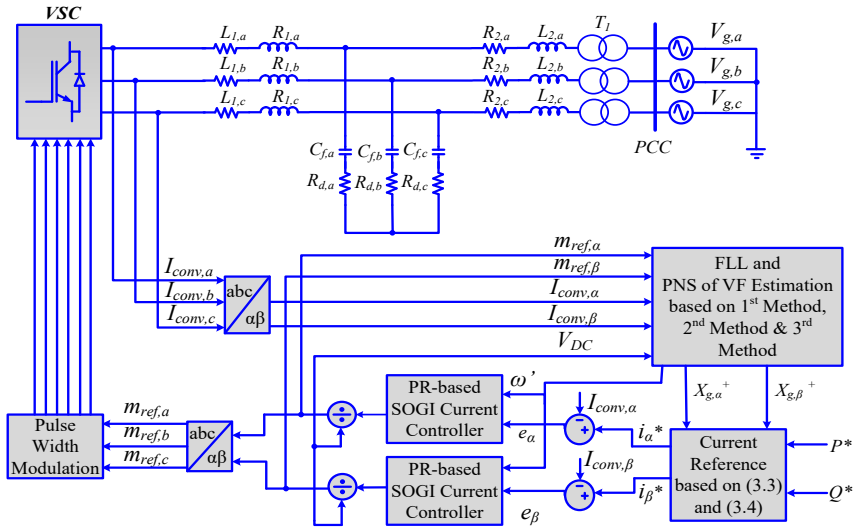
Fig. 3.8. Simulation Setup.

In this work, the 10 kHz sampling frequency is selected to work with the 10 kVA converter. This switching frequency is the most common working in this range of power as it has a good trade-off between passive sizing, ripple obtained and losses dissipated. If the switching and sampling is higher, the proposed solution would still work well. The increasing speed of microprocessors permits it to fit the VF algorithm in the pipeline. In the case of this chapter, even the code is not optimized, the code is executed in less than half of a cycle. The simulation has been carried out for all the three methods that have been proposed in previous section. The parameters are listed in Table 3.1. The design parameters are based on a 10 kW real power converter setup that will be later used in the experimental validation. The simulation studies have been conducted for two different scenarios.

Table 3.1. Simulation Parameters.

Abbreviation	Nomenclature	Values
S_N	Rated Apparent Power	10 kVA
$V_{g(p-p)}$	Phase to Phase Grid Voltage	400 V
$V_{g(p)}$	Phase Voltage	230 V
V_{DC}	dc-link Voltage	700 V
$L_{1(abc)}$	Inductor, L_1	3.4 mH
$L_{2(abc)}$	Inductor, L_2	588 µH
$L_{T(abc)}$	Inductor, L_T	35.28 µH
$C_{f(abc)}$	Filter Capacitor	4.7 µF
$R_{d(abc)}$	Damping Resistor	1.8 Ω
f_{sw}	Switching Frequency	10 kHz
f_s	Sampling Frequency	10 kHz

3.3.1   Active and Reactive Power Injection

The transient and steady state response of the system are monitored using the three VF-based control methods when the active power and reactive power reference is set to, P_{ref} = 10 kW (1 p.u.) and Q_{ref} = 0 kVar (0 p.u.). The value of K_p = 7 and K_r =19 are used in both simulation and experimental. A step in the references from zero is applied at t = 0.1s and the collected results are presented in the time domain in p.u. values. As it can be seen from Fig. 3.9, the performance of all the three methods is good. In Fig. 3.9 (a), the tracking capability of the PR current controller is verified, as the system is able to follow the current reference generation almost immediately when the reference step has been applied, for all the three methods. The converter currents show no transients overshoot, however in the third method, where the capacitor current measurement is involved, there is a noticeable noise in the current. The noise in the reference is due to the measured noise.

(a)
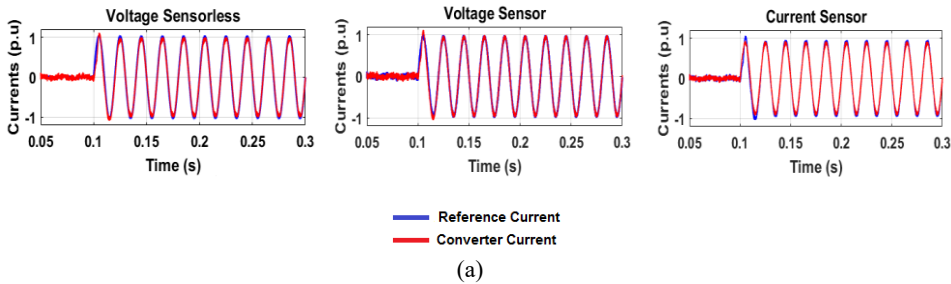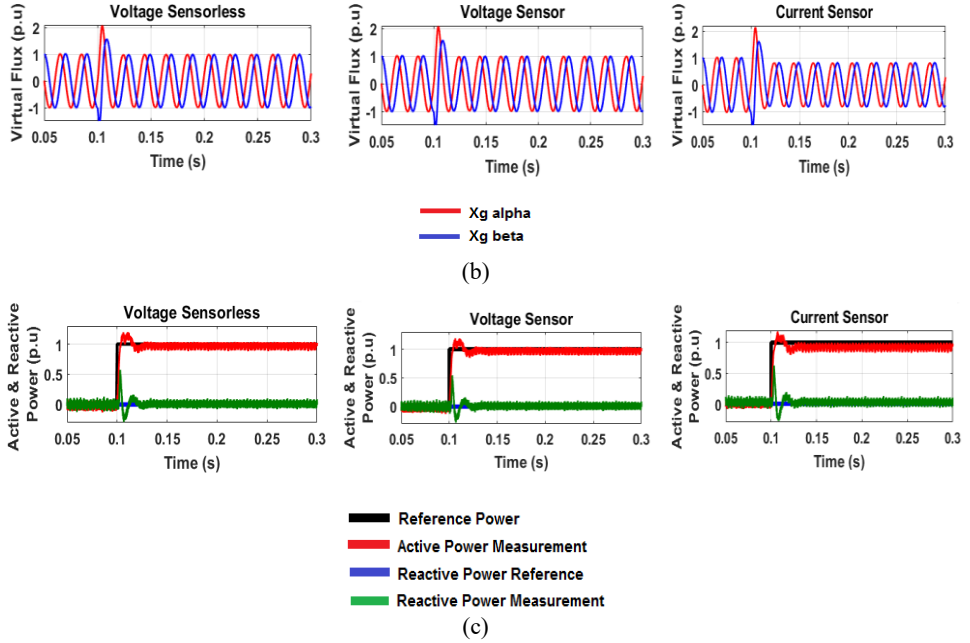
Fig. 3.9. Simulation Results. (a) Tracking capability of the proposed system, (b) Virtual flux estimation at the PCC, (c) Active and Reactive Power Injection.

These results also confirm that the PR current controller used in the proposed system is able to eliminate the tracking error and achieve zero error during the steady state. The positive sequence of VF estimation, shown in Fig. 3.9 (b), produces a balanced sinusoidal voltage with the beta component lags the alpha component by 90°. Based on the results obtained, it is proven that the precise parameters of the connection filter, as well as a good current measurement are crucial to ensure a good estimation of the grid voltage, which is essential for controlling the active and reactive power injected to the grid at the PCC.

However, in the case of the 3rd method, placing a current sensor for measuring directly the capacitor current has been shown to be a less preferable solution, because the ripple current in the capacitor is very large compared to the fundamental frequency component. Therefore, noise and ripple components might be transmitted into the control system and depreciate the performance of the VF estimation. This statement is referred to the plot shown in Fig. 3.9 (b) where it is clearly seen that the VF estimation at the PCC for the third method is a little bit less compared to the VF estimation shown in the case of first and second method.

In Fig. 3.9 (c), the values of active power in the time domain matches in all cases with the active power reference. Moreover, the proposed synchronization strategies are able to ensure that the active and reactive power injection to the grid is accurately controlled with only small overshoot in the measured reactive power occurring during the start-up for all

the three cases. However, the overshoot is quickly compensated, and the system reaches its steady state at approximately at t=0.103 s. As it can be seen in the plot shown in Fig. 3.9 (c), the active power measurement for the case of the third method is slightly lower compared to the active power reference that has been set. This is due to the affected virtual flux estimation at the grid side as shown in Fig. 3.9 (b).

3.3.2   Changes in Active and Reactive Power

Different values of active and reactive power references have been set in order to demonstrate that the system is still working well when different values of active and reactive power are injected to the grid. Based on the results obtained in section 3.3.1, the first method based on voltage sensorless and also the second method with voltage sensor to measure the capacitor voltage are promising. Thus in this section, the change in active and reactive power is only considering the first and the second method. For the 1st method, the active power reference, P_{ref} = 0.9 p.u. and the reactive power reference, Q_{ref} = 0.45 p.u. In the 2nd method, the P_{ref} = 0.8 p.u. and Q_{ref} = 0.2 p.u. The simulation results for the different values of active and reactive power injection are shown in Fig. 3.10.
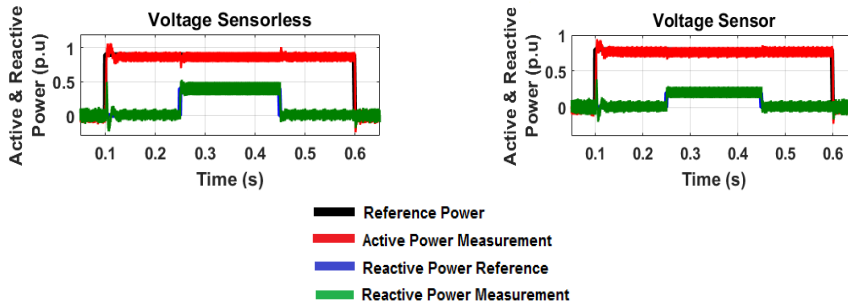
Fig. 3.10. Different injection of active and reactive power.

As per results shown in Fig. 3.9, the proposed system is able to control the active and reactive power precisely. In general, the results show a reliable accuracy of VF estimation, since the synchronization with the grid and the equivalent control of the active and reactive power injection to the PCC is based on the VF signals. By using the DSOGI-FLL in the VF estimation, the system is inherently adaptive to frequency variations and it is able to provide a very fast response. Based on the results obtained in Fig. 3.10, the propose systems are able to control the active and reactive power injections very well and this capability is very important for the system to respond to the variation of voltage and frequency.

3.4   Experimental Validation

The experimental setup used for the final validation is shown in Fig. 3.11. The system consists of a 10 kVA inverter which is connected to a three phase ac power source through a LCL filter. The inverter is powered by a dc-power supply that provides a 700 V dc-link voltage. The controller of the whole system is embedded in a dSpace1103 platform, which controls the switches of the converter through fibre-optic links.
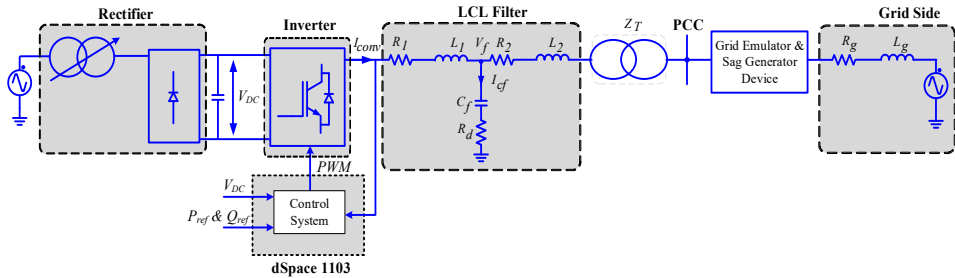
(a)
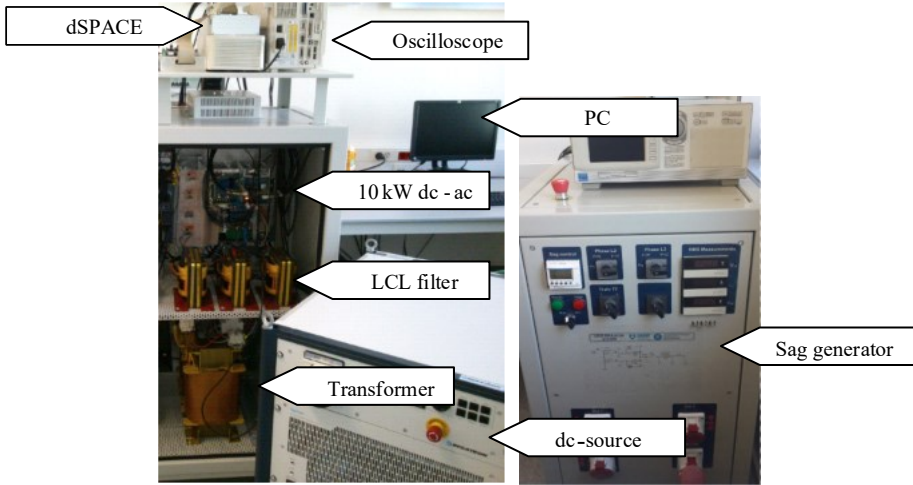
(b)

Fig. 3.11. (a) Block diagram of the experimental setup, (b) Experimental setup in the lab.

The block diagram of the system configuration is shown in Fig. 3.11 (a) and the experimental setup in the lab is shown in Fig. 3.11 (b). Considering the parameters listed in Table 3.1, the experimental validation has been carried out and the results have been structured into the SCADA layout. The SCADA layout is built using the control desk application of dSpace 1103. In the experimental validation, the overcurrent protection also includes an anti-saturation block, therefore the current will be always in the non-saturated

range. The saturation of the current should be avoided in the practical implementation because it may produce a current distortion larger than the expected. In any case, this limitation is also necessary in real power converter, as the THD should be lower than 3-4% in order to comply with the harmonic emission standards.

Considering the VF estimation methods explained in section 3.2, the approach without additional ac-side voltage or current sensors requires a more complex structure for practical implementation compared to the second and third method. As this method is relying on the converter output current as the only ac-side measurement, it is also considered as the most challenging one from the practical implementation point of view. If this method works well in the experimental platform and provides similar results as obtained from the simulation, it can be assumed that the performance of second and third method can be assessed according to the simulation results. Thus, only results from experimental verification of the first method will be presented in this chapter.

3.4.1   Active and Reactive Power Control

The value of K_p and K_r used in the experimental setup are the same as the ones used in the simulation. The plots in Fig. 3.12 show the experimental results where a power step of 0.8 p.u. (8 kW) of the active power reference has been applied.
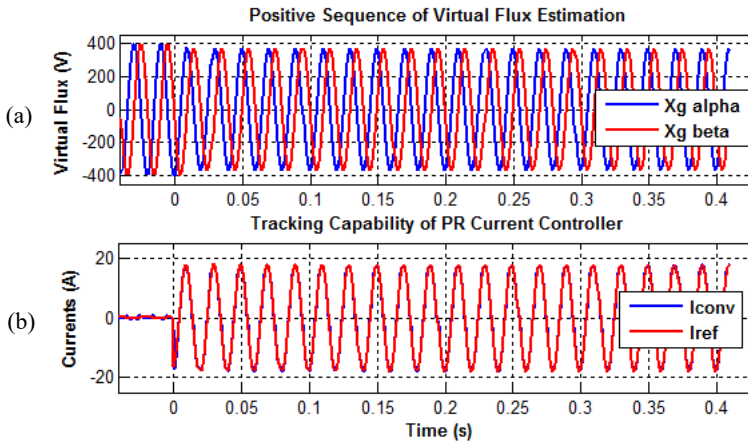
Fig. 3.12. Experimental results captured from control desk, (a) The plots of VF estimation at the grid side, (b) The tracking of converter currents.

The objective of this test is to investigate the performance of VF estimation and the inner loop control in the experimental implementation. In this experiment, the reactive power reference has been set to 0 p.u. (0 kVar). It should be noted that the results obtained in Fig. 3.12 are captured from the control desk of dSpace application and the values shown are the

real ones appreared on the control desk. Both signals show that the VF estimations at the grid side are free from the ripple and distortion. In these plots, it is proven that the VF based synchronization method works fine enabling the system to estimate the grid voltage for controlling the current. As shown in the plots, the inner loop control also works as it is required. The converter current is able to track the reference perfectly as shown in Fig. 3.12 (b). The proposed system tracks the reference with a fast dynamic response and has a zero steady state error. The quality of current reference generation plays an important role in the current tracking performances. The current reference generation depends on the estimation shown in (3.3) and (3.4). Therefore, the quality of VF estimation at the grid side in Fig. 3.12 (a) is very important because it will be essential in the calculation of current reference. In the case of voltage sensorless method, the capacitor current has been estimated based on the estimated capacitor voltage. Since there is no direct measurement of capacitor current, the reference current generation is free from the measurement noise, hence it produces a nice sinusoidal current in alpha and beta components. These results are very significant as any deviation in the estimation would affect the active and reactive power control.
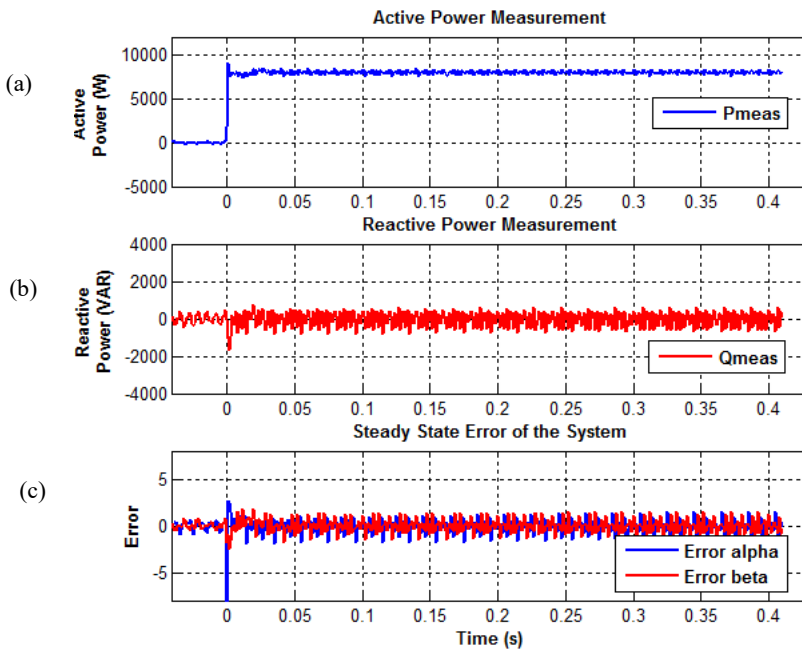
Fig. 3.13. (a) Active power measurement, (b) Reactive power measurement, (c) Steady state error of PR current controller.

In Fig. 3.13 (a) and Fig. 3.13 (b), the control of active and reactive power has been presented. It is clearly seen from the plots that the active and reactive power measurement match well with the active power and reactive power reference, proving thus that the

proposed system is able to control both active and reactive power without any errors in experimental implementation. The results also confirm that with a stable value of the filter parameters, the accuracy of the VF estimation is ensured, providing a good basis for controlling the active and the reactive power at the PCC. The steady state error shown in Fig. 3.13 (c) proves that the PR-current controller is working very well and capable to eliminate the steady state error.

3.4.2   Change in Active and Reactive Power Injection

Another test with different values of active power injection was carried out in order to observe the performance of the proposed system. The results obtained in this case are shown in Fig. 3.14, where it can be seen that the reference step change has been set to 1 p.u. and 0.8 p.u. respectively.
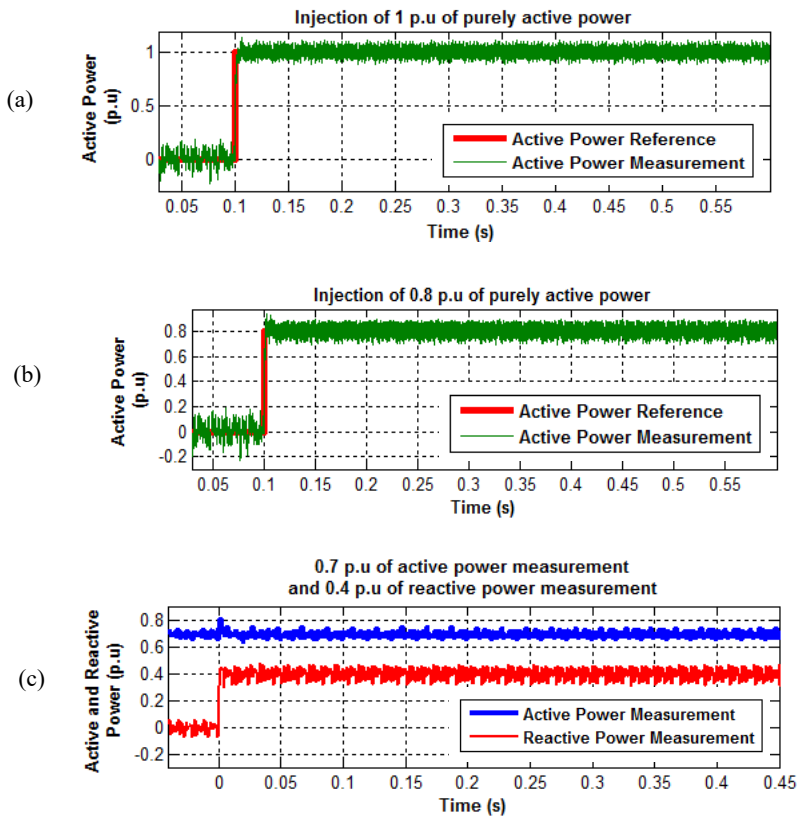
Fig. 3.14. Change in active and reactive power. (a) Active power measurement with reference step of 1 p.u., (b) Active power measurement with reference step of 0.8 p.u., (c) Change in reactive power measurement when reference step is applied from 0 to 0.4 p.u. while the active power is 0.7 p.u.

By observing the results shown in both Fig. 3.14 (a) and Fig. 3.14 (b), it can be concluded that the proposed system is able to control the active power perfectly without any noticeable overshoot in the transient response. Thus, the VF estimation and the active power control at the grid side are working properly. Change in reactive power is shown in Fig. 3.14 (c) with a reference step from 0 to 0.4 p.u. Based on this plot, the system is also capable to control the reactive power injection. The instantaneous power theory has been used to measure the active power, without including any filter. This is the reason why the power had a small ripple due to the inherent noise in the acquisition system boosted by the relatively high impedance of the experimental grid. However, the harmonic content in the current is below 2% (while up to 4% is admitted) and the performance of the overall controller is not affected. Moreover, this ripple could be considered as a proof that the system is able to work even if the sensing is not perfect or if the voltage is affected by some distortion.

It is important to observe the frequency and knowing the voltage magnitude at the point of connection to ensure a secure operation of the whole system. In AC network, the frequency should be ideally maintained as it is the most important global magnitude. In case of the frequency variations, the proposed system must be able to regulate the active power by increasing/decreasing the power when the frequency decreases/increases. In this work, the system frequency used is 50 Hz. Fig. 3.15 shows the injection of active and reactive power.
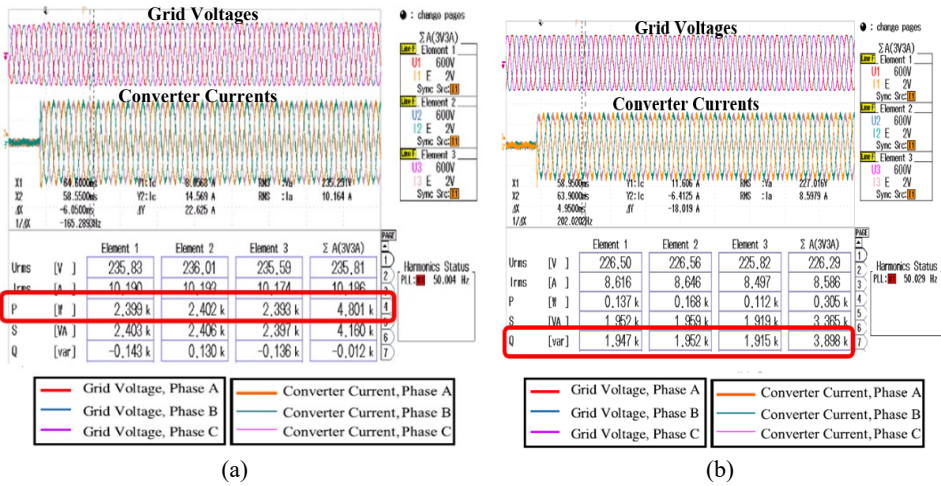
Fig. 3.15. Experimental result captured from the oscilloscope. (a) Injection of active power when reference step is from 0 to 7.5 kW (0.75 p.u.), (b) Injection of reactive power when the step reference is from 0 to 6kVar.

In Fig. 3.15 (a), the step reference has been applied from 0 to 7.5kW (0.75 p.u.). As seen in the plot, the system works well without any obvious transient overshoot during the injection of active power. In Fig. 3.15 (b), the reactive power is injected to the system with

a step reference from 0 to 6 kVar. In an electrical system, the magnitude of the voltage is controlled by the reactive power exchange. Any discrepancy between the supply and demand will give rise to a change of system voltage. The reactive power flow to be injected or absorbed in the line and vice versa is defined by the voltage gradient across the transmission line.

3.5   Summary of the Chapter

It can be summarized that, the VF based control for the case of VSC with LCL filter has been presented in three different methods taking into consideration the used of DSOGI-QSG into the estimation of VF. All the proposed methods have been investigated in both simulation and experimental studies. Based on the presented analysis, it is proven that the VF estimation based on either voltage sensorless operation or capacitor voltage measurements provide a reliable output compared to estimations using capacitor current measurements. VF estimation based on voltage sensorless operation can reduce cost, however for most practical implementations voltage sensors for measuring the capacitor voltage are essential to ensure safe and reliable operation. A highly dependent voltage measurement provides a stable output, thus contributing to a good estimation of virtual flux at the PCC. With a high consistency of VF estimation at PCC, detection of load imbalance is possible. Placing a current sensor to directly measure the capacitor current is not a good choice in a real implementation since the ripple current in the capacitor will attenuate the current flowing in the capacitor and deteriorate the performance of the VF estimation.

Remote Power Control Strategy based on VF Approach

R *enewable Energy Source (RES)-based power plants need to control the active and reactive power at the PCC with the grid, in order to comply with the requirements of the TSOs. This point is normally far away from the power converter station, and the cables as well as the step-up transformers have a non-negligible influence on the delivered power. In order to overcome this drawback, this chapter presents a control algorithm that permits one to control remotely the power injected at the PCC, by adjusting the local controller of the VSCs. As the same as the previous chapter, the synchronization with the grid is done based on the VF concept. The results reveals that the VF estimation is able to produce a reliable estimation of the grid voltage in any point of the network, and makes it possible to calculate the necessary current reference for injecting a desired active and reactive power at a point that can be some kilometres away. In this chapter, the main principle for this remote power control is presented. Likewise, the simulation and experimental results will be shown in order to analyse the effectiveness of the proposed system.*

4.1 Proposed Method of Remote Power Control Strategy

An overview of the system that will be considered as the case study in this chapter as shown in Fig. 4.1. As the same as previous chapter, the LCL filter will be considered due to the fact that it provides a good filtering response while optimizes the overall size and dimensions of the filter. The point of synchronization in previous works is normally located at the primary of the transformer, T_1 as shown in Fig. 4.1. As a difference, in this chapter,

the VF estimation point is considered to be after the transformer, T_2, which contributes to the uniqueness of this work, as the grid impedance is also considered in the VF estimation.
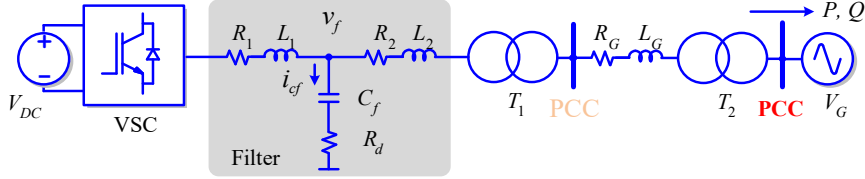
Fig. 4.1. Overview of proposed remote power control strategy.

The VF estimation enables to calculate the power at any point in the network and built controllers to regulate the active and reactive power delivery. Therefore, the VF estimation can regulate the active and reactive power not only at the output of the converter, but it is also possible to regulate the active and reactive power at the connection transformer that interfaces a plant with the main grid. Normally the connection point with the electrical company is far away from the converter. At this point, it is necessary to guarantee the cos phi required by the electrical company in many cases, hence the control proposed in this chapter permits to regulate the active and reactive power delivery in a remote point. The fact of controlling the power in a remote point is relevant as the standards requirement is to regulate the power at the connection point, which is not necessarily the output of the grid-side converter.

4.2   VF Estimation at the PCC

Since the implementation of the VF estimation with LCL filter is similar to the previous section, thus the equation stated in (3.5) - (3.8) as well as the figure shown in Fig. 3.3 - Fig. 3.7 is still valid to be considered. Since the effectiveness of the DSOGI-QSG and FLL to synchronize the VSC with the grid has been proven in the previous chapter, therefore, the implementation of VF estimation in this chapter will also take into consideration the used of DSOGI-QSG and FLL. As the performance of the PR current controller in the previous chapter is really good in the practical implementation, hence the PR current controller was used to accommodate the inner loop control of the VSC in this chapter. In this regard, the implementation of the PR current controller is still based on the transfer function stated in (2.7). The current reference needed for the PR current controller is based on the equation stated in (3.3) and (3.4) where in this regard; the virtual flux at the grid side is the estimation according to (4.1).

The estimation of the converter output voltage as well as the capacitor voltage can be calculated as the same implementation shown in Fig. 3.3. Since the capacitor current will be estimated based on the estimated capacitor voltage, therefore, Fig. 3.4 is still relevant to be considered in this work. However, the estimation at the grid side will have some

differences. Different from the work presented in Chapter 3, the voltage drop at the grid side is determined by multiplying the added value of R_2 and R_g with the integral of the grid current, $\vartheta_g^{\alpha\beta}$. The inductive fluxes drop at the grid side has been considered by multiplying the grid current by the addition of L_2, L_{T1}, L_g and L_{T2}. The values of L_{T1} and L_{T2} are the 3% of the transformer base impedance, namely Z_{T1} and Z_{T2} (the rated power of the transformer T_1 and T_2 are 20 kVA). The resulting positive sequence of VF estimation at the grid side in the stationary reference frame shown in (3.9) can be extended to (4.1) while considering the configuration shown in Fig. 4.1.

$$\chi_g^{\alpha\beta+}(t) = \chi_c^{\alpha\beta+}(t) - (r_2 + r_g) \cdot \vartheta_g^{\alpha\beta+}(t) - (l_2 + l_{T1} + l_g + l_{T2}) \cdot i_g^{\alpha\beta+}(t) \qquad (4.1)$$

The positive sequence coming from the virtual flux estimation at the grid side in (4.1) is shown graphically in Fig. 4.2.
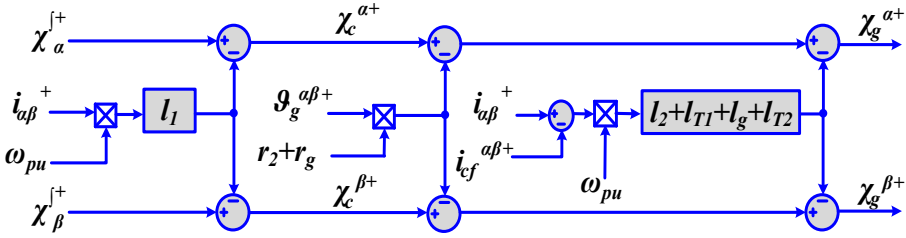
Fig. 4.2. Virtual flux estimation at the grid side.

As difference to the previous estimation shown in (3.9), the grid impedance has been included into the final estimation of the virtual flux. The active and reactive power measurement for both simulation and experimental are based on (4.2) and (4.3) respectively. In this regard, the positive sequence of the VF estimation at the grid side will be used to calculate the active and reactive power.

$$p = \chi_g^{\alpha+} \cdot i_\beta - \chi_g^{\beta+} \cdot i_\alpha = -\chi \perp \cdot i \qquad (4.2)$$

$$q = \chi_g^{\alpha+} \cdot i_\alpha - \chi_g^{\beta+} \cdot i_\beta = \chi \cdot i \qquad (4.3)$$

where $\perp$ is a set of signals that are lagging the original by 90° as the same implementation shown in [17]. As it has been previously mentioned, this work contributes to the actual state of the art by means of designing an application oriented to LCL filter-based configurations, which is broadly extended in the industry. Considering the per phase model of the LCL filter shown in Fig. 4.1, the transfer functions in (3.1) will be used in this work. The LCL-filter parameters and other operating nominal values used for both simulation and experimental studies are listed in Table 4.1.

Table 4.1. System Parameters for both Simulation and Experimental

Abbreviation	Nomenclature	Values
S_N	Rated Apparent Power	10 kVA
$V_g(p\text{-}p)$	Phase to Phase Grid Voltage	400 V
$V_g(p)$	Phase Voltage	230 V
V_{DC}	DC-Link Voltage	700 V
$L_{1(abc)}$	Inductor, L_1	3.4 mH
$L_{2(abc)}$	Inductor, L_2	0.588 mH
$L_{g(abc)}$	Grid Inductance, L_g	10 mH
$C_{f(abc)}$	Filter Capacitor	4.7 µF
$R_{d(abc)}$	Damping Resistor	1.8 Ω
f_{sw} & f_s	Switching & Sampling Frequency	10 kHz

4.3   Simulation Results

Based on the system overview shown in Fig. 4.1, the complete proposed method used for performing both the simulation and experimental analysis is shown in Fig. 4.3.
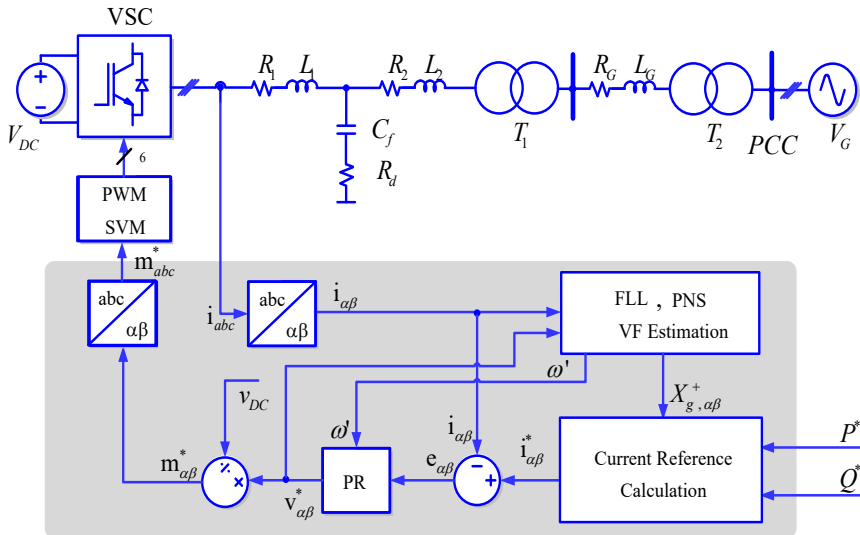
Fig. 4.3. Structure of the study case considered for the simulation and the experimental validation.

The system parameters listed in Table 4.1 are the ones used for both simulation and experimental studies. Considering the parameters listed in Table 4.1 and the proposed method shown in Fig. 4.3, the simulation has been done considering different scenarios.

4.3.1 Simulation Results at the Point After T_1

In order to evaluate the controllability of the proposed control, the first test is oriented to evaluate the performance of the system when tracking the active power after the point T_1, while the second test is focused on evaluating the performance of the system after the point of T_2 which is also the PCC according to Fig. 4.1. The first test is permitted to ensure that the system is working properly before the entire system is simulated. The reference step changes have been made and the results for the first test considering the per-unit values are shown in Fig. 4.4.
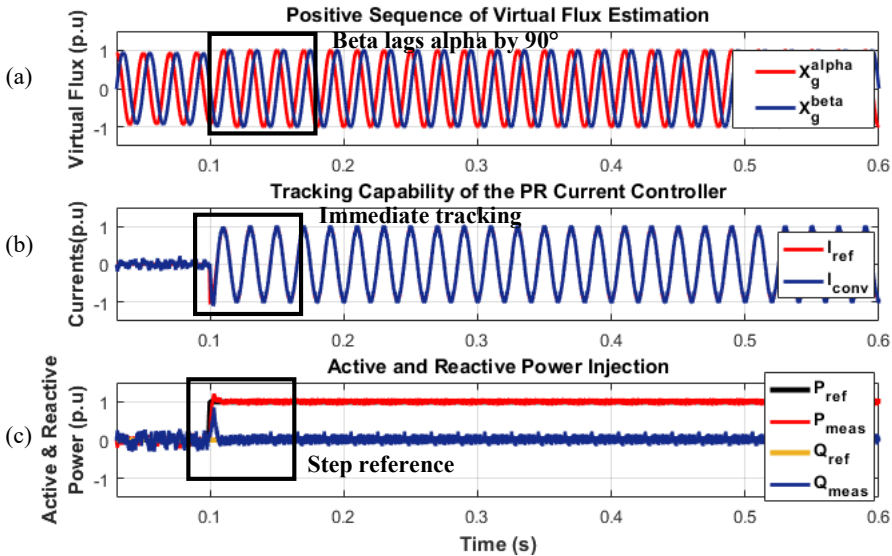
Fig. 4.4. Simulation results (a) Positive sequence of VF estimation after transformer, T_1, (b) Tracking capability of the system of the current controller, (c) Active & reactive power injection to the grid.

The power reference step is performed at $t = 0.1$s. The system is simulated from $t = 0.1$s until $t = 0.6$s. The proportional gain, K_p and the resonant gain K_r used in the simulation are set to 7 and 19 respectively. The plot in Fig. 4.4 (a) shows the positive sequence of the VF estimation after the transformer T_1. As similar to the plot shown in previous chapter, this simulation proves that the voltage sensor-less system is working well, as the positive

sequence VF estimations have been obtained without the need of measuring the grid voltage. The alpha and beta component of VF estimation have the same amplitude of the beta component but lagged 90°, what endorses the VF calculations. The PR current controller used in the inner loop still provides a very fast and good response. In fact, the converter current is able to follow the reference very fast, as it is shown in Fig. 4.4 (b). The active power reference, P_{ref} has been set to 1 p.u (10 kW) while the reactive power reference, Q_{ref} is set to zero. In the Fig. 4.4 (c), it can be seen that the measured active power and the reactive power matched with both power references.

4.3.2   Simulation Results at the PCC

The second test is focused on testing the remote power control. Since the VF estimation in this test is considered after the transformer T_2, it is important to make sure that the output of the VF estimation is perfect without any phase displacement. The power reference step applied in this simulation is performed at $t = 0.1$s and the power is stepped down to zero at $t = 0.4$s in order to observe the performance of the system during the transient as well as in the steady state. As per the first test, the active power reference, P_{ref} has been set to 1 p.u (10 kW) while the reactive power reference, Q_{ref} is set to zero. The simulation results for the proposed system are shown in Fig. 4.5.
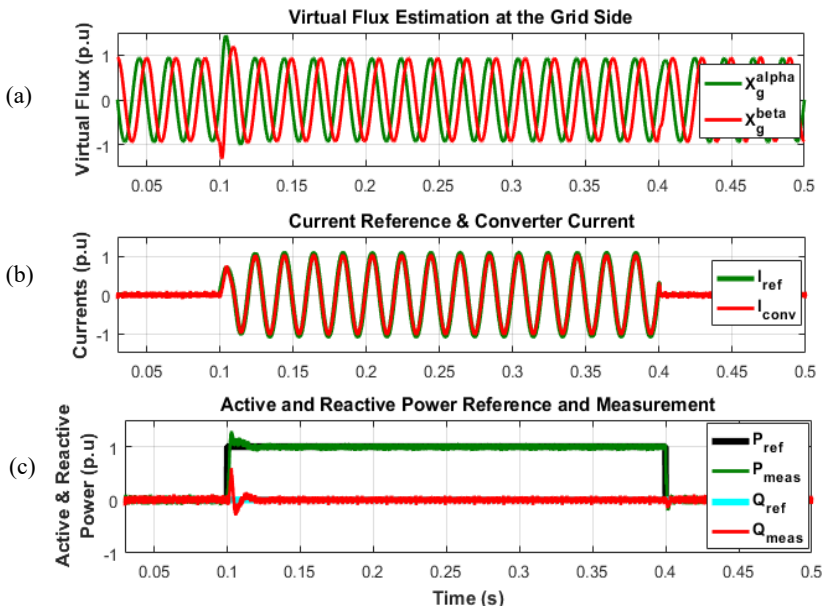
Fig. 4.5. Simulation results. (a) VF estimation at the PCC, (b) Current reference generation and converter current, (c) Active & reactive power reference and measurement.

Based on the simulation results obtained in Fig. 4.5 (a), the estimated virtual flux positive sequence is able to properly estimate the grid voltage conditions. The findings highlighted that the estimation performed by the DSOGI-QSG with FLL works accurately, as the positive sequence components of the virtual flux matches quite well with the value of the line-to-line voltage of the grid. The performance of the PR current controller is one of the important issues in this work because without a proper control, the tracking error will be attained during the steady state condition. However, based on the results shown in Fig. 4.5 (b), it can be concluded that the performance of the proposed control is very good, as the converter current is able to follow the reference without any errors and phase displacement. By referring to the results shown in Fig. 4.5, the proposed system is able to produce good results as long as the required parameters are available during the estimation. With reference to the measured active and reactive power is shown in Fig. 4.5 (c), it can be concluded that the proposed system is able to properly control the power at the remote point. Based on the results shown in Fig. 4.4 (c) and Figure Fig. 4.5 (c), a transient overshoot occurs when the step was applied at $t = 0.1$ s. However, this overshoot is soon attenuated and the system reaches its steady state at $t = 0.105$ s. However, this transient overshoot does not have any significant impact in the active and reactive power injection to the grid.

4.3.3   Change in Active and Reactive Power Injection to the Grid

The performance of the system presented as shown in Fig. 4.1 when different values of active and reactive power should be delivered to the grid will be analysed in this sub-chapter. In doing so, different step changes in both active and reactive power have been applied in order to ensure that the system is able to control remotely the active and reactive power injection. The performance of the system in these scenarios as shown in Fig. 4.6.
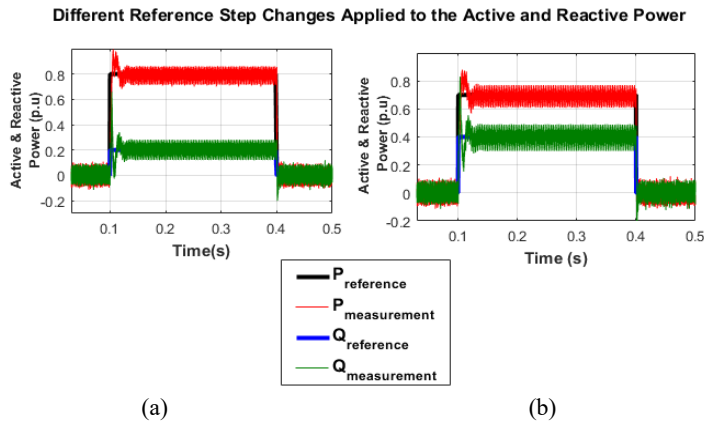
Fig. 4.6. Different step changes in the active and reactive power reference. (a) Step change of 0.8 p. u in active and 0.2 p. u in reactive power, (b) Step change of 0.7 p. u in active and 0.4 p. u in reactive power.

4.3.4   Change in Active and Reactive Power Injection Using Different Values of Grid Inductance.

A different scenario of active and reactive power injection has been captured in Fig. 4.7, where different values of grid inductance of 20 µH and 20 mH have been used. In all cases, the active power reference is set to 1 p.u and the reactive power reference is set to 0 p.u.
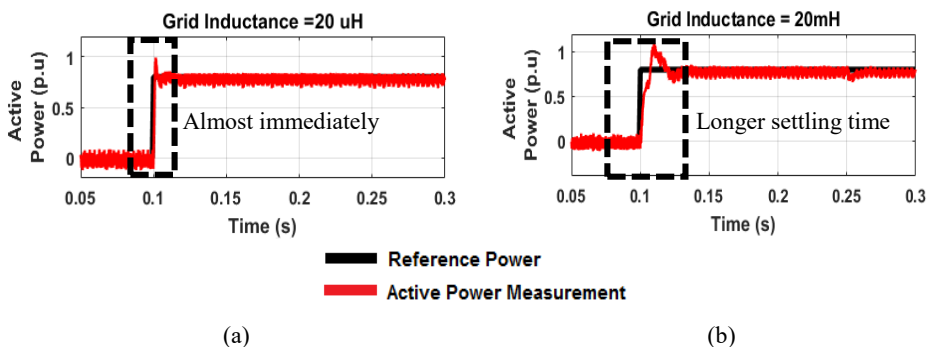
Fig. 4.7. Active power response when using different values of grid inductance. (a) With grid inductance of 20µH, (b) With grid inductance of 20mH.

In the first scenario as shown in Fig. 4.7 (a), the grid inductance used is 20 µH. In the second scenario shown in Fig. 4.7 (b), the grid inductance value used in the simulation is 20 mH. In real applications these values are mainly calculated from the impedance of the transformers and the effect of the cables, although the second one has a much lower influence. Considering the results obtained in Fig. 4.7, it can be concluded that the system has a good performance. All the results show a perfect tracking between the delivered active and reactive power and the corresponding references. The transient performance is also satisfactory in both cases, however, as expected, the lower the grid inductance used, the faster the settling time and steady state can be reached compared to the higher values of the grid inductance.

4.4   Experimental Results

The same experimental setup presented in Fig. 3.11 (b) will be used for the final validation, hence, the 10 kVA inverter is connected to a controlled 230 V phase-to-phase (400 V line-to-line), 50 Hz three phase AC power source through the LCL filter. The programmable dc power supply provides a 700 V dc-link and the proposed control method has been programmed on a dSpace1103 platform (dSPACE Inc., Wixom, MI, USA). The converter, filter as well as the transformer are located in the converter cabinet. In this study, the block diagram of the experimental setup shown in Fig. 3.11 (a) is modified and presented in Fig. 4.8.
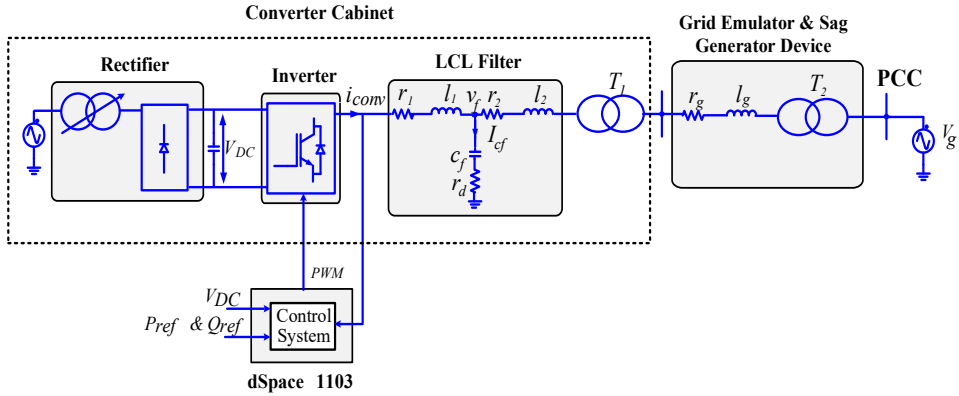
Fig. 4.8. Block diagram of the experimental setup.

As for the experimental investigation, the "grid emulator-voltage sag generator device" has been used for setting a grid inductance value of 10 mH. It is important to remark that the layout of the experimental setup has the same structure of the one used in the simulation analysis presented in the previous section. Moreover, in the experimental setup, it has the same parameters as the ones provided for the simulation, which are listed in Table 4.1. In this workbench the active and reactive power references can be changed easily and the values of measured as well as estimated signals can be easily plotted and captured by using SCADA system which is built using the Control Desk application of dSpace.

4.4.1 Performance of VF-based Controller

The first step of the experimental validation will be focused on testing the performance of the VF based controller, which is now running on dSpace. This first test permits us to evaluate whether the digital implementation of the controller works properly or not. Since the proposed system has been tested in the simulation, the experimental result obtained here is the verification that the proposed method works well in a real platform. As it is shown, the performance achieved is satisfactory and the pipeline of the controller is ensured working at the sampling frequency of the DSP which is embedded in the dSpace. At a first test, the value of the resonant controller is changed in order to carry out a preliminary evaluation of the transient performance. This scenario can be observed in Fig. 4.9.

The waveforms of grid voltages and converter currents have been captured when the reference power has been boosted up from zero to 7 kW (0.7 p. u). In Fig. 4.9 (a) and (b), the K_p and K_r value has been set to 7 and 70 respectively. When the step has been applied, there is transient overshoot occurred on the current even though the system is stable in both open and closed loop.

However, when the resonant gain is reduced for instance to 19, this transient overshoot is eliminated as shown in Fig. 4.9 (c) and (d) improving thus the performance of the system.
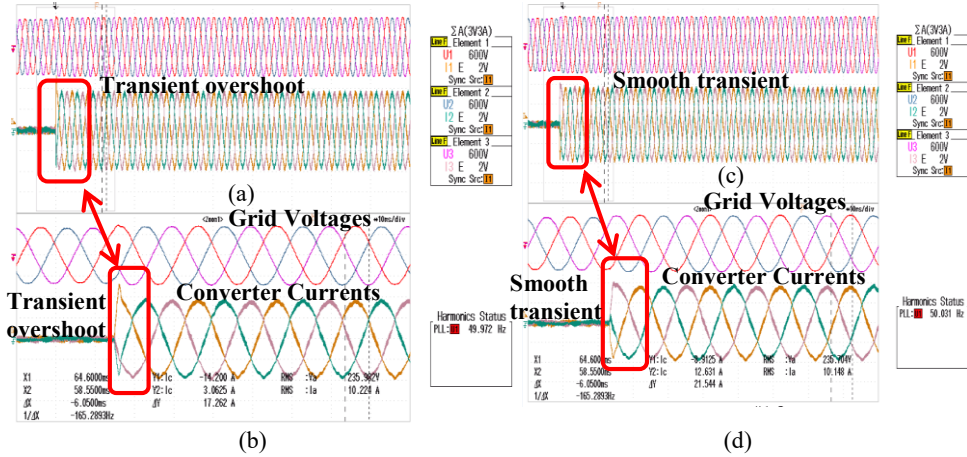
Fig. 4.9. Experimental results captured from the oscilloscope. (a) Experimental results of grid voltages and converter current when $K_p = 7$ and $K_r = 70$, (b) Zoom in version of the grid voltages and converter currents shown in (a), (c) Experimental results of grid voltages and converter current when $K_p = 7$ and $K_r = 19$, (d) Zoom in version of the grid voltages and converter currents shown in (c).

4.4.2   Control of Active Power Delivery

The main objective of this work is to control the active and reactive power injection remotely, monitoring the frequency and knowing the voltage magnitude at the point of connection. It is very important in order to ensure a secure operation of the whole system. Theoretically, in an electrical system, the magnitude of the voltage is controlled by the reactive power exchange. Based on the understanding that any mismatching between the supply and demand will give rise to a change of system voltage, the voltage gradient across the transmission line defines the reactive power flow to be injected or absorbed in the line and vice versa. This is the reason why the positive sequence VF estimation is so significant and important for controlling the reactive power remotely. In Fig. 4.10, the results captured from the oscilloscope are shown when 9.5 kW (0.95 p. u) are injected to the grid.

The result shown in Fig. 4.10 prove that the proposed system works properly. Since the frequency is the most important global magnitude in AC network, it should be ideally maintained by all the interconnected elements in a cooperative manner. It is understandable that in case of the frequency variations, regulating the active power is essential, increasing/decreasing the power when the frequency decreases/increases. In this work, the system frequency used is 50 Hz.
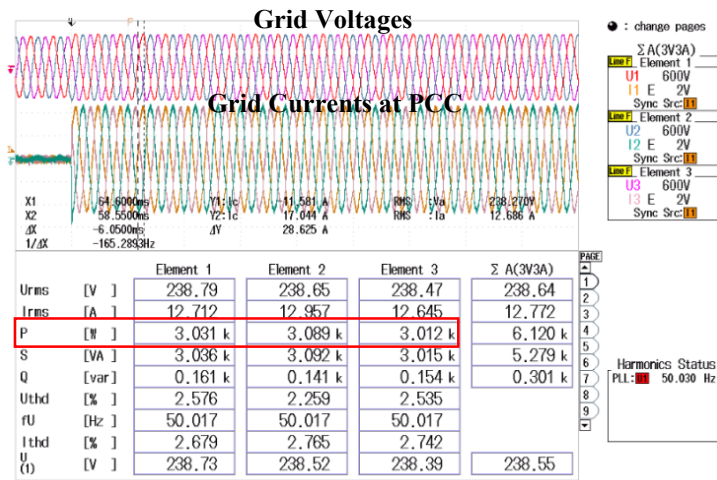
Fig. 4.10. Experimental results captured from the oscilloscope.

When the step reference has been applied, the system works well without any transient overshoot, as shown in Fig. 4.11.
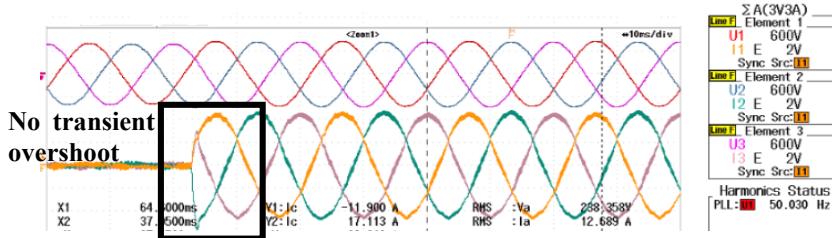
Fig. 4.11. Grid voltages and currents when the step reference from 0 to 10kW (1 p. u) has been applied.

A different value of purely active power reference has been injected to the grid and the experimental results captured from the control desk are shown in Fig. 4.12. The active power reference step has been applied from zero to 7 kW (0.7 p. u) in Fig. 4.12 (a) and 9 kW active power reference has been set in Fig. 4.12 (b). The system is working well and the system has reached its steady state condition at t = 0.02s. In this test, the reactive power measurement in the two cases shown in Fig. 4.12 are equal to zero, which matches with the value of reactive power reference that has been set in the experiments.
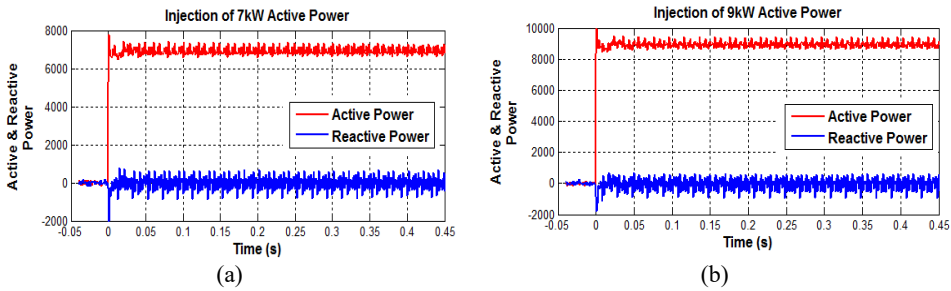
Fig. 4.12. Injection of purely active power. (a) Results captured from the control desk when power reference is set to 7 kW (0.7 p. u); (b) Results captured from the control desk when power reference is set to 9 kW (0.9 p. u).

4.4.3 Control of Reactive Power Delivery

In these case studies, the reactive power reference step of 6kVar (0.6 p. u) has been applied in order to see the behavior of the system at both transients and steady state condition. It can be concluded from the plots, a very smooth transient state condition of the reactive power injection can be seen in Fig. 4.13.
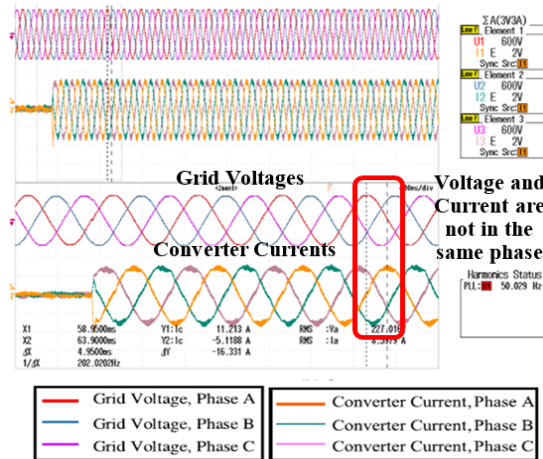
Fig. 4.13. Purely reactive power injection.

It is also clear that the voltages and currents are not in phase when reactive power has been injected. It can be seen that the converter current, I1 lags the grid voltage, U1 by almost 90°.

Considering that the system is working at 50Hz fundamental frequency, the time for one full cycle is equal to 20ms. Since one full cycle is equivalent to 360°, $\Delta X = 4.95$ms is considered as 89.1° phase lag $((360° \times 4.95 \text{ ms}) /20\text{ms})$.

In Fig. 4.14, the experimental results captured from the control desk considering different values of active and reactive power injections to the grid have been presented. The reactive power reference step has been applied in order to see the behavior of the system at both transients and steady state condition. It can be concluded from the plots; a very smooth transient state condition of the reactive power injection can be seen.
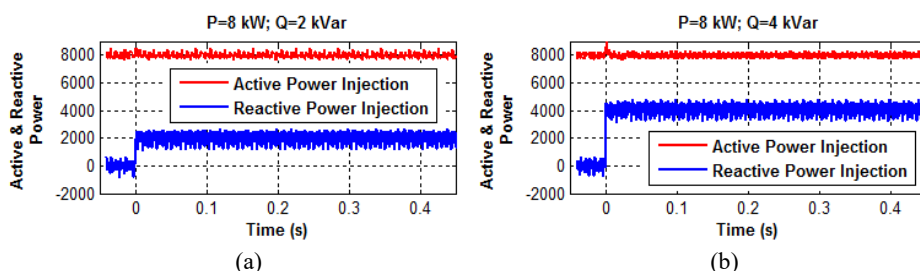
Fig. 4.14. Injection of reactive power: (a) Step change from 0 to 2 kVar when active power injection is 8 kW; (b) Step change from 0 to 4 kVar when active power injection maintains at 8 kW.

Based on the simulation and experimental results shown in this chapter, it can be concluded that the proposed system based on the VF-based synchronization is able to control the injection of active and reactive power to the grid. In general, the presented results at both simulation and experimental validated the accuracy of VF estimation, since the synchronization with the grid and the corresponding control of the active and reactive power injection to the PCC is based on the VF signals. All the parameters involved in Chapter 3 and Chapter 4 are easy to control and change by considering the control desk application. In this regard, it is also easy to control the injection of active and reactive power and monitoring the behavior of other signals. Fig. 4.15 shows the screenshot of the control desk application.
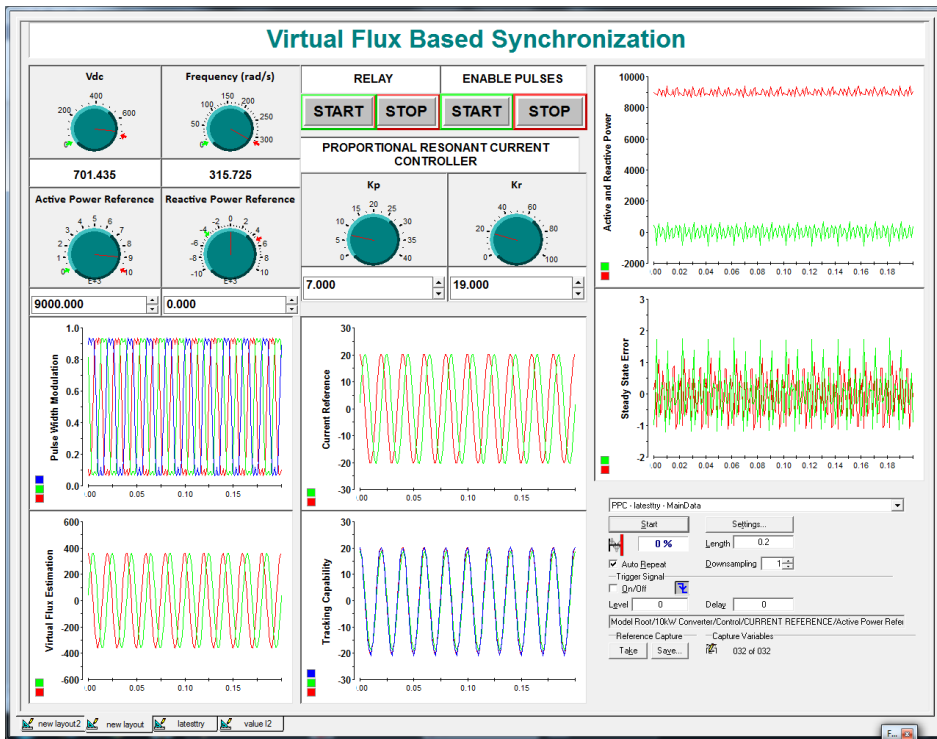
Fig. 4.15. Control Desk Application.

4.5 Summary of the Chapter

In summary, this chapter presented the control strategy based on virtual flux approach to control the active and reactive power injection to the grid remotely. As the point of common connection is not after the second inductor of the filter, the parameters of the grid needs to be considered in the virtual flux estimation. With the configurations shown in Fig. 4.1 and the results presented in both simulation and experimental, the active and reactive power can be controlled remotely as long as all the parameters needed are available and the measurement of the current is good.

Virtual Synchronous Flux Controller (VSFC)

T *his chapter presents a VSFC as a new control solution for the grid connected power converter. Taking into consideration the virtual flux approach, this control strategy could provide an inherent synchronous connection with the grid without the need of having any additional synchronization system. Its advanced synchronous behavior enables the controller to comply with the* grid code requirements. VSFC proposes Magnetic Controller in the inner control loop of a grid connected power converter which in this regard, the controller is responsible to generate the modulation reference to the converter. The proposed system is an alternative to the classic current control, as it is based on controlling an output flux in the power converter. It derives from the main idea that grid connected power converter can be controlled as a virtual synchronous generator where flux is a variable to control the operation. The main concept of the VSFC as well as the experimental results will be presented to validate the effectiveness of the proposed system. The remaining part of the chapter is organized as follows: In the first section, there is an overview of the proposed control methods which includes the explanation of the magnetic controller. The explanation also includes the structure of virtual reluctance and the flux controller used in the inner loop control and the control strategy used in the outer loop control of the power converters. It will be continued with the simulation and experimental results before concluding the paper with a discussion about the obtained performances.*

5.1   VSFC-based Power Converter Control

The VSFC presented in this chapter is totally different from the remarkable works conducted in the virtual flux concept that has been applied in the power generation application. The VF presented in [15-17] and [112, 113] are used to estimate the grid

voltage condition without measuring directly the voltage with sensors. The integral of virtual flux is the estimated voltage at the output of the filter's inductance. However, the estimation of VF is highly dependent on the accurate values of the filter as well as a good measurement of the currents. The virtual flux discussed in [15-17] and [112, 113] are just used to perform the grid synchronization and the information is used in the power/current reference calculations.

The power converters equipped with the VSFC are designed to be able to work in all kind of networks, no matter the short circuit ratio between the grid and the converters or the X/R ratio of the line. The VSFC is able to force an inductive behavior permitting to standardize the frequency and voltage regulation loops. This controller combines a magnetic controller in the electrical part of the system which is responsible to regulate the virtual flux at the output of the power converter, while the outer loop control is used to provide the flux reference to be tracked by the magnetic controller. The VSFC does not use any additional synchronization system because it is capable to perform an inherent synchronous connection with the grid. The VSFC also does not require any specific hardware or power converter topology as it can be applied in any commercial power converter by just changing its control layer. Considering the control structure will be implemented in stationary reference frame, an overview of VSFC that includes the magnetic controller and the outer loop control is shown in Fig. 5.1.
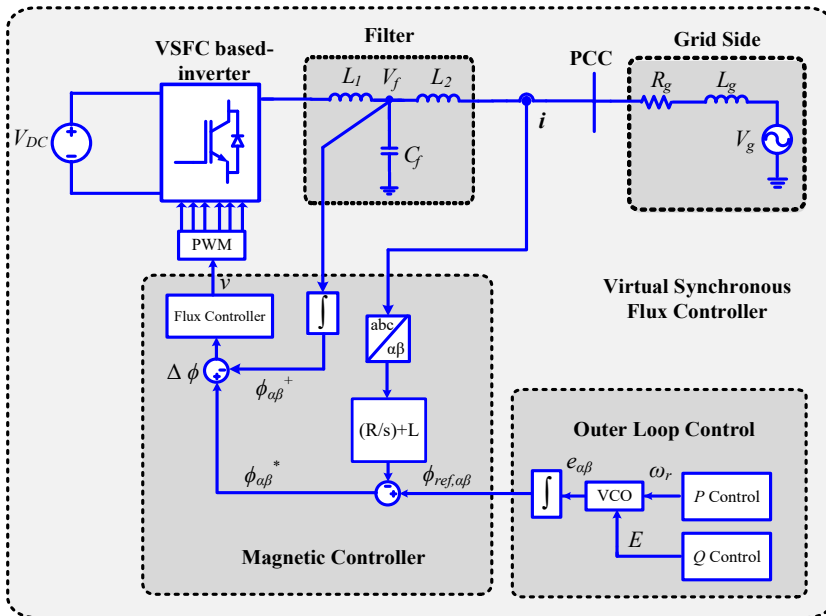
Fig. 5.1. Simplified diagram of the implementation of Virtual Synchronous Flux Controller.

The flux controller will regulate the error between the reference flux and the measurement flux as depicted in Fig. 5.1. The error is generated by subtracting the flux measurement, $\phi_{\alpha\beta}{}^{+}$ from the virtual flux reference, $\phi_{\alpha\beta}{}^{*}$. The flux measurement can be obtained by integrating the measured voltage. The voltage sensor is normally available at the capacitor so that the V_f in this analysis is known as the voltage across the capacitor. The converter output voltage can be formalized as follows;

$$V_{conv} = L\frac{di}{dt} + V_f \tag{5.1}$$

The equation stated in (5.1) can be integrated to obtain the virtual flux as shown in (5.2).

$$\int V_{conv} = L \cdot i + \int V_f \rightarrow \phi_{conv} = L \cdot i + \phi_f \tag{5.2}$$

5.2   Inner Regulation based on Magnetic Controller

The magnetic controller as shown in Fig. 5.2 is able to perform the electrical performance emulation as the same as a synchronous generator.
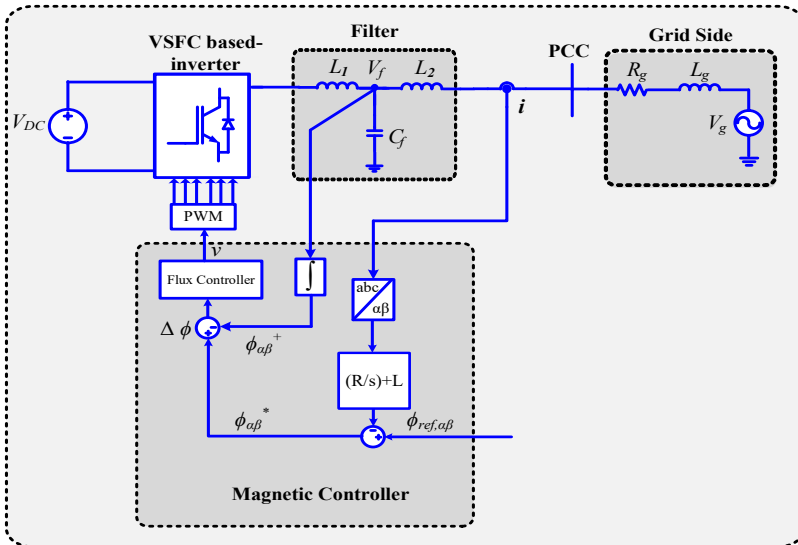
Fig. 5.2. The structure of Magnetic Controller.

One of the advantages of magnetic controller compared to the previous solutions, is that, this structure permits not having two cascaded controllers in the inner regulation but just a single controller to control the flux. This feature makes it suitable for systems with low switching frequency where the delay of cascaded loop can affect the overall performance of the system. In this regard, the dynamic performance of the VSFC could be improved as delay of cascaded loop can be avoided.

The behavior of the power converter controlled by this controller is more harmonious with the overall performance of the electrical network. The magnetic controller directly regulates the virtual flux injected by the grid connected power converter which is totally different from the classical current controller or those based on emulation of synchronous machine. Contrary to the previous solution, in this work, virtual reluctance structure will be used to emulate the electrical part in order to suit with the virtual flux implementation.

An implementation of the virtual reluctance on the other hand also inherits the electrical characteristics of the synchronous generator. In contrast with the virtual impedance concept, this system does not perform as a voltage control, hence it is possible to get rid of the drawbacks related to the use of derivative terms. It is also different from the virtual admittance concept as there is no need to calculate the internal voltage in an outer loop that is later regulated by an inner current control loop. However, as the same as virtual admittance, the virtual reluctance is programmable, so that the values can be changed in order to achieve the most convenient performance. By controlling this magnitude, it is possible to set a predominant inductive behavior between the connection of the power converter and the grid. The closed loop structure of the Magnetic Controller is shown in Fig. 5.3.
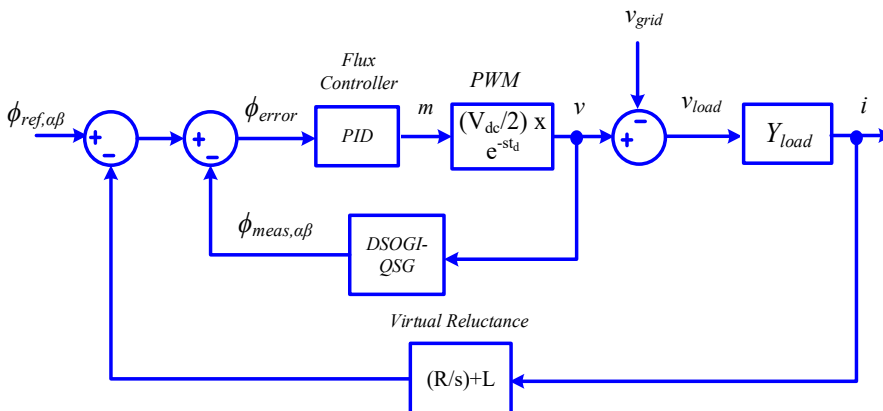
Fig. 5.3. Closed loop structure of Magnetic Controller

Fig. 5.4 shows the equivalent vector diagram of magnetic controller when considering the virtual resistance, R_{vir} almost equal to 0. In this regards, the flux drop is obtained just by multiplying the measured current with the virtual inductance, L_{vir}. It is clearly seen that the virtual flux reference ϕ^* has 90° phase shift from the converter voltage, v. The reference generated by the outer loop controller, ϕ_{ref} is based on the integration of the virtual emf, e_{vir} hence the 90°phase shifted can be clearly seen from the vector diagram.
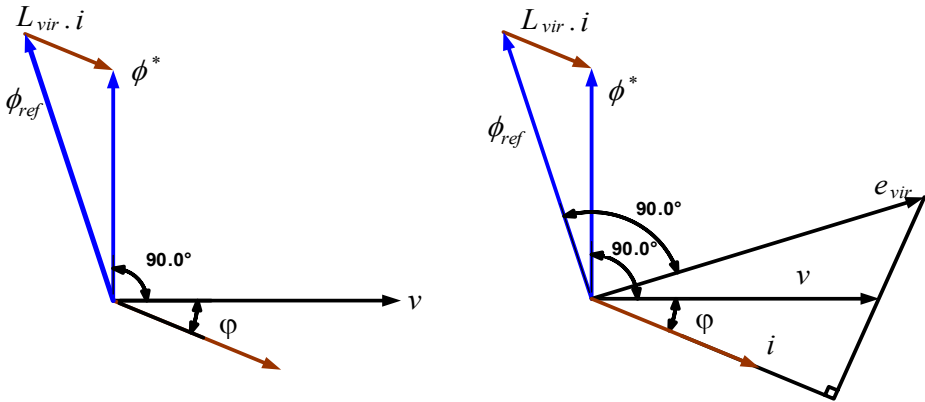
Fig. 5.4. Equivalent vector diagram of Magnetic Controller considering $R_{vir} \approx 0$.

5.2.1 Emulation of Electrical Part

Before going further on the explanation of electrical part of VSFC, it is worth to consider the grid connection of Synchronous Generator as shown in Fig. 5.5.
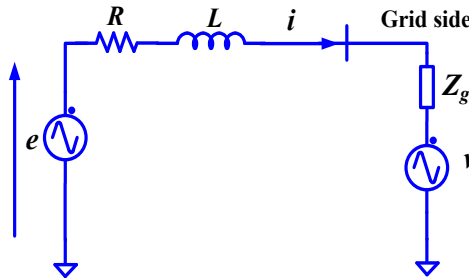
Fig. 5.5. Connection of grid connected synchronous generator.

Referring to Fig. 5.5, the point of connection is represented by the AC grid voltage, v, where the AC internal induced electromotive force is represents by 'e' and the output impedance of the generator is denoted as R-L. The dynamic performance of the principle shown in Fig. 5.5, therefore, can be described in (5.3) and the Laplace transform differential equation is given by (5.4) respectively.

$$v(t) = e(t) - Ri(t) - L\frac{di(t)}{dt} \tag{5.3}$$

$$v(s) = e(s) - i(s)(R + Ls) \tag{5.4}$$

Based on the dynamical equation stated in (5.4), it clearly shows that the grid connected power converter works as a controlled voltage source. The voltage drops across the virtual impedance, $R+Ls$ is subtracted from the emf induced, e, in order to calculate the voltage reference, v. The measured current, i, in this case will be affected by the derivative term in order to calculate the voltage reference. The measured current is also possible to be affected by the noise and other interferences. In most application of virtual impedance concept, the current is normally filtered to avoid overshoot caused by the derivative term. The filter plays a very important role to stabilize the performance. In the virtual impedance concept shown in Fig. 5.6 (a), the internal voltage loop is needed and the classic synchronization is still required in order to obtain the phase angle. The other concern is the grid impedance estimation algorithms require quite a complex structure and it is difficult to guarantee the accuracy.
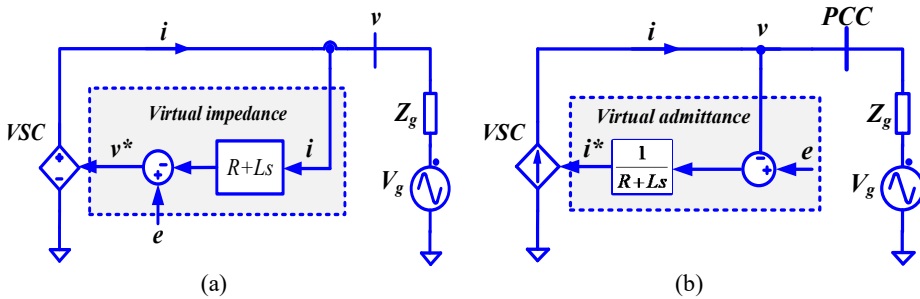
Fig. 5.6. Electrical emulation approach: (a) Implementation based on Virtual impedance concept, (b) Implementation based on Virtual admittance concept.

The other approach to emulate the electrical part is by implementing the virtual admittance as shown in Fig. 5.6 (b). With such an implementation, the derivatives term of current can be avoided thus the differential equation given in (5.4) can be modified to (5.5).

$$i(s) = \frac{1}{R + sL}(e(s) - v(s))$$

(5.5)

In this regards, it can be clearly seen that virtual admittance working in an opposite principle of the virtual impedance. It works as a current source instead of the voltage source as describe in [52] and [53]. By adopting the virtual admittance in the control layer the need of the filter is not necessary anymore. Contrary to the previous solution, in this work, a virtual reluctance structure will be used to emulate the electrical part in order to suit with the virtual flux implementation. Implementation of the virtual reluctance on the other hand inherits the same electrical characteristics of the synchronous generator. By rearranging the impedance of the line, the virtual reluctance can be obtained and the implementation of the virtual reluctance is shown in Fig. 5.7 respectively.
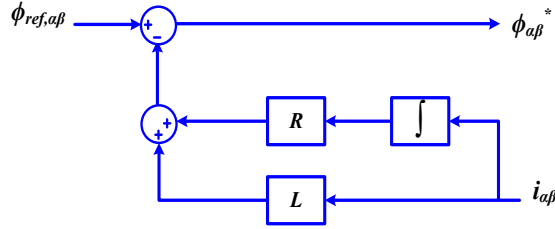
Fig. 5.7. Implementation of virtual reluctance.

The flux reference, $\phi_{\alpha\beta}{}^*$ is generated by considering the subtraction of the flux drop from the reference, $\phi_{ref,\alpha\beta}$ generated by the outer loop controller. Thus the reference flux, $\phi_{\alpha\beta}{}^*$ is given by (5.6).

$$\phi_{\alpha\beta}{}^*(s) = \phi_{ref,\alpha\beta}(s) - \left[\left(i_{\alpha\beta}(s) \right) \cdot \left(\frac{R}{s} + L \right) \right]$$

(5.6)

Table 5.1 shows the parameters of the Magnetic Controller that will be used in the simulation and experimental studies.

Table 5.1. Magnetic Controller Parameters.

Symbol	Quantity	Value
R	Virtual resistance	0.1 p.u
L	Virtual inductance	0.3 p.u
H	Virtual inertia constant	2
ζ	Damping ratio	0.707
K_P	Proportional gain	3.5
K_R	Resonant gain	10
ω	Nominal AC frequency	314.159 rad/s

5.2.2   Stability Analysis

Since the flux controller is a new control structure in a grid connected power converter control, the system stability analysis need to be done in order to ensure that the system is stable enough to be implemented in the experimental validation. Furthermore, the system stability is very important to ensure that the inner loop controller is working on the optimal performance within its stability region. The whole system can be defined as a stable system, if the closed loop system is also in a stable condition. A stable system is expected to have a frequency response at the closed loop system that decays over time. The closed loop system will be unstable if the frequency response is larger over time. The closed loop system of the flux controller shown in Fig. 5.8 will be considered in the stability analysis in this section. The closed loop system shown in Fig. 5.8 includes the processing delay and filter in continuous domain.
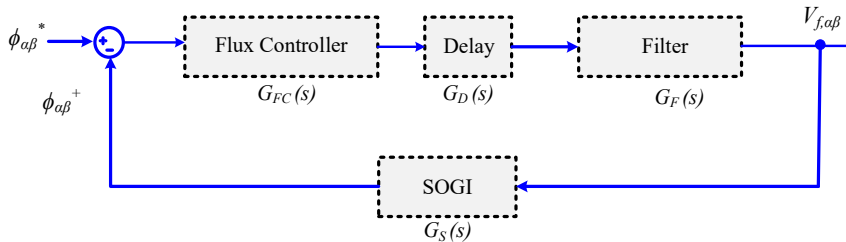
Fig. 5.8. Closed loop structure of the flux controller.

As explained in Chapter 5.1, flux controller is used to regulate the error of the flux signal in order to achieve zero error during the steady state condition. Based on figure shown in Fig. 5.8, the $V_{f,\,\alpha\beta}$ is the converter output voltage which is used as a feedback. The closed loop transfer function of the flux controller can be described in (5.7). Based on this transfer function, $G_{FC}(s)$ is the structure of flux controller where in this regard, the structure of Proportional Resonant is adopted. The delay of the system, $G_D(s)$ can be based on (5.8) where the T_s is the sampling time. Considering the filter structure shown in Fig. 5.1 and Fig. 5.2, the transfer function of the filter, $G_F(s)$ is given in (5.9) respectively.

$$FC_{CL}(z) = \frac{G_{FC}(z) \cdot G_D(z) \cdot G_F(z)}{1 + G_{FC}(z) \cdot G_D(z) \cdot G_F(z) \cdot G_s(z)} \tag{5.7}$$

$$G_D(s) = \frac{1}{1 + sT_s} \tag{5.8}$$

$$G_F(s) = \frac{1}{L_1 C_f L_2 s^3 + \left(L_1 L_2\right)s^2} \tag{5.9}$$

As shown in Fig. 5.2, the flux measurement is obtained by integrating the measured capacitor voltage. In the practical implementation, this integration is obtained by using the SOGI-QSG, therefore the stability analysis carried out in this section will also consider the transfer function of the SOGI-QSG. The transfer function of the closed loop system in (5.7) is discretized using the 'c2d' function in MATLAB. This function is used to convert from continuous domain to the discrete domain by means of using the Zero Order Hold (ZOH) method. In practice, there are a lot of discretization methods such as First Order Hold, Forward Euler, Backward Euler, Tustin, Tustin with Prewarping, Zero-pole Matching and Impulse Invariant. However, the ZOH provides a good representation of the average voltage output from the converter PWM operation on the filter inductor during one sampling period. The stability analysis is carried out using the SISO tool in MATLAB and the root locus as well as the bode diagram of the system described in (5.7) are shown in Fig. 5.9 and Fig. 5.10 respectively.

As shown in Fig. 5.10 the gain and phase margin are the two important elements to describe the stability status of the system in the stability analysis. If the system has a lower margin, it means that it is less stable. The greater the margin, the more the system stables. This shows that the system become marginally stable after varying the gain and phase up to a certain threshold. The best way to describe the margin is how far it is from the unstable point. For the case of the gain margin, the unstable point is at 0dB gain while the unstable point for the phase margin is at -180° phase. However, further variation of gain and phase could lead to unstable system. The gain margin is expressed in dB and the phase margin is expressed in degree. It is worth to mention that, even though the gain margin is stable,

it is important for the system should at least have a phase margin of 60° for a good and stable system. Based on the bode diagram shown in Fig. 5.10, the system is stable with a gain margin of 12.3 dB and the phase margin is equal to 67 degree. This analysis is taking into consideration the K_P and K_R value as stated in Table 5.1, ω_o = 314 rad/s and ω_c = 5 rad/s.
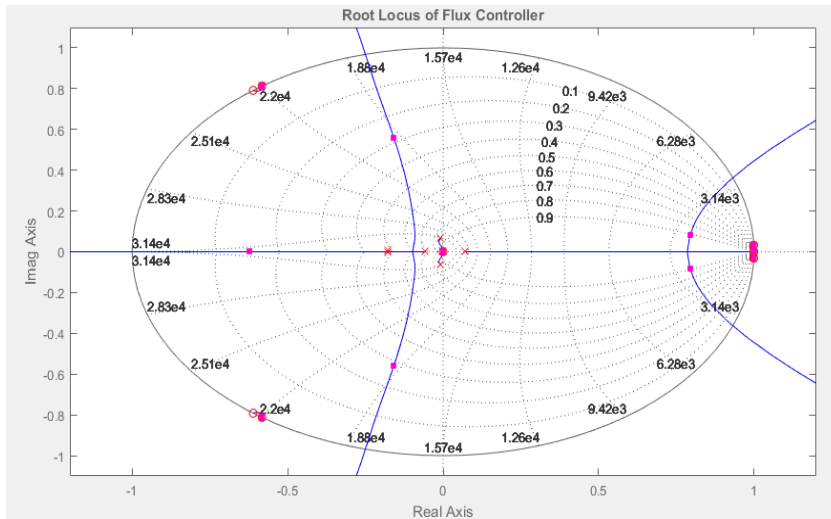
Fig. 5.9. Root locus of the system.
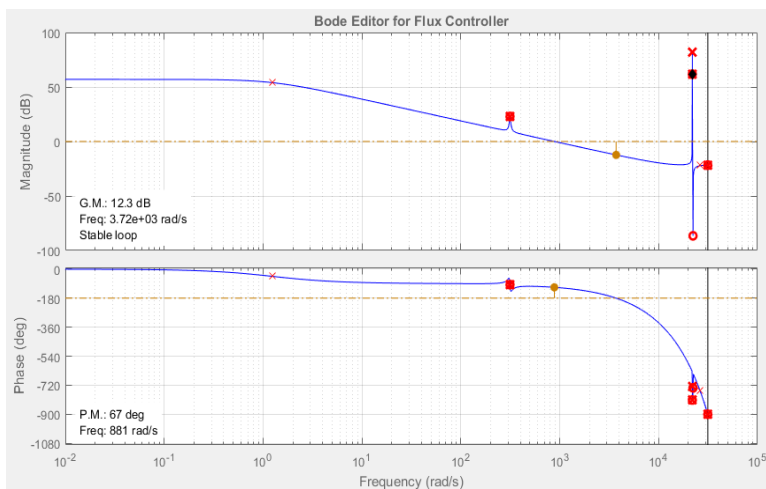
Fig. 5.10. Bode diagram of the Flux Controller.

5.3   Outer Loop Control

The implementation of the outer loop control of the VSFC is shown in Fig. 5.11. The structure shown in Fig. 5.11 is used to provide the reference to the magnetic controller. The input needed by the Voltage Controlled Oscillator (VCO) is come from the frequency generated by the active power control (P Control) and the amplitude, E generated by the reactive power control (Q Control). The main components of the P Control and Q Control are shown in Fig. 5.12 (a) and Fig. 5.12 (b) respectively.
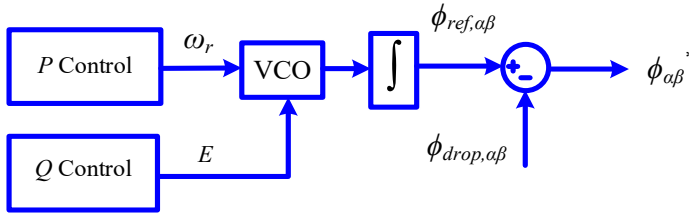
Fig. 5.11. Simplified structure of the outer loop control.

| (a) | (b) |
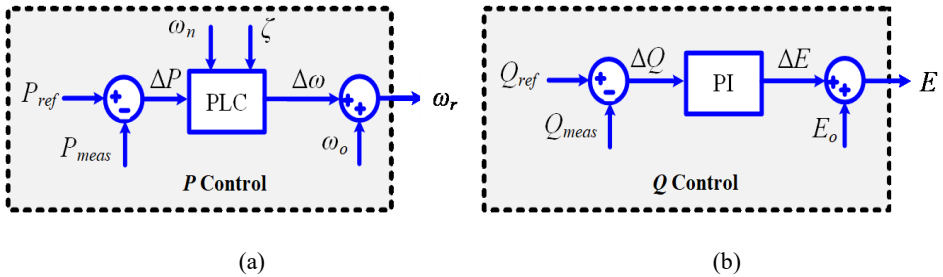
Fig. 5.12. Outer loop control of the VSFC (a) Active Power Control, (b) Reactive Power Control.

As shown in Fig. 5.12 (a), the main component of the P Control is the Power Loop Controller (PLC). The PLC transfer function is given by (5.10) respectively.

$$PLC(s) = k\,\frac{\omega_c}{s + \omega_c} \tag{5.10}$$

where the k is the gain and ω_c is the cut off frequency which can be obtained by (5.11);

$$\omega_c = 2 \cdot \zeta \cdot \omega_n \tag{5.11}$$

The symbol ζ indicates the damping factor and ω_n is the natural frequency of the virtual electromechanical model. The natural frequency, ω_n can be calculated by (5.12) respectively.

$$\omega_n = \sqrt{\frac{P_{max}}{J\omega_s}} \quad \text{or} \quad \omega_n = \sqrt{k\omega_c P_{max}} \tag{5.12}$$

The k and ω_c are the two control parameters to be adjusted to set the natural frequency and the damping factor. The active power transfer equation considering that the synchronous generator is mainly inductive is given by (5.13).

$$P = P_{max} \cdot \delta \tag{5.13}$$

where δ is the phase angle difference between the virtual electromotive force, e given by the controller and the grid voltage, v. The P_{max} is represents the maximum value of active power that can be delivered by the synchronous generator and the P_{max} can be calculated by (5.14).

$$P_{max} = \frac{E \cdot V}{X} \tag{5.14}$$

where the E and V are the RMS values of e and v respectively. The reactance is denoted as X. The dynamic relationship between the input and output power can be written as (5.15).

$$\frac{P_s}{P_{in}}(s) = \frac{k\omega_c P_{max}}{s^2 + 2\zeta\omega_c s + k\omega_c P_{max}} \tag{5.15}$$

The inertia as well as the damping behavior can be controlled by specifying the values of the natural frequency, ω_n and the damping factor, ζ. The damping factor can be determined as (5.16).

$$\zeta = \sqrt{\frac{\omega_c}{4kP_{max}}} \tag{5.16}$$

As shown in Fig. 5.12 (b), a simple Proportional Integral (PI) is used in the Q Control in order to provide the amplitude, E. The transfer function of the PI controller is given in (5.17).

$$G_{PI}(s) = \frac{K_i}{s} \tag{5.17}$$

The VCO block illustrated in Fig. 5.11 is a simple oscillator that used to provide the virtual *emf* signal in $\alpha\beta$ components. The implementation of the VCO block can be based on (5.18).

$$e = \begin{bmatrix} e_\alpha \\ e_\beta \end{bmatrix} = VCO(E, \omega) = \sqrt{3}E \begin{bmatrix} \cos\theta & -\sin\theta \\ \sin\theta & \cos\theta \end{bmatrix} \cdot \begin{bmatrix} E_d \\ E_q \end{bmatrix} \tag{5.18}$$

The reference, $\phi_{ref,\,\alpha\beta}$ is the integration output generated by the VCO, e. The angle, θ in this case is the frequency of virtual *emf* in rad and E is the amplitude of the virtual *emf* respectively. The integration of e_α and e_β will provide a set of virtual flux reference, needed in the magnetic controller of VSFC.

$$\phi_{ref,\alpha\beta}(t) = \int e_{\alpha\beta}(dt) \tag{5.19}$$

5.4   Simulation Results

The simulation study conducted in this section is to ensure that the Magnetic Controller is working fine and the Flux Controller is able to track the reference flux. Considering the parameters listed in Table 5.2, the simulation has been carried out. Since, the Flux Controller adopted the PR control, the same values of K_P, K_R, ω_c and ω_o were used in the stability analysis, and have been considered in the simulation.

Table 5.2. VSFC-based power converter technical data used in the simulation.

Symbol	Quantity	Value
S_{VSFC}	Nominal power	10 kVA
V_{AC}	Nominal AC-voltage	380V
ω	Frequency	314.15926 rad/s
f_{sw} & f_s	Switching & Sampling Frequency	10 kHz
$L_{1(abc)}$	Output filter inductors	3.4 mH
$L_{2(abc)}$	Inductor, L_2	0.588 mH
$C_{f(abc)}$	Output filter capacitors	4.7 μF
R	Virtual Resistance	0.1 p.u
L	Virtual Inductance	0.3 p.u

The simulation results is shown in Fig. 5.13. In Fig. 5.13 (a), the simulation of the virtual flux measurement in $\alpha\beta$ is presented. The flux measurement in this plot is the output after integrating the measured voltage using the DSOGI-QSG. It can be clearly seen in the plot that both virtual flux at alpha and beta components have the same amplitude with beta component is 90° phase shifted from the alpha component.
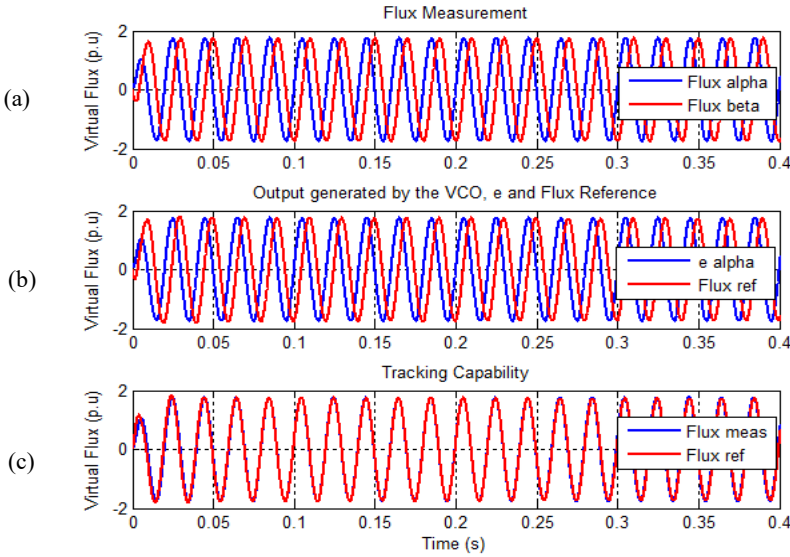
Fig. 5.13. Simulation Results of VSFC.

Fig. 5.13 (b) shows the amplitude of *emf* in alpha component and the flux reference, ϕ_{ref} also in alpha component that is generated after integrating the amplitude of *emf, e*. It should be noted that the flux reference should be lagged the *emf, e* by 90° and based on the plot shown in Fig. 5.13 (b), the system is working as it is required. The performance of the flux controller is shown in Fig. 5.13 (c). In this plot, it shows that the tracking capability of the system is good where the flux controller is capable to force the measurement flux to follow the reference flux.

5.5   Experimental Validation of VSFC

The experimental setup for the final validation consists of a 5 kVA VSFC based-inverter which is connected to a controlled 380 V line-to-line, 50 Hz three phase AC power source through the LCL filter. The second inductor of the filter is based on 5% of the 20kVA isolating transformer impedance. The inverter has been powered by a

programmable dc power supply that provides a 650V dc-link. The inverter, LCL filter and the transformer are located inside the converter cabinet. The control loop of the VSFC has been programmed on a dSpace1103 platform (dSPACE Inc., Wixom, MI, USA). Similar to the results shown in Chapter 3 and Chapter 4, the control parameters can be easily changed and all the required signals can be easily captured by using SCADA system which is built using the Control Desk application of the dSpace. An overview of the experimental setup is shown in Fig. 5.14 (a) and the real structure is shown Fig. 5.14 (b).
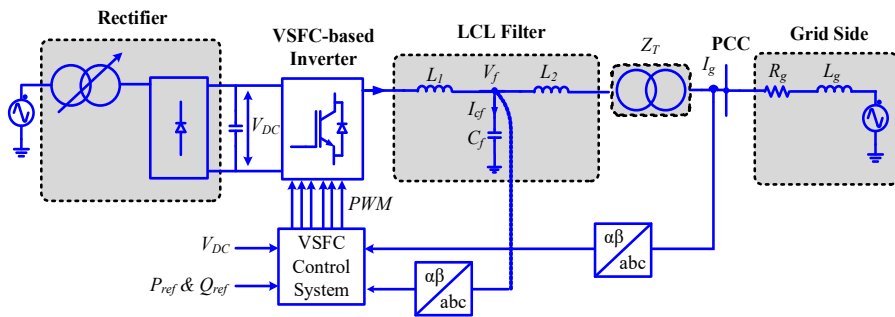
(a)
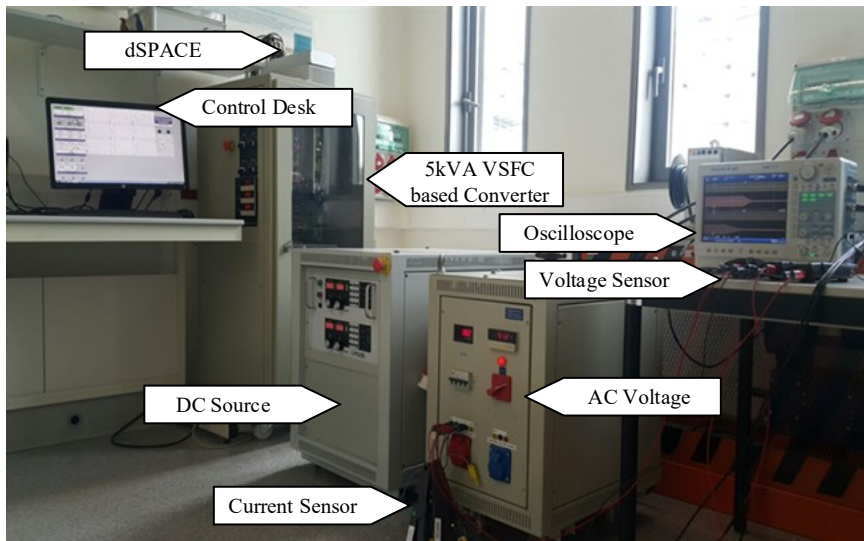
(b)

Fig. 5.14. (a) Overview of experimental setup, (b) The real experimental setup used in the lab.

The technical data for the VSFC-based power converter is listed in Table 5.3.

Table 5.3. VSFC-based power converter technical data.

Symbol	Quantity	Value
S_{VSFC}	Nominal power	5 kVA
V_{DC}	Nominal DC-voltage	650V
V_{AC}	Nominal AC-voltage	380V
f_{AC}	Nominal AC-frequency	50Hz
f_{sw} & f_s	Switching & Sampling Frequency	10 kHz
$L_{1(abc)}$	Output filter inductors	6 mH
$L_{2(abc)}$	Inductor, L_2	0.588 mH
$C_{f(abc)}$	Output filter capacitors	4.7 μF

5.5.1   Start-Up Process

In the case of VSFC-based converter, it is important to initialize the controller properly before it successfully enabled, and the system is seamlessly connected to the grid. This process is essential to avoid the possibility of inrush current in the converter due to the large flux reference injected. This problem normally happened when the voltage difference between the virtual electromotive force and the grid voltage are relatively high. The process starts with the connection of the converter with the DC source and AC source, where both DC and AC voltage are set at the nominal value as shown in Table 5.3. The system starts with the enabling of the modulation pulses and the flux controller with a flux reference is set to zero. At this stage, the value of the virtual inductance is set to be ten times higher from the per unit value stated in the important parameters of the Magnetic Controller tabulated in Table 5.1. However, this high value is set only for a very short time. After this step, the power converter is ready to start its synchronization with the grid. It is worth to mention that during this stage, the active and reactive power references are set to zero. The power measurement in this case calculated the reference flux from the virtual reluctance block that is already working instead of the measured flux. Hence, the flux reference tracked by the flux controller is equal to zero.

5.5.2   Performance of VSFC in the Digital Implementation

The first step of the experimental validation was to focused on testing the performance of the magnetic controller. This first test is carried out in order to evaluate whether the magnetic controller works properly or not in the digital implementation. The performance

of magnetic controller is very important to ensure that the system is capable to achieve zero error during the steady state condition and also to have a good performance during the transient state condition. The experimental result obtained here permits to verify that the proposed method is also working well in a real platform. It should be noted that the parameters listed in Table 5.1 and Table 5.3 have been considered in the practical test.

Fig. 5.15 shows the tracking capability of the flux controller captured from the control desk application. It is proven that the tracking capability shown in Fig. 5.15 is perfect without any significant tracking error. The flux measurement shown in Fig. 5.16 has a nice sinusoidal because the integration of voltage is performed using the DSOGI-QSG, therefore, the input voltage has been filtered by the filtering component of the DSOGI-QSG. The flux reference on the other hand has been shaped by the virtual reluctance where in this case the high value of the inductance is set in the beginning just to reduce the possibility of high current when the reference step is applied.
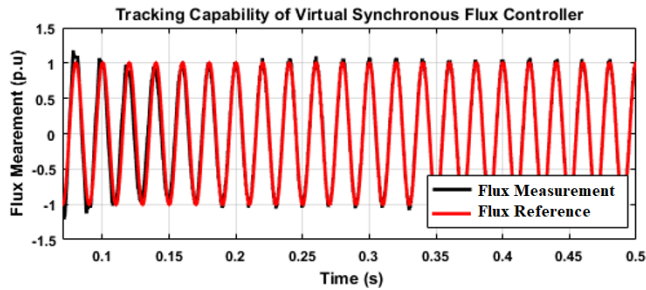
Fig. 5.15. Tracking performance.
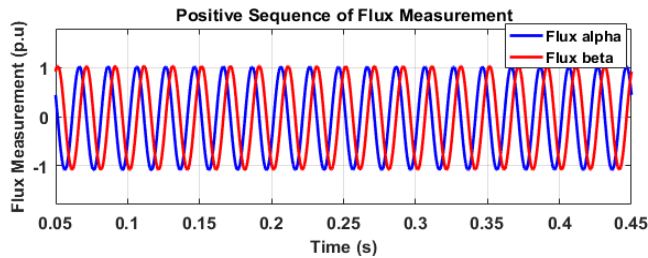
Fig. 5.16. Flux measurement in alpha and beta components.

As proven, the DSOGI-QSG performed the integration of the measured voltage perfectly as the positive sequence of the virtual flux measurement is balanced and has a nice sinusoidal. The alpha component on the other hands leads the beta component by 90°. However, as can be understood by the theoretical, the beta components of the virtual flux measurement lagged the alpha component of the capacitor voltage by 90°. This analysis is also the same in the case of virtual flux reference, $\phi_{ref,\,\alpha\beta}$. It should be noted that the integration of e_α and e_β also will be based on the DSOGI-QSG. The integration of e_α

and e_β is important to obtain a set of virtual flux reference, $\phi_{ref,\,\alpha\beta}$ needed by the magnetic controller. In this analysis, only positive sequence of the flux measurement will be considered. In all cases, a constant frequency of 314.159 rad/s is fed to the DSOGI-QSG.

Fig. 5.17 on the other hand, shows the performance of the controller during the transient and steady state condition. In this test, the active power reference is set from 0 to 4 kW and from 4kW to 0 in order to observe the capability of the system in controlling the flux. The system is working properly where it can be observed that the system performance during the transient and steady state is normal without any excessive transient overshoot when the reference step is applied. Both voltage profile and the current did not suffer from any unwanted perturbation.
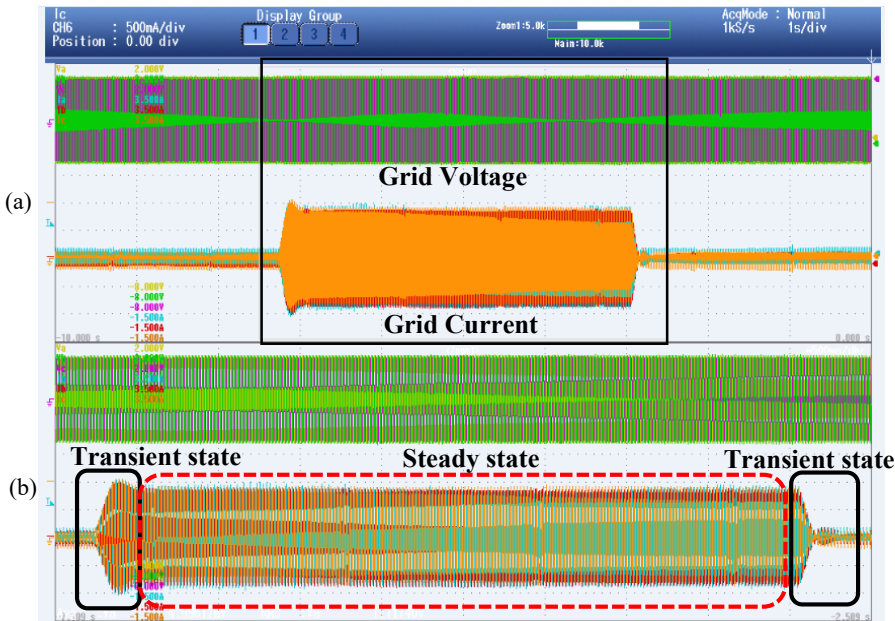
Fig. 5.17. Performance of the flux controller during transient and steady state condition (a) The waveforms of grid voltage and current, (b) Zoom version of the waveforms shown in (a).

The test continued with an evaluation of the voltage and current during the transient state where at this stage the reference power has been stepped up and stepped down in order to analyze the behavior of the system. Fig. 5.18 (a) shows the voltage and current when the reference power is stepped up from 0 to 4kW and Fig. 5.18 (b) on the other hand shows the voltage and current when the reference power is stepped down to 0. Based on the results obtained, the current and voltage profile seems good and it is proven that obtaining the virtual flux using the DSOGI-QSG in digital implementation of VSFC is working fine.

(a)   (b)
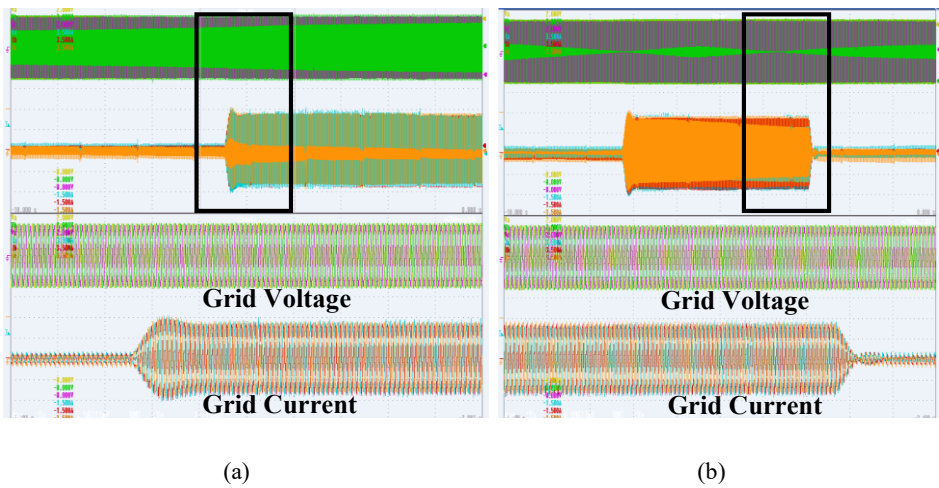
Fig. 5.18. Grid voltage and current waveform. (a) Step-up in reference power, (b) Step-down in reference power.

Fig. 5.19 shows the quality of the three phase voltage and current using the control of VSFC. The good performance of the system keeps the three phase voltage and current in a balanced sinusoidal. Based on the results shown, the VSFC control loop implementation is able to keep the voltage and current at the PCC as stable as possible.
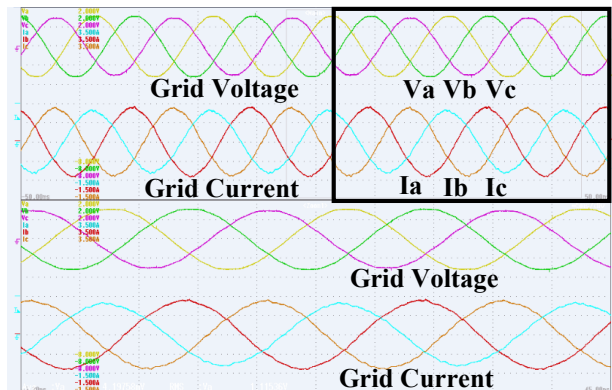
Fig. 5.19. Zoom-in of grid voltage and grid current.

5.5.3   Control of Active and Reactive Power Delivery

The control of active and reactive power at the PCC is one of the most important studies in the VSFC control system. In this test, the reactive power reference is set to zero. Fig.

5.20 shows the active and reactive power measurement when the active power reference changed from 0 to 4kW and stepped down from 4kW to 0.
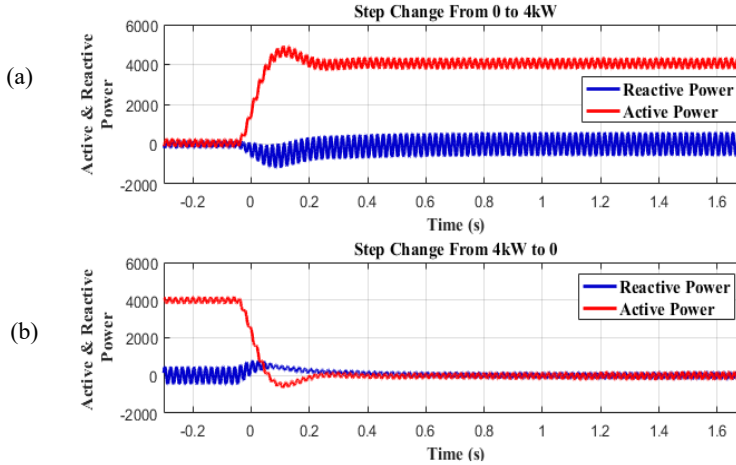
Fig. 5.20. Active and reactive power measurement captured from the control desk. (a) When active power reference is changed from 0 to 4kW, (b) When active power reference is stepped down from 4kW to 0.

It is clear that both active and reactive power measurement are matched with the active and reactive power reference thus proved that VSFC control system is able to properly control the active and reactive power of the system in digital implementation.

5.5.4   Performance of VSFC using Ideal Integration with High Pass Filter

Another test has been carried out just to observe the performance of VSFC if the virtual flux is obtained by using the ideal integration that includes the high pass filter. Fig. 5.21 shows the voltage and current when the active power reference is stepped from 0 to 4kW. In this experimental validation, it is clearly seen that the system is working as it is required. It proved that the ideal integration can still be considered in the experimental validation but it requires the high pass filter in order to provide a satisfactory performance. As discussed in [15], ideal integration will cause a drift and offset problems in the digital implementation. However, if compared the quality of current shown in Fig. 5.21 (b) with the quality of current shown in Fig. 5.19, it can be said that the quality of the current is better by using the DSOGI-QSG.
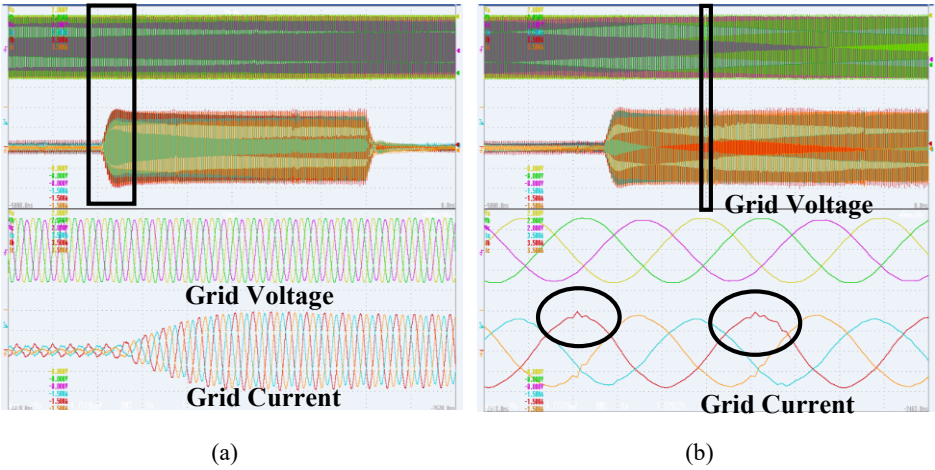
Fig. 5.21. Output from oscilloscope when the virtual flux is obtained by using ideal integration. (a) Grid voltage and current when active power reference is stepped up from 0 to 4kW, (b) Quality of voltage and current.

However, when the system was analyzed under the transient state condition, the system worked well during the step up and step down of reference power as shown in Fig. 5.22 as long as the high pass filter is included in the practical implementation.
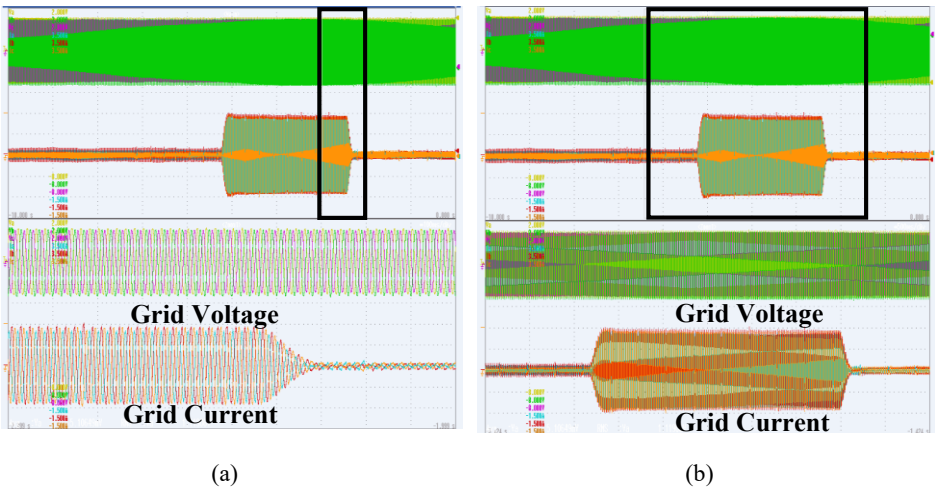
Fig. 5.22. The grid voltage and current (a) Zoom in version when the active power reference is stepped down to 0, (b) Zoom in version when the active power is stepped up from 0 to 4kW and from 4kW to 0.

5.6   Summary of the Chapter

In summary, the VSFC-based control for the case of VSC with LCL filter has been presented. In this work, the flux measurement obtained by integrating the converter output voltage. The DSOGI-QSG has been considered in the integration of converter output voltage because of its good performance as proven in the previous chapters. The proposed methods of VSFC have been investigated in the experimental studies and, based on the presented analysis, it is proven that the magnetic controller is able to regulate the virtual flux injected by the grid connected power converter. With a reliable output as shown in the test, the magnetic controller can be an alternative solution to the conventional current controller. The outer loop control of the VSFC is capable to provide a good transient response when the active power reference has been stepped-up and stepped-down. In general, the experimental results prove that the VSFC is reliable and able to provide an effective control solution for the power converters which are integrated in power generation facilities based on distributed generation systems.

Conclusion and Future Work

6.1 Conclusion

The research question stated in Chapter 1.5 has been resolved in Chapter 3, Chapter 4 and Chapter 5. In Chapter 3, a comparative study of three different implementations of VF estimation for grid synchronization of VSC with LCL filter has been presented, which permits to control the active and reactive power flow at the grid side of the filter. The results from simulation of all the three methods confirmed that accurate parameters of the connection filter, as well as a good current measurement are crucial to ensure a good estimation of the grid voltage, which is necessary for controlling the active and reactive power injected to the grid at the PCC.

The fast synchronization and the smooth reference tracking achieved in transient conditions, have demonstrated the effectiveness of the DSOGI-VF and the PR current controller used in the proposed system. Among the investigated methods, the VF estimation based on voltage sensor-less operation offers several advantages in terms of cost reduction and improvement of the system modularity. However, for most practical applications, the measurement of the capacitor voltages is not a significant disadvantage. This voltage measurement is a stable output and contributes positively to carry out a good estimation of the virtual flux at the PCC. However, when combined with VF-estimation, the synchronization method can also maintain operation in case of voltage sensor failure. On the other hand, placing a current sensor for measuring directly the capacitor current has been shown to be a less preferable solution especially in practical implementation, since the ripple current in the capacitor is very large compared to the fundamental frequency component.

Thus, noise and ripple components might propagate into the control system and deteriorate the performance of the VF estimation which in this case is better to be avoided.

The experimental verification has demonstrated that the VF approach based entirely on estimated signals for the LCL filter configurations and can provide good grid synchronization for controlling the power delivered to the PCC. Among the three investigated estimation methods, the voltage sensorless operation was selected for validation as it is the most complex scenario, and the results achieved permits also to validate the performance of the other two methods presented.

The other topics that have been presented is the control method based on VF synchronization that permits to control the active/reactive power delivery in a remote point of the grid, as for instance at the transformer connection point. The results from the simulation as well as the experimental studies prove that the VF based synchronization is a good method to estimate the grid voltage condition without considering any voltage sensor. Furthermore, the proposed VF-based synchronization has shown to have a good behaviour which contributes to achieve a good performance of overall systems in the experimental validation. Similar to the findings in Chapter 3, the synchronization with the grid is very fast and the smooth reference tracking is achieved in transient conditions. The most obvious finding that emerges from this study is that the VF estimation is reliable to estimate the voltage at different points along the grid as long as the parameters needed for the estimation are available. Therefore, it is possible to control the power injection/absorption remotely. Additionally, the presented control solution in this dissertation offers a flexible way to control the active and reactive power. The possibility of controlling the active and reactive power flow at remote location in the grid can be useful for several applications.

In Chapter 5, this dissertation presented a new control solution based on VSFC approach. The VSFC works perfectly with the magnetic controller as a new invention for the inner control of grid connected power converter. As the magnetic controller directly regulates the virtual flux, it is totally different from the classical current controller or those based on emulation of synchronous machine. As shown in the practical implementation in the lab, the magnetic controller is able to get self-synchronized without external synchronization system. In the electrical part, the virtual reluctance has been adopted instead of considering the virtual impedance or virtual admittance. The values of virtual reluctance are programmable; hence it is easy to change in order to achieve the most convenient performance. By controlling this magnitude, it is possible to set a predominant inductive behavior between the connection of the power converter and the grid. The VSFC is very useful for the control of power converters with low switching frequencies as it does not require two cascaded controllers, therefore, it is capable to reduce the delays in experimental implementation. The VSFC not only meets the requirement set by the grid codes but offers advanced functionalities that are followed in the new grid codes.

The findings of research studies presented in Chapter 3, Chapter 4 and Chapter 5 meets all the scope of works listed in Chapter 1.4 and most importantly meets the aim and objectives of the PhD Dissertation. However, the limitation of the research works opens for further discussion and research that will be highlighted in the following section.

6.2 Future Work

There are a few topics that are relevant to be considered as a future research works based on the results and limitation of research presented in the previous chapters. The future works on virtual flux approach can be either focused in the area of VF estimation and power control or in the local control of VSFC based power converter.

The possible issues in the VF-based Synchronization for the power converter with the LCL Filter that are relevant to be investigated in the future are listed as follows:

- The VF estimation structure shown in Chapter 3 and Chapter 4 considered the used of LCL Filter with a passive damping. This analysis could be expanded by considering the active damping in the filter configurations.
- The scope of investigated VF-based synchronization for power converter with LCL Filter in this dissertation is focused on balanced condition only. Therefore, the work can be expanded with an investigation of VF estimation for power converter with LCL Filter under unbalanced conditions.
- The current controller used in both Chapter 3 and Chapter 4 are based on Proportional Resonant Current Controller. The presented strategies can be further studied with a various types of current controller and the results can be compared with the one presented in this dissertation.
- The implementation of VF-based synchronization in this dissertation is implemented in stationary reference frame, more exploration can be done by considering the implementation of VF estimation with positive and negative sequence component in decouple double synchronous reference frame. This method may require more complex structure in digital implementation compared to the one presented in this dissertation.

Since the topic of VSFC-based power converter control is still new, many future works can be done to improve the performance of VSFC. The methods and results presented in Chapter 5 can be used as a basis for future works. The possible topics that can be further studied are listed as follows:

- Further elaborations and studies on the magnetic controller performance. The focus of the studies can be based on the effect of ranging values of virtual reluctance. Further analysis can be made on how the ranging values of virtual reluctance will affect the overall performance of VSFC.
- This dissertation only focuses on the balance conditions therefore further research on the unbalanced conditions or weak grid will add more values to the research area. The implementation in digital platform should take care on the inrush current or transient overshoot that might occur when the step reference is applied.
- Further investigations can be made on the stability of the magnetic

     controller. It could focus on the analysis of stable and unstable loop and how the values of proportional gain and integral gain term will affect the stability of the system.

- Further studies can be focus on the outer loop control of the VSFC. Different control strategies can be proposed to control the dynamical performance of the VSFC-based converter.

- The implementation of VSFC in this dissertation considered the used of LCL filter, hence, the analysis on VSFC with L filter and LC filter can be further explored and the stability analysis of this system should be simpler. The performance of VSFC considering the L and LC filter can be compared with the results presented in this dissertation.

6.3   Closing Remarks

    The control strategies of power electronics converter based on virtual flux approach which have been presented in Chapter 3, Chapter 4 and Chapter 5 respectively. Virtual flux estimation in Chapter 3 and Chapter 4 is applied to estimate the grid voltage that includes the filter values into the calculation. The virtual flux estimation is used to perform a synchronization of the power converter with the grid where the output of the estimation is used to generate the reference needed for the current controller. The control structure presented in Chapter 5 on the other hand is different from those two control strategies where no synchronization system is needed since it is capable to seamlessly connect to the electrical network. All the control strategies presented in this dissertation can be applied in any commercial power converter, without having a specific converter topology. The results and analysis of the proposed control strategies answered the research question stated in Chapter 1.5.

References

[1]   "The First Decade 2004 - 2014 : Ten Years of Renewable Energy Progress," Renewable Energy Policy Network for the 21st Century (REN21), Paris, France, 2014.

[2]   "Renewable 2019 - Global Status Report," Renewable Energy Policy Network for the 21st Century, Paris, France, 2019.

[3]   "Global Renewables Outlook - Energy Transformation 2050," International Renewable Energy Agency, Abu Dhabi, 2020.

[4]   "World Energy Outlook 2020 : Renewable Energy Market Update," International Energy Agency, Paris, 2020.

[5]   "Renewables 2020 - Analysis and Forecast to 2025," International Energy Agency, Paris, France, 2020.

[6]   "Sustainable Recovery - World Energy Outlook Special Report," International Energy Agency, Paris, France, 2020.

[7]   F. Blaabjerg, K. Ma and Y. Yang, "Power Electronics - The Key Technology for Renewable Energy System," in *Proc. EVER*, 2014.

[8]   F. Blaabjerg, Y. Yang, D. Yang and X. Wang, "Distributed Power-Generation Systems and Protection," *Proceedings of the IEEE,* vol. 105, no. 7, pp. 1311-1331, 2017.

[9]   R. Teodorescu, M. Liserre and P. Rodríguez, Grid Converters for Photovoltaic
        and Wind Power Systems, United Kingdom: Wiley, 2011.

[10]   N. Vasquez, L. D. C. Garcia, C. Hernandez, E. Vazquez, H. Lopez, I. Cervantes
        and J. Iturria, "A Grid Connected Multilevel Current Source Inverter and its
        Protection for Grid Disconnection," *International Journal of Photoenergy,* vol.
        vol. 2013, 2013.

[11]   K. K. Gupta and S. Jain, "A Multilevel Voltage Source Inverter (VSI) to Maximize
        the Number of Levels in Output Waveform," *International Journal of Electrical
        Power & Energy Systems,* vol. 44, no. 1, pp. 25-36, 2013.

[12]   P. Rodriguez, A. Luna, J. I. Candela, R. Mujal, R. Teodorescu and F. Blaabjerg,
        "Multiresonant Frequency-Locked Loop for Grid Synchronization of Power
        Converters Under Distorted Grid Conditions," *IEEE Transactions on Industrial
        Electronics,* vol. 58, no. 1, pp. 127-138, 2011.

[13]   P. Rodriguez, A. Luna, R. S. Munoz Aguilar, R. Teodorescu, F. Blaabjerg and I.
        E. Otadui, "A Stationary Reference Frame Grid Synchronization Converters
        Under Adverse Grid Conditions," *IEEE Transactions on Power Electronics,* vol.
        27, no. 1, p. 99–112, 2012.

[14]   A. Luna, J. Rocabert, J. I. Candela, J. R. Hermoso, R. Teodorescu, F. Blaabjerg
        and P. Rodriquez, "Grid Voltage Synchronization for Distributed Generation
        Systems Under Grid Fault Conditions," *IEEE Transactions on Industry
        Applications,* vol. 51, pp. 3414-3425, 2015.

[15]   A. Kulka, "Sensorless Digital Control of Grid Connected Three Phase Converters
        for Renewable Sources," Ph.D Dissertation, Norwegian Univ. Sci. Technology,
        Trondheim, Norway, 2009.

[16]   J. A. Suul, A. Luna, P. Rodríguez and T. Undeland, "Voltage Sensorless
        Synchronization to Unbalanced Grids by Frequency-Adaptive Virtual Flux
        Estimation," *IEEE Transactions on Industrial Electronics,* vol. 59, p. 2910–2923,
        2012.

[17]   J. A. Suul, "Control of Grid Integrated Voltage Source Converters Under
        Unbalanced Conditions – Development of An Online Frequency Adaptive Virtual
        Flux Based Approach," Ph.D Dissertation, Norwegian Univ. Sci. Technology,
        Trondheim, Norway, 2012.

[18]   M. Malinowski, M. P. Kazmierkowski, S. Hansen, F. Blaabjerg and G. D. Marques, "Virtual-Flux-based Direct Power Control of Three-Phase PWM Rectifiers," *IEEE Transactions on Industry Applications,* vol. 37, no. 4, p. 1019–1027, 2001.

[19]   M. Malinowski, M. P. Kazmierkowski and A. M. Trzynadlowski, "A Comparative Study of Control Techniques for PWM Rectifiers in AC Adjustable Speed Drives," *IEEE Transactions on Power Electronics,* vol. 18, no. 6, pp. 1390 - 1396, 2003.

[20]   M. Malinowski, G. Marques, M. Cichowlas and M. Kazmierkowski, "New Direct Power Control of Three-Phase PWM Boost Rectifiers under Distorted and Imbalanced Line Voltage Conditions," in *2003 IEEE International Symposium on Industrial Electronics*, Rio de Janeiro, Brazil, Brazil, 9-11 June 2003.

[21]   J. A. Suul and T. Undeland, "Flexible Reference Frame Orientation of Virtual Flux Based Dual Frame Current Controllers For Operation in Weak Grids," in *2011 IEEE Trondheim PowerTech*, Trondheim, Norway, 2011.

[22]   J. A. Suul, M. Molinas and P. Rodríguez, "Exploring the Range of Impedance Conditioning by Virtual Inductance for Grid Connected Voltage Source Converters," in *2012 3rd IEEE PES International Conference and Exhibition on Innovative Smart Grid Technologies*, Berlin, Germany, 2012.

[23]   A. Egea-Alvarez, S. Fekriasl, F. Hassan and O. Gomis-Bellmunt, "Advanced Vector Control for Voltage Source Converters Connected to Weak Grids," *IEEE Transactions on Power Systems,* vol. PP, no. 99, pp. 1-10, 2015.

[24]   J. C. Vasquez, R. A. Mastromauro, J. M. Guerrero and M. Liserre, "Voltage Support Provided by a Droop-Controlled Multifunctional Inverter," *IEEE Transactions on Industrial Electronics,* vol. 56, no. 11, p. 4510–4519, 2009.

[25]   J. C. Vasquez, J. M. Guerrero, A. Luna, P. Rodríguez and R. Teodorescu, "Adaptive Droop Control Applied to Voltage-Source Inverters Operating in Grid-Connected and Islanded Modes," *IEEE Transactions on Industrial Electronics,* vol. 56, p. 4088–4096, 2009.

[26]   J. Kim, J. M. Guerrero, P. Rodriguez and R. Teodorescu, "Mode Adaptive Droop Control with Output Impedances for an Inverter-based Flexible AC Microgrid," *IEEE Transactions on Power Electronics,* vol. 26, no. 3, p. 689–701, 2011.

[27]   W. Yao, M. Chen, J. Matas, J. M. Guerrero and Z. M. Qian, "Design and Analysis of the Droop Control Method for Parallel Inverters Considering the Impact of the Complex Impedance on the Power Sharing," *IEEE Transactions on Industrial Electronics,* vol. 58, no. 2, pp. 576 - 588, 2011.

[28]   Q. C. Zhong, "Robust Droop Controller for Accurate Proportional Load Sharing Among Inverters Operated in Parallel," *IEEE Transactions on Industrial Electronics,* vol. 60, p. 1281–1290, 2013.

[29]   K. D. Brabandere, B. Bolsens, J. V. D. Keybus, A. Woyte, J. Driesen and R. Belmans, "A Voltage and Frequency Droop Control Method for Parallel Inverters," *IEEE Transactions on Power Electronics,* vol. 22, no. 4, pp. 1107-1115, 2007.

[30]   J. M. Guerrero, J. C. Vasquez, J. Matas, L. G. DeVicuna and M. Castilla, "Hierarchical Control of Droop -Controlled AC and DC Microgrids-A General Approach Towards Standardization," *IEEE Transactions on Industrial Electronics ,* vol. 58, no. 1, pp. 158-172, 2011.

[31]   J. Rocabert, A. Luna, F. Blaabjerg and P. Rodriguez, "Control of Power Converters in AC Microgrids," *IEEE Transaction on Power Electronics,* vol. 27, no. 11, p. 4734–4749, 2012.

[32]   T. K. Vrana and C. Hille, "A Novel Control Method for Dispersed Converters Providing Dynamic Frequency Response," *Electrical Engineering,* vol. 93, no. 4, p. 217 – 226 , 2011.

[33]   J. Zhu, C. D. Booth, G. P. Adam, A. J. Roscoe and C. G. Bright, "Inertia Emulation Control Strategy for VSC-HVDC Transmission Systems," *IEEE Transactions on Power Systems,* vol. 28, no. 2, p. 1277 – 1287, 2013.

[34]   M. A. Torres, L. A. Lopes, L. A. Moran and J. R. Espinoza, "Self-Tuning Virtual Synchronous Machine : A Control Strategy for Energy Storage Systems to Support Dynamic Frequency Control," *IEEE Transactions on Energy Conversion,* vol. 29, no. 4, pp. 833 - 840, 2014.

[35]   S. I. Nanou, A. G. Papakonstantinou and S. A. Papathanassiou, "A Generic Model of Two-Stage Grid-Connected PV Systems with Primary Frequency Response and Inertia Emulation," *Electrical Power System Research,* vol. 127, p. 186 – 196, 2015.

[36]   M. P. N. Van Wesenbeeck, S. W. H. De Haan, P. Varela and K. Visscher, "Grid Tied Converter with Virtual Kinetic Storage," *IEEE Bucharest PowerTechnology,* pp. 1 - 7, 2009.

[37]   S. D. Arco, J. A. Suul and O. B. Fosso, "Control System Tuning and Stability Analysis of Virtual Synchronous Machines," in *2013 IEEE Energy Conversion Congress and Exposition (ECCE 2013)*, Denver, Colorado, 15 - 19 September 2013.

[38]   M. Guan, W. Pan, J. Zhang, Q. Hao, J. Cheng and X. Zheng, "Synchronous Generator Emulation Control Strategy for Voltage Source Converter (VSC) Station," *IEEE Transactions on Power Systems,* vol. 30, no. 6, p. 3093 – 3101, 2015.

[39]   Q. C. Zhong and G. Weiss, "Static Synchronous Generators for Distributed Generation and Renewable Energy," in *2009 IEEE/PES Power Systems Conference and Exposition*, Seattle, WA, USA, 2009.

[40]   Q. C. Zhong and G. Weiss, "Synchronverters: Inverters That Mimic Synchronous Generators," *IEEE Transactions on Industrial Electronics,* vol. 58, no. 4, p. 1259 – 1267, 2011.

[41]   S. M. Ashabani and Y. A. R. I. Mohamed, "A flexible control strategy for grid connected and islanded microgrids with enhanced stability using nonlinear microgrid stabilizer," *IEEE Transactions on Smart Grid,* vol. 3, no. 3, p. 1291 – 1301, 2012.

[42]   S. D. Arco and J. A. Suul, "Equivalence of Virtual Synchronous Machines and Frequency-Droops for Converter-Based MicroGrids," *IEEE Transactions on Smart Grid,* vol. 5, no. 1, p. 394 – 395, 2014.

[43]   Q. C. Zhong, P. Nguyen, Z. Ma and W. Sheng, "Self-Synchronized Synchronverters : Inverters Without a Dedicated Synchronization Unit," *IEEE Transactions on Power Electronics,* vol. 29, no. 2, p. 617 – 630, 2014.

[44]   J. Alipoor, Y. Miura and T. Ise, "Power System Stabilization Using Virtual Synchronous Generator With Alternating Moment of Inertia," *IEEE Journal of Emerging and Selected Topics in Power Electronics,* vol. 3, no. 2, pp. 451-458, 2015.

[45]   M. Ashabani, F. D. Freijedo, S. Golestan and J. M. Guerrero, "Inducverters: PLL-less Converters with Auto-Synchronization and Emulated Inertia Capability," *IEEE Transactions on Smart Grid,* vol. 7, no. 3, p. 1660 – 1674, 2016.

[46]   J. Matas, M. Castilla, L. G. Vicuña, J. Miret and J. C. Vasquez, "Virtual Impedance Loop for Droop-Controlled Single-Phase Parallel Inverters Using a Second-Order General-Integrator Scheme," *IEEE Transactions on Power Electronics,* vol. 25, no. 12, pp. 2993-3002, 2010.

[47]   J. He and Y. W. Li, "Analysis, Design, and Implementation of Virtual Impedance for Power Electronics Interfaced Distributed Generation," *IEEE Transactions on Industry Applications,* vol. 47, no. 6, pp. 2525-2538, 2011.

[48]   J. He, Y. W. Li, J. M. Guerrero, F. Blaabjerg and J. C. Vasquez, "An Islanding Microgrid Power Sharing Approach Using Enhanced Virtual Impedance Control Scheme," *IEEE Transactions on Power Electronics,* vol. 28, no. 11, pp. 5272-5282, 2013.

[49]   X. Wang, Y. Wei Li, F. Blaabjerg and P. C. Loh, "Virtual-Impedance-Based Control for Voltage-Source and Current-Source Converters," *IEEE Transactions on Power Electronics,* vol. 30, no. 12, pp. 7019-7037, 2015.

[50]   Y. Chen, R. Hesse, D. Turschner and H. Beck, "Dynamic Properties of the Virtual Synchronous Machine (VISMA)," in *International Conference on Renewable Energy and Power Quality Journal* , Las Palmas de Gran Canaria, 13 - 15 April 2011.

[51]   H. Alatrash, A. Mensah, E. Mark, G. Haddad and J. Enslin, "Generator Emulation Controls for Photovoltaic Inverters," *IEEE Transactions on Smart Grid,* vol. 3, no. 2, pp. 996 - 1011, 2012.

[52]   P. Rodriguez, I. Candela and A. Luna, "Control of PV Generation Systems Using the Synchronous Power Controller," in *2013 IEEE Energy Conversion Congress and Exposition*, Denver, CO, USA, 2013.

[53]   P. Rodriguez, I. Candela, C. Citro, J. Rocabert and A. Luna, "Control of Grid-Connected Power Converters based on a Virtual Admittance Control Loop," in *15th European Conference in Power Electronics and Applications (EPE)*, Lille, France, 2013.

[54]   D. Remon, A. M. Cantarellas, E. Rakhshani, I. Candela and P. Rodriguez, "An Active Power Self-Synchronizing Controller for Grid-Connected Converters

Emulating Inertia," in *International Conference on Renewable Energy Research and Applications (ICRERA)*, Milwaukee, WI, USA, 19-22 October 2014.

[55] S. D'Arco, J. A. Suul and O. B. Fosso, "A Virtual Synchronous Machine Implementation for Distributed Control of Power Converters in Smart Grid," *Elsevier-Electric Power Systems Research,* vol. 122, pp. 180-197, 2015.

[56] P. Rodriguez, C. Citro, I. Candela, J. Rocabert and A. Luna, "Flexible Grid Connection and Islanding of SPC- based PV Power Converters," in *Seventh Annual IEEE Energy Conversion Congress and Exposition (ECCE)*, Montreal, Canada, 20 - 24 September 2015.

[57] F. Katiraei, R. Iravani, N. Hatziargyriou and A. Dimeas, "Microgrids Management," *IEEE Power Energy Magazine,* vol. 6, no. 3, pp. 54-65, 2010.

[58] L. Che, M. Shahidehpour, A. Alabdulwahab and Y. Al-Turki, "Hierarchical Coordination of a Community Microgrid with AC and DC Microgrids," *IEEE Transactions on Smart Grid,* vol. 6, no. 6, pp. 3042-3051, 2015.

[59] M. Datta, T. Senjyu, A. Yona, T. Funabashi and C. H. Kim, "A Frequency Control Approach by Photovoltaic Generator in a PV Diesel Hybrid Power System," *IEEE Transactions in Energy Conversions,* vol. 26, no. 2, pp. 559-571, 2011.

[60] D. Chen and L. Xu, "Autonomous DC Volatge Control of DC Microgrid with Multiple Slack Terminals," *IEEE Transactions in Power Systems,* vol. 27, no. 4, pp. 1897-1905, 2012.

[61] S. Moayedi and A. Davoudi, "Distributed Tertiary Control of DC Microgrid Clusters," *IEEE Transactions on Power Electronics,* vol. 31, no. 2, pp. 1717-1733, 2016.

[62] S. Salomonsson, L. Soder and A. Sannino, "An Adaptive Control System for a DC Microgrid for Data Centers," *IEEE Transactions on Industrial Applications,* vol. 44, no. 6, pp. 1910-1917, 2008.

[63] A. Kwasinski, "Quantitative Evaluation of DC Microgrids Availability: Effects of System Architecture and Converter Topology Design Choices," *IEEE Transactions on Power Electronics,* vol. 26, no. 3, pp. 835-851, 2011.

[64]   Y. Gu, X. Xiang, W. Li and X. He, "Mode-Adaptive Decentralized Control for Renewable DC Microgrid with Enhanced Reliability and Flexibility," *IEEE Transactions on Power Electronics,* vol. 29, no. 9, pp. 5072-5080, 2014.

[65]   H. Kakigano, Y. Miura and T. Ise, "Low Voltage Bipolar-Type DC Microgrid for Super High Quality Distribution," *IEEE Transactions on Power Electronics ,* vol. 25, no. 12, pp. 3066-3075, 2010.

[66]   Y. K. Chen, Y. C. Wu, C. C. Song and Y. S. Chen, "Design and Implementation of Energy Management System with Fuzzy Control for DC Microgrid Systems," *IEEE Transactions on Power Electronics,* vol. 28, no. 4, pp. 1563-1570, 2013.

[67]   P. C. Loh, D. Li, Y. K. Chai and F. Blaabjerg, "Autonomous Operation of Hybrid Microgrid with AC and DC Subgrids," *IEEE Transactions on Power Electronics,* vol. 28, no. 5, pp. 2214-2223, 2013.

[68]   N. Bottrell, M. Prodanovic and T. C. Green, "Dynamic Stability of a Microgrid with an Active Load," *IEEE Transactions on Power Electronics,* vol. 28, no. 11, pp. 5107-5119, 2013.

[69]   J. C. Vasquez, J. M. Guerrero, J. Miret, M. Castilla and L. G. DeVicuna, "Hierarchical Control of Intelligent Microgrids," *IEEE on Industrial Electronics Magazine,* vol. 4, no. 4, pp. 23-29, 2010.

[70]   A. Kwasinski and C. N. Onwuchekwa, "Dynamic Behaviour and Stabilization of DC Microgrids with Instantaneous Constant Power Loads," *IEEE Transactions on Power Electronics,* vol. 26, no. 3, pp. 822-834, 2011.

[71]   B. T. Patterson, "DC, Come Home: DC Microgrids and the Birth of 'Enernet'," *IEEE Power Energy Magazine,* vol. 10, no. 6, pp. 60-69, 2012.

[72]   J. M. Guerrero, M. Chandorkar, T. L. Lee and P. C. Loh, "Advanced Control Architectures for Intelligent Microgrids - Part I: Decentralized and Hierarchical Control," *IEEE Transactions on Industrial Electronics,* vol. 60, no. 4, pp. 1254-1262, 2013.

[73]   Y. Han, H. Li, P. Shen, E. A. A. Coelho and J. M. Guerrero, "Review of Active and Reactive Power Sharing Strategies in Hierarchical Controlled Microgrids," *IEEE Transactions on Power Electronics,* vol. 32, no. 3, pp. 2427-2451, 2017.

[74]   S. K. Khadem, M. Basu and M. F. Conlon, "Intelligent Islanding and Seamless Reconnection Technique for Microgrid with UPQC," *IEEE Journal Emerging Selected Topics on Power Electronics ,* vol. 3, no. 2, pp. 483-492, 2015.

[75]   A. Micallef, M. Apap, C. S. Staines and J. M. Guerrero, "Single Phase Microgrid with Seamless Transition Capabilities Between Modes of Operation," *IEEE Transactions on Smart Grid,* vol. 6, no. 6, pp. 2736-2745, 2015.

[76]   M. C. Chandorkar, D. M. Divan and R. Adapa, "Control of Parallel Connected Inverters in Stand-alone AC Supply Systems," *IEEE Transactions on Industrial Application,* vol. 29, no. 1, pp. 136-143, 1993.

[77]   J. M. Guerrero, L. DeVicuna, J. Matas, M. Castilla and J. Miret, "A Wireless Controller To Enhanced Dynamic Performance of Parallel Inverters in Distributed Generation System," *IEEE Transactions on Power Electronics,* vol. 19, no. 5, pp. 1205-1213, 2004.

[78]   Y. A. R. I. Mohamed, H. H. Zeineldin, M. M. A. Salama and R. Seethapathy, "Seamless Formation and Robust Control of Distributed Generation Microgrids via Direct Voltage Control and Optimized Dynamic Power Sharing," *IEEE Transactions on Power Electronics,* vol. 27, no. 3, pp. 1283-1294, 2012.

[79]   Y. A. R. I. Mohamed and E. F. E. Saadany, "Adaptive Decentralized Droop Controller to Preserve Power Sharing Stability of Paralleled Inverters in Distributed Generation Microgrids," *IEEE Transactions on Power Electronics,* vol. 23, no. 6, pp. 2806-2816, 2008.

[80]   Y. W. Li and C. N. Kao, "An Accurate Power Control Strategy for Power Electronics-Interfaced Distributed Generation Units Operating in A Low Voltage Multibus Microgrid," *IEEE Transactions on Power Electronics,* vol. 24, no. 12, pp. 2977-2988, 2009.

[81]   J. W. He and Y. W. Li, "An Enhanced Microgrid Load Demand Sharing Strategy," *IEEE Transactions on Power Electronics,* vol. 27, no. 9, pp. 3984-3995, 2012.

[82]   Y. D. Chen, A. Luo, J. Zhou, L. S. Bai and Z. H. Dou, "Rapid Reactive Power Control Method for Parallel Inverters Using Resistive-Capacitive Output Impedance," in *Proceedings 1st International Future Energy Electronics Conference*, 2013.

[83]   H. Mahmood, D. Michealson and J. Jiang, "Reactive Power Sharing In Island Microgrids Using Adaptive Volatge Droop Control," *IEEE Transactions on Smart Grid,* vol. 6, no. 6, pp. 3052-3060, 2015.

[84]   P. Li, X. B. Wang, W. J. Lee and D. Xu, "Dynamic Power Conditioning Method of Microgrid via Adaptive Inverse Control," *IEEE Transactions on Power Delivery,* vol. 30, no. 2, pp. 906-913, 2015.

[85]   M. Q. Mao, Z. Dong, Y. Ding and L. C. Chang, "A Unified Controller for a Microgrid Based on Adaptive Virtual Impedance and Conductance," in *IEEE Energy Conversion Congress Expo*, 2014.

[86]   H. Mahmood, D. Michealson and J. Jiang, "Accurate Reactive Power Sharing in an Island Microgrid Using Adaptive Virtual Impedances," *IEEE Transactions on Power Electronics,* vol. 30, no. 3, pp. 1605-1617, 2015.

[87]   Y. J. Gu, W. H. Li and X. N. He, "Frequency Coordinating Virtual Impedance for Autonomous Power Management of DC Microgrid," *IEEE Transactions on Power Electronics,* vol. 30, no. 4, pp. 2328-2337, 2015.

[88]   H. Han, X. C. Hou, J. Yang, J. Wu, M. Su and J. M. Guerrero, "Review of Power Sharing Control Strategies for Islanding Operation of AC Microgrids," *IEEE Transaction on Smart Grid,* vol. 7, no. 1, pp. 200-2015, 2016.

[89]   S. C. Liu, X. Y. Wang and P. X. P. Liu, "Impact of Communication Delays On Secondary Frequency Control in an Islanded Microgrid," *IEEE Transactions on Industrial Electronics,* vol. 62, no. 4, pp. 2021-2031, 2015.

[90]   V. Nasirian, Q. Shafiee, J. M. Guerrero, F. L. Lewis and A. Davoudi, "Droop - Free Distributed Control for AC Microgrids," *IEEE Transactions on Power Electronics,* vol. 31, no. 2, pp. 1600-1617, 2016.

[91]   C. Ahumada, R. Cardenas, D. Saez and J. M. Guerrero, "Secondary Control Strategies for Frequency Restoration in Islanded Microgrids with Consideration of Communication Delays," *IEEE Transactions on Smart Grid,* vol. 7, no. 3, pp. 1430-1441, 2016.

[92]   J. Schiffer, T. Seel, J. Raisch and T. Sezi, "Voltage Stability and Reactive Power Sharing in Inverter-based Microgrids with Consensus-based Distributed Voltage Control," *IEEE Transactions on Control Systems Technology,* vol. 24, no. 1, pp. 96-109, 2016.

[93]   J. W. He, Y. W. Li, J. M. Guerrero, F. Blaabjerg and J. C. Vasquez, "Microgrid Reactive and Harmonic Power Sharing Using Enhanced Virtual Impedance," in *IEEE 28th Appl. Power Electron. Conf. Expo Annual Conference*, 2013.

[94]   M. Savaghebi, Q. Shafiee, J. C. Vasquez and J. M. Guerrero, "Adaptive Virtual Impedance Scheme For Selective Compensation of Voltage Unbalanced and Harmonics in Microgrids," in *IEEE Power Energy Soc. General Meeting*, 2015.

[95]   T. Vu Van, K. Visscher, J. Diaz, V. Karapanos, A. Woyte, M. Albu, J. Bozelie, T. Loix and D. Federenciuc, "Virtual Synchronous Generator: An Element of Future Grids," in *2010 IEEE PES Innovative Smart Grid Technologies Conference Europe (ISGT Europe)*, Gothenberg, Sweden, 2010.

[96]   H. Bevrani, T. Ise and a. Y. Miura, "Virtual synchronous generators: A survey and new perspectives," *International Journal of Electrical Power & Energy Systems,* vol. 54, p. 244–254, 2014.

[97]   T. Shintai, Y. Miura and Y. Ise, "Oscillation Damping of a Distributed Generator Using a Virtual Synchronous Generator," *IEEE Transaction on Power Delivery,* vol. 29, no. 2, pp. 668-676, 2014.

[98]   J. Liu, Y. Miura and T. Ise, "Comparison of Dynamic Characteristics Between Virtual Synchronous Generator and Droop Controling Inverter-Based Distributed Generators," *IEEE Transaction on Power Electronics,* vol. 31, no. 5, pp. 3600-3611, 2016.

[99]   C. Wu, A. Luo, L. Zhou, X. Zhou, L. Yang, Y. Dong and J. M. Guerero, "A Virtual Inertia Control Strategy for DC Microgrids Analogized With Virtual Synchronous Machines," *IEEE Transactions on Industrial Electronics,* vol. 64, no. 7, pp. 6005 - 6016, 2017.

[100]   K. Shi, H. Ye, W. Song and G. Zhou, "Virtual Inertia Control Strategy in Microgrid Based on Virtual Synchronous Generator Technology," *IEEE Access,* vol. 6, pp. 27949-27957, 2018.

[101]   K. Visscher and S. De Haan, "Virtual Synchronous Machines (VSG's) for Frequency Stabilisation in Future Grids with a Significant Share of Decentralized Generation," in *CIRED Seminar 2008: SmartGrids for Distribution*, Frankfurt, Germany, 2008.

[102] T. Loix, S. D. Breucker, P. Vanassche, J. V. D. Keybus, J. Driesen and K. Visscher, "Layout and Performance of the Power Electronic Converter Platform for the VSYNC Project," in *2009 IEEE Bucharest Power Tech Conference*, Bucharest, Romania, 2009.

[103] W. G. and Q. C. Zhong, "Static Synchronous Generators". Patent WO 2010/055322 A, 2008.

[104] L. Zhang, L. Harnefors and H. P. Nee, "Power Synchronization Control of Grid-Connected Voltage Source Converters," *IEEE Transactions on Power Systems,* vol. 25, no. 2, p. 809–820, 2010.

[105] L. Zhang, L. Harnefors and H. P. Nee, "Interconnection of Two Very Weak AC Systems by VSC-HVDC Links Using Power-Synchronization Control," *IEEE Transactions on Power Systems,* vol. 26, no. 1, p. 344–355, 2011.

[106] L. Zhang, L. Harnefors and a. H. P. Nee, "Modeling and Control of VSC-HVDC Links Connected to Island Systems," *IEEE Transactions on Power Systems,* vol. 26, no. 2, p. 783–793, 2011.

[107] Z. Weiyi, A. M. Cantarellas, J. Rocabert, A. Luna and P. Rodriguez, "Synchronous Power Controller with Flexible Droop Characteristics for Renewable Power Generation Systems," *IEEE Transactions on Sustainable Energy,* vol. 7, no. 4, pp. 1572-1582, 2016.

[108] W. Gullvik, "Modeling, Analysis and Control of Active Front End (AFE) Converter," Ph.D Dissertation, Norwegian University of Science and Technology, Trondheim, Norway, 2007.

[109] W. Gullvik, L. Norum and R. Nilsen, "Active Damping of Resonance Oscillations in LCL-Filters based on Virtual Flux and Virtual Resistor," in *Proceedings of 12th European Conference on Power Electronics and Applications*, Aalborg, Denmark, 2007.

[110] G. Wrona and K. Malon, "Sensorless Operation of an Active Front End Converter with LCL Filter," in *Proceedings of 2014 IEEE 23rd International Symposium on Industrial Electronics, ISIE*, Istanbul, Turkey, 2014.

[111] J. Zhang, H. Wang, M. Zhu and X. Cai, "Control Implementation of the Full-Scale Wind Power Converter Without Grid Voltage Sensors," in *Proceedings of 2014 International Power Electronics Conference*, Hiroshima, Japan, 2014.

[112] N. F. Roslan, J. A. Suul, A. Luna, J. I. Candela and P. Rodriguez, "A Simulation Study of Proportional Resonant Controller based on the Implementation of Frequency Adaptive Virtual Flux Estimation with the LCL Filter.," in *Proceedings of the IEEE Industrial Electronics Society*, Yokohama, Japan, 2015.

[113] J. A. Suul, A. Luna, P. Rodriguez and T. Undeland, "Frequency-Adaptive Virtual Flux Estimation for Grid Synchronization Under Unbalanced Conditions," in *IECON 2010 - 36th Annual Conference on IEEE Industrial Electronics Society*, Glendale, AZ, USA, 2010.

[114] E. Hossain, M. R. Tur, S. Padmanaban, S. Ay and I. Khan, "Analysis and Mitigation of Power Quality Issues in Distributed Generation Systems Using Custom Power Devices," *IEEE Access,* vol. 6, pp. 16816 - 16833, 2018.

[115] A. A. Alkahtani, S. T. Y. Alfalahi, A. A. Athamneh, A. Q. Al-Shetwi, M. Mansur, M. A. Hannan and V. G. Agelidis, "Power Quality in Microgrids Including Supraharmonics: Issues, Standards, and Mitigations," *IEEE Access,* vol. 8, pp. 127104 - 127122, 2020.

[116] Y. Han, Y. Feng, P. Yang, L. Xu, Y. Xu and F. Blaabjerg, "Cause, Classification of Voltage Sag, and Voltage Sag Emulators and Applications: A Comprehensive Overview," *IEEE Access,* vol. 8, pp. 1922 - 1934, 2020.

[117] S. K. Gawre, N. P. Patidar and R. K. Nema, "Application of wavelet Transform in power Quality: A Review," *International Journal of Computer Applications,* vol. 39, no. 18, pp. 30 - 36, 2012.

[118] M. Ramachandran, A. Mariya Chithra Mary, M. Muthukumaran, J. Ganesan, A. Krishnaveni and D. Edison Selvaraj, "A Review on Basic Concepts and Important Standards of Power Quality in Power Systems," *International Journal of Science and Engineering Applications,* vol. 4, no. 5, pp. 299 - 303, 2015.

[119] N. K. Roy and H. R. Pota, "Current Status and Issues of Concern for the Integration of Distributed Generation Into Electricity Networks," *IEEE Systems Journal,* vol. 9, no. 3, pp. 933 - 943, 2015.

[120] Q. Fu, L. F. Montoya, A. Solanki, A. Nasiri, V. Bhavaraju, T. Abdallah and D. C. Yu, "Microgrid Generation Capacity Design With Renewables and Energy Storage Addressing Power Quality and Surety," *IEEE Transactions on Smart Grid,* vol. 3, no. 4, pp. 2019 - 2027, 2012.

[121]   "Scaling Up Variable Renewable Power : The Role of Grid Codes," International Renewable Energy Agency, Barbados, Germany, 2016.

[122]   N. Ruban, A. Kinshin and A. Gusev, "Review of Grid Codes: Ranges of Frequency Variation," in *International Youth Scientific Conference "Heat and Mass Transfer in the Thermal Control System of Technical and Technological Energy Equipment"*, Tomsk, Russia, 2019.

[123]   Q. Zheng, J. Li, X. Ai, J. Wen and J. Fang, "Overivew of Grid Codes for Photovoltaic Integration," in *2017 IEEE Conference on Energy Internet and Energy System Integration (EI2)*, Beijing, China, November 2017.

[124]   Y. Xue, K. C. Divya, G. Griepentrog, M. Liviu, S. Suresh and M. Manjrekar, "Towards Next Generation Photovoltaic Inverters," in *2011 IEEE Energy Conversion Congress and Exposition*, Phoenix, AZ, USA, 2011.

[125]   J. D. Van Wyk and F. C. Lee, "On A Future for Power Electronics," *IEEE Journal of Emerging and Selected Topics in Power Electronics,* vol. 1, no. 2, pp. 59-72, 2013.

[126]   K. O. Kovanen, "Photovoltaic and Power Distribution," *Renew. Energy Focus,* vol. 14, no. 3, pp. 20-21, 2013.

[127]   H. Gerard, E. I. R. Puente and D. Six, "Coordination Between Transmission and Distribution System Operators in the Electricity Sector: A Conceptual Framework," *Elsevier-Utilities Policy,* vol. 50, pp. 40-48, 2018.

[128]   N. Femia, G. Petrone, G. Spagnuolo and M. Vitelli, "Optimization of Perturb and Observe Maximum Power Point Tracking Method," *IEEE Transactions on Power Electronics,* vol. 20, no. 4, pp. 963-973, 2005.

[129]   J. H. R. Enslin, M. S. Wolf, D. B. Snyman and W. Swiegers, "Integrated Photovoltaic Maximum Power Point Tracking Converter," *IEEE Transaction on Industrial Electronics,* vol. 44, no. 6, pp. 769-773, 1997.

[130]   C. W. Tan, T. C. Green and C. A. Hernandez-Aramburo, "Analysis of Perturb and Observe Maximum Power Point Tracking Algorithm for Photovoltaic Applications," in *2008 IEEE 2nd International Power and Energy Conference*, Johor Bahru, Malaysia, 2008.

[131]   L. Piegari, R. Rizzo, I. Spina and P. Tricoli, "Optimized Adaptive Perturb and Observe Maximum Power Point Tracking Control for Photovoltaic Generation," *Energies,* vol. 8, no. 5, pp. 3418-3436, 2015.

[132]   A. A. Elbaset, H. Ali, M. A. El Sattar and M. Khaled, "Implementation of a Modified Perturb and Observe Maximum Power Point Tracking Algorithm for Photovoltaic System Using an Embedded Microcontroller," *IET Renewable Power Generation,* vol. 10, no. 4, pp. 551-560, 2016.

[133]   S. B. Kjær, "Evaluation of the "Hill Climbing" and the"Incremental Conductance" Maximum Power PointTrackers for Photovoltaic Power Systems," *IEEE Transaction on Energy Conversion,* vol. 27, no. 4, pp. 922-929, 2012.

[134]   G. C. Hsieh, H. I. Hsieh, C. Y. Tsai and C. H. Wang, "Photovoltaic Power-Increment-Aided Incremental-Conductance MPPT With Two-Phased Tracking," *IEEE Transaction on Power Electronics,* vol. 28, no. 6, pp. 2895-2911, 2013.

[135]   N. Kumar, I. Hussain, B. Singh and B. K. Panigrahi, "Self-Adaptive Incremental Conductance Algorithm for Swift and Ripple-Free Maximum Power Harvesting From PV Array," *IEEE Transaction on Industrial Informatics,* vol. 14, no. 5, pp. 2031-2041, 2018.

[136]   T. Esram, J. W. Kimball, P. T. Krein, P. L. Chapman and P. Midya, "Dynamic Maximum Power Point Tracking of Photovoltaic Arrays Using Ripple Correlation Control," *IEEE Transaction on Power Electronics,* vol. 21, no. 5, pp. 1282-1291, 2006.

[137]   J. W. Kimball and P. T. Krein, "Discrete-Time Ripple Correlation Control forMaximum Power Point Tracking," *IEEE Transaction on Power Electronics,* vol. 23, no. 5, pp. 2353-2362, 2008.

[138]   A. Costabeber, M. Carraro and M. Zigliotto, "Convergence Analysis and Tuning of a Sliding-ModeRipple-Correlation MPPT," *IEEE Transaction on Energy Conversion,* vol. 30, no. 2, pp. 696-706, 2015.

[139]   H. Ahmed Sher, A. F. Murtaza, A. Noman, K. E. Addoweesh, K. Al-Haddad and M. Chiaberge, "A New Sensorless Hybrid MPPT Algorithm Basedon Fractional Short-Circuit Current Measurementand P&O MPPT," *IEEE Transactions on Sustainable Energy,* vol. 6, no. 4, pp. 1426-1434, 2015.

[140]   Z. Lubosny, Wind Turbine Operation in Electric Power Systems Advance Modelling, Berlin: Heidelberg: Springer, 2003.

[141]   T. Ackermann, Wind Power in Power Systems, John Wiley & Sons, 2005.

[142]   T. K. A. Brekken and N. Mohan, "Control of a Doubly Fed Induction Wind Generator Under Unbalanced Grid Voltage Conditions," *IEEE Transactions on Energy Conversion,* vol. 22, no. 1, pp. 129-135, 2007.

[143]   K. Protsenko and D. Xu, "Modeling and Control of Brushless Doubly-Fed Induction Generators in Wind Energy Applications," *IEEE Transactions on Power Electronics,* vol. 23, no. 3, pp. 1191-1197, 2008.

[144]   R. Fadaeinedjad, M. Moallem and G. Moschopoulos, "Simulation of a Wind Turbine With Doubly Fed Induction Generator by FAST and Simulink," *IEEE Transactions on Energy Conversion,* vol. 23, no. 2, pp. 690-700, 2008.

[145]   Y. You, T. A. Lipo and B. Kwon, "Optimal Design of a Grid-Connected-to-Rotor Type Doubly Fed Induction Generator for Wind Turbine Systems," *IEEE Transactions on Magnetics,* vol. 48, no. 11, pp. 3124-3127, 2012.

[146]   J. Carroll, A. McDonald and D. McMillan, "Reliability Comparison of Wind Turbines With DFIG and PMG Drive Trains," *IEEE Transactions on Energy Conversion,* vol. 30, no. 2, pp. 663-670, 2015.

[147]   F. Valenciaga and P. F. Puleston, "High-Order Sliding Control for a Wind Energy Conversion System Based on a Permanent Magnet Synchronous Generator," *IEEE Transactions on Energy Conversion,* vol. 23, no. 3, pp. 860 - 867, 2008.

[148]   S. M. Dehghan, M. Mohamadian and A. Y. Varjani, "A New Variable-Speed Wind Energy Conversion System Using Permanent-Magnet Synchronous Generator and Z-Source Inverter," *IEEE Transactions on Energy Conversion,* vol. 24, no. 3, pp. 714 - 724, 2009.

[149]   C. N. Bhende, S. Mishra and S. G. Malla, "Permanent Magnet Synchronous Generator-Based Standalone Wind Energy Supply System," *IEEE Transactions on Sustainable Energy,* vol. 2, no. 4, pp. 361 - 373, 2011.

[150]   T. L. Vandoorn, B. Meersman, J. D. M. De Kooning and L. Vandevelde, "Directly-Coupled Synchronous Generators With Converter Behavior in Islanded

Microgrids," *IEEE Transactions on Power Systems,* vol. 27, no. 3, pp. 1395 - 1406, 2012.

[151]   A. E. Leon, M. F. Farias, P. E. Battaiotto, J. A. Solsona and M. I. Valla, "Control Strategy of a DVR to Improve Stability in Wind Farms Using Squirrel-Cage Induction Generators," *IEEE Transactions on Power Systems,* vol. 26, no. 3, pp. 1609 - 1617, 2011.

[152]   H. Chen and D. C. Aliprantis, "Analysis of Squirrel-Cage Induction Generator With Vienna Rectifier for Wind Energy Conversion System," *IEEE Transactions on Energy Conversion ,* vol. 26, no. 3, pp. 967 - 975, 2011.

[153]   H. Polinder, J. Ferreira, B. B. Jensen, A. B. Abrahamsen, K. Atallah and R. A. McMahon, "Trends in Wind Turbine Generator Systems," *IEEE Journal of Emerging and Selected Topics in Power Electronics,* vol. 1, no. 3, pp. 174 - 185, 2013.

[154]   V. Yaramasu, B. Wu, P. C. Sen, S. Kouro and M. Narimani, "High-Power Wind Energy Conversion Systems: State-of-the-Art and Emerging Technologies," *Proceedings of the IEEE,* vol. 103, no. 5, pp. 740 - 788, 2015.

[155]   A. Rolan, F. C. Lopez, S. Bogarra, L. Monjo and J. Pedra, "Reduced-Order Models of Squirrel-Cage Induction Generators for Fixed-Speed Wind Turbines Under Unbalanced Grid Conditions," *IEEE Transactions on Energy Conversion,* vol. 31, no. 2, pp. 566 - 577, 2016.

[156]   F. González-Espín, E. Figueres and G. Garcerá, "An Adaptive Synchronous-Reference-FramePhase-Locked Loop for Power QualityImprovement in a Polluted Utility Grid," *IEEE Transaction on Industrial Electronics,* vol. 59, no. 6, pp. 2718-2731, 2012.

[157]   S. Golestan, M. Monfared and F. D. Freijedo, "Design-Oriented Study of Advanced Synchronous Reference Frame Phase-Locked Loops," *IEEE Transactions on Power Electronics,* vol. 28, no. 2, pp. 765-778, 2013.

[158]   M. Reyes, P. Rodríguez, S. Vázquez, A. Luna and J. M. Carrasco, "Decoupled Double Synchronous Reference Frame Current Controller for Unbalanced Grid Voltage Conditions," in *2012 IEEE Energy Conversion Congress and Exposition*, 2012.

[159]   X. Wu, T. Huang, X. Chen, H. Hu and G. He, "Frequency Characteristic and Impedance Analysis on Three-Phase Grid-Connected Inverters Based on DDSRF-PLL," in *2019 10th International Conference on Power Electronics and ECCE Asia (ICPE 2019 - ECCE Asia)*, Busan, Korea, 2019.

[160]   P. Rodriguez, A. Luna, J. I. Candela, R. Teodorescu and F. Blaabjerg, "Grid Synchronization of Power Converters Using Multiple Second Order Generalized Integrators," in *2008 34th Annual Conference of IEEE Industrial Electronics*, Orlando, FL, USA, 2008.

[161]   P. Rodriguez, A. Luna, I. Etxeberria, J. R. Hermoso and R. Teodorescu, "Multiple Second Order Generalized Integrators for Harmonic Synchronization of Power Converters," in *2009 IEEE Energy Conversion Congress and Exposition*, San Jose, California, USA, 2009.

[162]   G. Shen, X. Zhu, J. Zhang and D. Xu, "A New Feedback Method for PR Current Control of LCL-Filter-Based Grid-Connected Inverter," *IEEE Transactions on Industrial Electronics,* vol. 57, no. 6, pp. 2033 - 2041, 2010.

[163]   A. G. Yepes, F. D. Freijedo, O. Lopez and J. Doval-Gandoy, "Analysis and Design of Resonant Current Controllers for Voltage-Source Converters by Means of Nyquist Diagrams and Sensitivity Function," *IEEE Transactions on Industrial Electronics,* vol. 58, no. 11, pp. 5231 - 5250, 2011.

[164]   Y. Jia, J. Zhao and X. Fu, "Direct Grid Current Control of LCL-Filtered Grid-Connected Inverter Mitigating Grid Voltage Disturbance," *IEEE Transactions on Power Electronics,* vol. 29, no. 3, pp. 1532 - 1541, 2014.

[165]   F. Hans, W. Schumacher, S. F. Chou and X. Wang, "Design of Multifrequency Proportional–Resonant Current Controllers for Voltage-Source Converters," *IEEE Transactions on Power Electronics,* vol. 35, no. 12, pp. 13573 - 13589, 2020.

[166]   A. Timbus, M. Liserre, R. Teodorescu, P. Rodriguez and F. Blaabjerg, "Evaluation of Current Controllers for Distributed Power Generation Systems," *IEEE Transaction on Power Electronics,* vol. 24, no. 3, pp. 654-664, 2009.

[167]   M. Hojabri, A. Z. Ahmad, A. Toudeshki and M. Soheilirad, "An Overview on Current Control Techniques for Grid Connected Renewable Energy Systems," in *2nd International Conference on Power and Energy Systems (ICPES 2012)*, 2012.

[168]   D. Zammit, C. S. Staines and M. Apap, "Comparison Between PI and PR Current Controllers in Grid Connected PV Inverters," *International Journal of Electrical, Computer, Electronics and Communication Engineering,* vol. 8, p. 224–229, 2014.

[169]   R. Teodorescu and F. Blaabjerg, "A New Control Structure for Grid-Connected LCL PV Inverters with Zero Steady-State Error and Selective Harmonic Compensation," in *Nineteenth Annual IEEE Applied Power Electronics Conference and Exposition*, 2004.

[170]   A. Kuperman, "Proportional-Resonant Current Controllers Design Based on Desired Transient Performance," *IEEE Transactions on Power Electronics,* vol. 30, no. 10, p. 5341–5345, 2015.

[171]   F. Blaabjerg, R. Teodorescu, M. Liserre and A. Timbus, "Overview of Control and Grid Synchronization for Distributed Power Generation Systems," *IEEE Transactions on Industrial Electronics,* vol. 53, no. 5, pp. 1398-1409, 2006.

[172]   E. Twining and D. G. Holmes, "Grid Current Regulation of a Three-Phase Voltage Source Inverter With an LCL Input Filter," *IEEE Transaction on Power Electronics,* vol. 18, no. 3, pp. 888-895, 2003.

[173]   C. A. Busada, S. G. Jorge and J. A. Solsona, "A Synchronous Reference Frame PI Current Controller With Dead Beat Response," *IEEE Transaction on Power Electronics,* vol. 35, no. 3, pp. 3097-3105, 2020.

[174]   M. Ramezani, S. Li and S. Golestan, "Analysis and Controller Design for Stand-Alone VSIs in Synchronous Reference Frame," *IET Power Electronics,* vol. 10, no. 9, pp. 1003-1012, 2017.

[175]   J. A. Suul, K. Ljokelsoy, T. Midtsund and T. Undeland, "Synchronous Reference Frame Hysteresis Current Control for Grid Converter Applications," *IEEE Transactions on Industry Applications,* vol. 47, no. 5, p. 2183–2194, 2011.

[176]   H. Mao, X. Yang, Z. Chen and Z. Wang, "A Hysteresis Current Controller for Single-Phase Three-Level Voltage Source Inverters," *IEEE Transactions on Power Electronics,* vol. 27, no. 7, p. 3330–3339, 2012.

[177] R. Davoodnezhad, D. G. Holmes and B. P. McGrath, "A Novel Three-Level Hysteresis Current Regulation Strategy for Three-Phase Three-Level Inverters," *IEEE Transactions on Power Electronics,* vol. 29, no. 11, p. 6100–6109, 2014.

[178] F. Blaabjerg, K. Ma and D. Zhou, "Power Electronics and Reliability in Renewable Energy Systems," in *IEEE International Symposium on Industrial Electronics*, 2012.

[179] O. Lopez, R. Teodorescu and J. Doval-Gandoy, "Multilevel Transformer-less Topologies for Single-Phase Grid-Connected Converters," in *IECON Proceedings (Industrial Electronics Conference)*, 2006.

[180] I. Agirman and V. Blasko, "A Novel Control Method of a VSC Without AC Line Voltage Sensors," *IEEE Transaction on Industry Applications,* vol. 39, no. 2, pp. 519-524, 2003.

[181] Y. A.-R. I. E.-S. E. F. Mohamed and M. M. A. Salama, "Adaptive Grid Voltage Sensorless Control Scheme for Inverter-Based Distribution Generation," *IEEE Transaction on Energy Conversion,* vol. 24, no. 3, pp. 683-694, 2009.

[182] R. Rahoui, A. Bechouche, H. Seddiki and D. O. Abdeslam, "Grid Voltages Estimation for Three-Phase PWM Rectifiers Control Without AC Voltage Sensors," *IEEE Transactions on Power Electronics,* vol. 33, no. 1, pp. 859-875, 2018.

[183] H. Gholami-Khesht, M. Monfared and S. Golestan, "Low Computational Burden Grid Voltage Estimation for Grid Connected Voltage Source Converter-based Power Applications," *IET Power Electronics,* vol. 8, no. 5, p. 656–664, 2015.

[184] M. B. Ketzer and C. B. Jacobina, "Virtual Flux Sensorless Control for Shunt Active Power Filters with Quasi-Resonant Compensators," *IEEE Transactions on Power Electronics,* vol. 31, no. 7, p. 4818–4830, 2016.

[185] T. Noguchi, H. Tomiki, S. Kondo and I. Takahashi, "Direct Power Control of PWM Converter Without Power-Source Voltage Sensors," *IEEE Transaction on Industry Applications,* vol. 34, no. 3, pp. 473-476, 1998.

[186] S. Hansen, M. Malinowski, F. Blaabjerg and M. P. Kazmierkowski, "Sensorless Control Strategies for PWM Rectifier," in *Proceedings of the Fifteenth Annual IEEE Applied Power Electronics Conference and Composition*, New Orleans, Louisiana, USA, 2000.

[187]   Y. A. R. I. Mohamed and E. F. El-Saadany, "Adaptive Discrete Time Grid Voltage Sensorless Interfacing Scheme for Grid Connected DG-Inverters Based on Neural-Network Identification and Deadbeat Current Regulation," *IEEE Transactions on Power Electronics,* vol. 23, no. 1, pp. 308 - 321, 2008.

[188]   J. G. Norniella, J. M. Cano, G. A. Orcajo, C. H. Rojas, J. F. Pedrayes, M. F. Cabanas and M. G. Melero, "Improving the Dynamics of Virtual Flux-based Control of Three-Phase Active Rectifiers," *IEEE Transactions on Industrial Electronics,* vol. 61, no. 1, p. 177–187, 2014.

[189]   Z. Zhang, H. Xu, M. Xue, Z. Chen, T. Sun, R. Kennel and C. M. Hackl, "Predictive control with novel virtual-flux estimation for back-to-back power converters," *IEEE Transactions on Industrial Electronics,* vol. 62, no. 5, pp. 2823 - 2834, 2015.

[190]   Y. Cho and K.-B. Lee, "Virtual-Flux-based Predictive Direct Power Control of Three-Phase PWM Rectifiers with Fast Dynamic Response," *IEEE Transactions on Power Electronics,* vol. 31, no. 4, p. 3348–3359, 2016.

[191]   K.-J. Lee, B.-G. Park, R.-Y. Kim and D.-S. Hyun, "Robust Predictive Current Controller based on a Disturbance Estimator in a Three-Phase Grid Connected Inverter," *IEEE Transactions on Power Electronics,* vol. 27, no. 1, p. 276 – 283, 2012.

[192]   H. Yoo, J.-H. Kim and S.-K. Sul, "Sensorless operation of a PWM rectifier for a distributed generation," *IEEE Transactions on Power Electronics,* vol. 22, no. 3, p. 1014 –1018, 2007.

[193]   K. H. Ahmed, A. M. Massoud, S. J. Finney and B. W. Williams, "Sensorless Current Control of Three-Phase Inverter-based Distributed Generation," *IEEE Transactions on Power Delivery,* vol. 24, no. 2, p. 919–929, 2009.

[194]   R. Guzman, L. G. de Vicuña, J. Morales, M. Castilla and J. Miret, "Model-based Control for a Three-Phase Shunt Active Power Filter," *IEEE Transactions on Industrial Electronics,* vol. 63, no. 7, p. 3998 – 4007, 2016.

[195]   J. Kukkola, M. Hinkkanen and K. Zenger, ""Observer-Based State-Space Current Controller for a Grid Converter Equipped With an LCL Filter: Analytical Method for Direct Discrete-Time Design," *IEEE Transactions on Industry Applications,* vol. 51, no. 5, p. 4079 – 4090, 2015.

[196]   J. Kukkola and M. Hinkkanen, "State observer for grid-voltage sensorless control of a converter equipped with an LCL filter: direct discrete-time design," *IEEE Transactions on Industry Application,* vol. 52, no. 4, pp. 3133 - 3145, 2016.

[197]   Y. A.-R. I. Mohamed and E. F. El-Saadany, ""A Robust Natural-Frame based Interfacing Scheme for Grid-Connected Distributed Generation Inverters," *IEEE Transactions on Energy Conversion,* vol. 26, no. 3, p. 728 – 736, 2011.

[198]   M. Malinowski, "Sensorless Control Strategies for Three Phase PWM Rectifiers," PhD Thesis, Warsaw University of Technology, Warsaw, Poland, 2001.

[199]   M. Malinowski, M. Jasinki and M. P. Kazmierkowski, "Simple Direct Power Control of Three Phase PWM Rectifier Using Space Vector Modulation (DPC-SVM)," *IEEE Transactions on Industrial Electronics,* vol. 51, no. 2, pp. 447 - 454, 2004.

[200]   R. Pollanen, "Converter-flux-based Current Control of Voltage Source PWM Rectifiers: Analysis and Implementation," Ph.D Dissertation, Lappeenranta University Technology, Finland, 2003.

[201]   J. Luukko, M. Niemela and J. Pyrhonen, "Estimation of the Flux Linkage in a Direct Torque Controlled Drive," *IEEE Transactions on Industrial Electronics,* vol. 50, no. 2, pp. 283 - 287, 2003.

[202]   L. A. Serpa, S. D. Round and J. W. Kolar, "A Virtual Flux Decoupling Hysteresis Current Controller for Mains Connected Inverter Systems," *IEEE Transactions on Power Electronics,* vol. 22, no. 5, pp. 1766 - 1777, 2007.

[203]   G. Tan, X. Wu, H. Li and M. Liu, "Novel Control Strategy for Multi-Level Active Power Filter Without Phase Locked Loop," *Energy and Power Engineering,* vol. 2, no. 4, pp. 262 - 270, 2010.

[204]   C. Bian, C. Shi, C. Song and A. Wang, "Study of the Control System of a Three Level PWM Rectifier Based on Virtual Flux Oriented," in *Proceeedings of the Third International Conference on Intelligent Human Machine Systems and Cybernetics*, Hangzhou, China, 2011.

[205]   P. Kundur, Power System Stability and Control, New York, USA / New Delhi, India: Mc Graw-Hill / Tata Mc Graw-Hill, 2006.

[206]   R. F. Camargo and H. Pinheiro, "Synchronization Method for Three Phase PWM Converters Under Unbalanced and Distorted Grid," *IEEE Proceedings on Electric Power Applications,* vol. 153, no. 5, pp. 763 - 772, 2006.

[207]   J. Svensson, M. Bongiorno and A. Sannino, "Practical Implementation of Delayed Signal Cancellation Method for Phase-Sequence Separation," *IEEE Transactions on Power Delivery,* vol. 22, no. 1, pp. 18 - 26, 2007.

[208]   R. Cárdenas, M. Dı´az, F. Rojas and J. Clare, "Fast Convergence Delayed Signal Cancellation Method for Sequence Component Separation," *IEEE Transactions on Power Delivery,* vol. 30, no. 4, pp. 2055 - 2057, 2015.

[209]   P. Rodríguez, R. Teodorescu, I. Candela, A. V. Timbus, M. Liserre and F. Blaabjerg, "New Positive-Sequence Voltage Detector for Grid Synchronization of Power Converters Under Faulty Grid Conditions," in *2006 37th IEEE Power Electronics Specialists Conference*, Jeju, South Korea, 18-22 June 2006.

[210]   M. Jasinski, M. P. Kazmierkowski, M. Bobrowska and P. Okon, "Control of AC-DC-AC Converter Under Unbalanced and Distorted Input Conditions," in *CPE 2009 - 6th International Conference-Workshop - Compatability and Power Electronics*, Badajoz, Spain, 2009.

[211]   R. Peña-Alzola, M. Liserre, F. Blaabjerg, R. Sebastían, J. Dannehl and F. W. Fuchs, "Analysis of the Passive Damping Losses in LCL-Filter-based Grid Converters," *IEEE Transactions in Power Electronics,* vol. 28, p. 2642–2646, 2013.

dSpace 1103 Controller Board

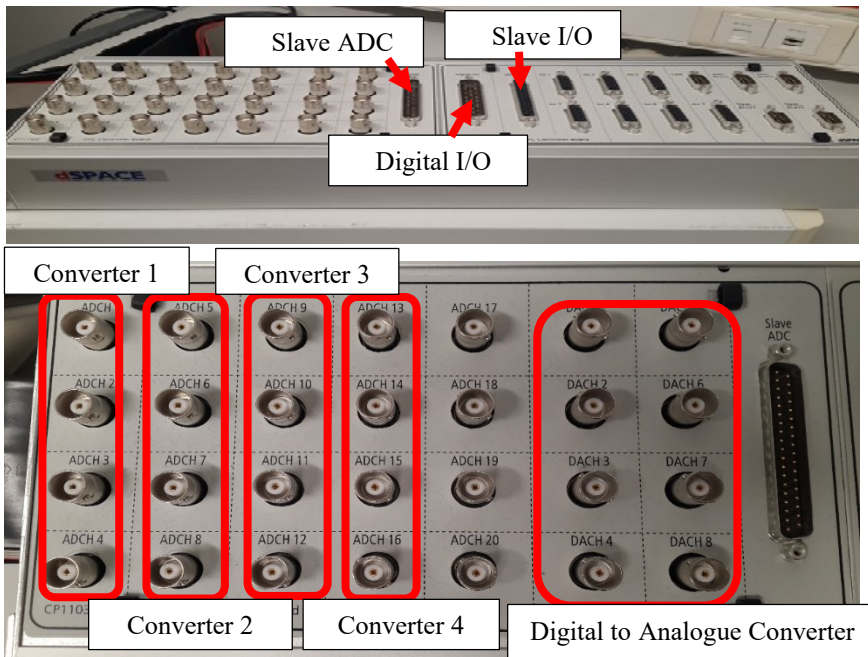This Appendix presented the configuration of the dSpace 1103 Controller Board used in the experimental works.
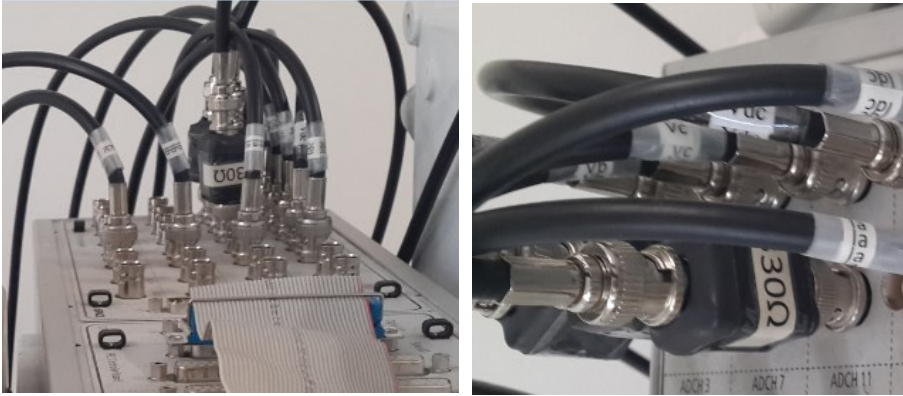

Fig. A.1. dSpace 1103 port.

Fig. A.1 shows the controller board where 20 analogue to digital converter channels and 8 digital to analogue converter channels are available. The DS1103MUX ADC Multiplexed A/D conversion is used for the acquisition data of three phase voltages at both converter and the grid side. The ADC multiplexed A/D conversion provides read access to 16 channels of 4 parallel A/D converters. The unit specification consists of 4 converter number where each number has 4 channels selection as shown in Fig. A.1. For the channel number 17 to 20, the DS1103ADC A/D conversion is used. By using the ADC, it will provides read access to 4 parallel A/D converters. The output from this controller board will be sent to the dSpace Fiber Optic Board to generate the pulse width modulation signal as shown in Fig. A.2 and this Fiber Optic Board is powered by the 24Vdc source. The key features of the dSpace 1103 controller board are described in Table A.1.
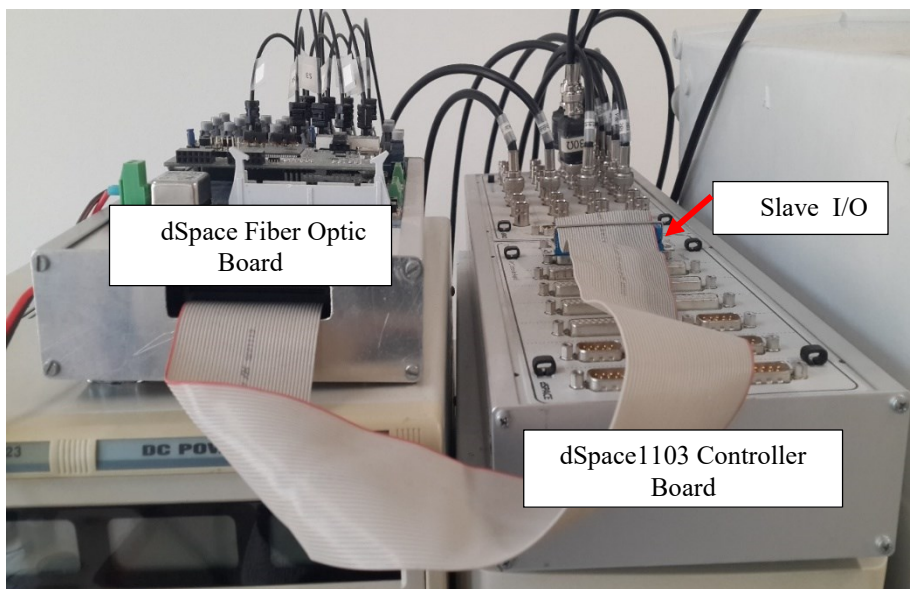
Fig. A.2. Output ports of the dSpace1103 controller board connected to the fiber optic board.

Fig. A.3. Connection of 330Ω to the coaxial cable before connecting to the dSpace ADC Input port.

Table A.1. dSpace 1103 controller board features.

Board	BNC Connectors	Sub-D Connectors
DS1103	• 20 ADC	• Digital I/O
	• 8 DAC	• Slave DSP I/O
		• Incremental Encoder Interfaces
		• CAN Interface
		• Serial Interface